Analyzing the impact of astrocyte-oligodendrocyte gap junction coupling on neuronal activity in the thalamus

Dissertation

zur

Erlangung des Doktorgrades (Dr. rer. nat.)

der

Mathematisch-Naturwissenschaftlichen Fakultät

der

Rheinischen Friedrich-Wilhelms-Universität Bonn

vorgelegt von

Camille Monique Madeleine Philippot

aus

Louviers, Frankreich

Bonn, 2019

Angefertigt mit Genehmigung der Mathematisch-Naturwissenschaftlichen Fakultät der
Rheinischen Friedrich-Wilhelms-Universität Bonn

1. Gutachter: **Prof. Dr. Christian Steinhäuser**
Institut für Zelluläre Neurowissenschaften
Universität Bonn

2. Gutachter: **Prof. Dr. Michael Hofmann**
Institut für Zoologie
Universität Bonn

Tag der Promotion: 04.03.2020

Erscheinungsjahr: 2020

« Il faut bien que je supporte deux ou trois chenilles si je veux connaître les papillons. »

-Le Petit Prince (1943) de Antoine de Saint-Exupéry

Acknowledgements

First of all, I would like to thank my supervisor Prof. Dr. Christian Steinhäuser for giving me the opportunity to work on this fascinating project while doing my PhD in his lab. I am very thankful for the scientific guidance, constant support, constructive discussions, and for sparking my enthusiasm to learn more about glial cells in the very special region of the thalamus.

I am grateful to Prof. Dr. Michael Hofmann, Prof. Dr. Karl Schilling and Prof. Dr. Christa Müller for accepting my request to be part of the examination committee and for their time and efforts in reviewing my thesis.
Additionally, I would like to thank PD Dr. Ronald Jabs for excellent support in the field potential analysis and with Igor tools. I am thankful for all the support in 2P imaging and for answering in all kind of questions about microscopy and electrophysiology throughout the years.
Special thanks go to PD Dr. Gerald Seifert for organizing the animal breeding for all the transgenic mice used for my work, the constant support in genotyping all the connexin 32/47 ko mice, and the fruitful scientific discussions.
Besides, I would like to thank Prof. Dr. Christian Henneberger for his time and fruitful discussion on the thalamus project.
My sincere thanks go to Thomas Erdman for excellent technical support, especially in ordering the stimulation electrodes and the genotyping of the connexin 32/47 ko mice. I am thankful to Dr. Ines Heuer und Dr. Silke Künzel for their help in administrative matters.

My special thanks go to Dr. Stephanie Griemsmann for introducing me to the thalamus field and to the field of electrophysiology, sharing valuable experience, scientific discussions, advices (throughout the years, even after leaving the lab) and her time for providing constructive criticisms on my thesis manuscript. I also want to thank Linda Patt for her time and valuable inputs in correcting my thesis manuscript. I would like to thank Lena Claus for introducing me to the field of thalamic barreloids, sharing knowledge and scientific discussion for our successful publication. I want to thank Paula Baum her commitment and enthusiasm in following the barreloid project.

Besides, I would like to thank Monika Plescher for being a wonderful patch colleague during her time in our lab, for her support through our time together in Bonn, for all our shared diner, conferences and travel trips. I am so glad that our friendship is continuing while you moved to Sweden!

A very special thank go to Aline Timmermann. Thank you for being the best colleague and friend I could have asked for before coming to Bonn! For all our good times, tea times, lunch times, conferences (18!), for her valuable help in the lab and our productive scientific discussions, for helping me in everything involving German and most

importantly for always being so enthusiastic and bringing such a good atmosphere to the lab (especially early mornings).

My warm thanks go to Sabrina and Vicky. Thank you both for bringing a bit of France in the lab next door, as well as for the coffee breaks, the diner, board games and cocktail nights.

Of course, I would like to thank all the members of the IZN institute for an excellent work environment, all the help and the great time together, soccer betting, workout days, lunch times, travel to conferences, Christmas parties and more: Alberto, Antonia, Björn, Cátia, Daniel, Dario, Dilaware, Dmitry, Julia, Kirsten, Lukas, Magda, Michel, Nehal, Peter, Petr, Stefan H, Stefan P, Steffi A, Tushar and Zhou.

I would like to express my warmest thanks to my parents and sisters. Maman, Papa, Hélène et Julie, merci pour votre soutien constant et vos encouragements, toujours sans failles et spécialement au cours de ces cinq dernières années. Merci!

Finally, my deepest thanks go to my boyfriend Jascha. Merci, vielen Dank, thank you for your love, patience, constant support and encouragement throughout the years.

Table of Contents

Abbreviations **9**

1 Introduction **11**

1.1 The thalamus 11

1.2 Thalamic barreloids 13

1.3 Glial cells in the brain 14

1.3.1 Astrocytes 15

1.3.2 Oligodendrocytes 17

1.4 Connexin gap junction channels 18

1.4.1 Astrocyte connexins 20

1.4.2 Oligodendrocyte connexins 21

1.4.3 Panglial gap junction coupling 22

1.5 Neuron-glia interactions and metabolism 23

1.5.1 Tripartite synapse and calcium waves 23

1.5.2 Astrocytes and neurovascular coupling 25

1.5.3 Astrocyte Neuron Lactate Shuttle hypothesis 26

1.5.4 Oligodendrocytes and metabolic support to axons 28

2 Aim of the Study **31**

3 Materials **33**

3.1 Chemicals 33

3.2 General materials 34

3.3 Software 34

3.4 Equipment 34

3.5 Antibodies 35

3.6 Solutions and buffers 36

3.6.1 Solutions for electrophysiology 36

3.6.2 Solutions and buffers for immunohistochemistry 37

3.7 Animals 38

3.7.1 C57BL/6J mice 38

3.7.2 hGFAP-EGFP mice ... 38
3.7.3 PLP-GFP mice ... 39
3.7.4 Cx32/Cx47 dko mice ... 39
4 Methods ... 40
4.1 Electrophysiology ... 40
4.1.1 Preparation of acute brain slices ... 40
4.1.2 Electrophysiological set up ... 40
4.1.3 Whole-cell patch-clamp recording ... 41
4.1.4 Recording of thalamic field potentials and data analysis ... 43
4.2 Confocal and 2-photon microscopy ... 46
4.3 Immunohistochemistry ... 46
4.3.1 Immunofluorescence staining ... 46
4.3.2 Microscopy of fixed slices ... 47
4.3.3 Data analysis ... 47
4.4 Statistics ... 47
5 Results ... 48
5.1 Thalamic barreloids ... 48
5.1.1 Properties of oligodendrocytes localized on barreloid borders ... 48
5.1.2 Functional impact of neuronal activity on glial coupling in thalamic barreloids ... 50
5.2 Effect of extracellular glucose deprivation on post synaptic field potentials in the thalamus ... 52
5.2.2 Analyses at physiological temperature ... 52
5.2.1 Analyses at room temperature ... 53
5.3 Decline of fPSPs during EGD cannot be rescued by extracellular bath application of lactate or pyruvate ... 54
5.4 Effect of filling glial cells with energy metabolites during EGD on neuronal activity ... 56
5.4.1 Effect of filling an astrocyte ... 56
5.4.2 Effect of filling an oligodendrocyte ... 58
5.5 The impact of Cx32 and Cx47 ... 60
5.5.1 Impact on panglial networks ... 60
5.5.2 Impact on neuronal activity ... 62
5.6 Effect of glucose and monocarboxylate transporters on neuronal activity ... 64
6 Discussion ... 66
6.1 Barreloid borders are mostly shaped by weakly coupled oligodendrocytes ... 67

6.2 Neuronal activity shapes panglial networks in thalamic barreloids 68

6.3 Thalamic fPSPs are sensitive to EGD and extracellular lactate or pyruvate cannot replace glucose to maintain fPSPs 70

6.4 Loading an astrocyte with energy metabolites can rescue the EGD-induced decline of thalamic fPSPs 72

6.5 Oligodendrocytes in gap junction networks are essential to maintain fPSP activity in the thalamus 73

6.6 Glucose and monocarboxylate transporters are involved in providing energy substrates through thalamic panglial networks to sustain neuronal activity 74

7 Summary 76

8 Perspective 78

References 79

Abbreviations

2-NBDG	2-(N-(7-nitrobenz-2-1,3-diazol-4-yl)amino)-2-deoxyglucose
ACSF	artificial cerebrospinal fluid
AG	astrocyte glucose
AL	astrocyte lactate
Aldh1L1	aldehyde dehydrogenase 1 family, member L1
AMPA	α-amino-3-hydroxy-5-methyl-4-isoxazolepropionic acid
ANLS	astrocyte-neuron lactate shuttle
ATP	adenosine triphosphate
Biocytin	N-biotinyl-L-lysine
Camp	cyclic adenosine monophosphate
Cm	membrane capacitance
CNP	2',3'-Cyclic-nucleotide 3'-phosphodiesteras
CNS	central nervous system
CO	cortex
CT	cortico-thalamic
Cx	connexin
D-AP5	DL-2-amino-5-phosphonovaleric acid
DIC	differential interference contrast
dko	double knockout
DNA	deoxyribonucleic acid
e.g.	for example
EAAT	excitatory amino acid transporters
ECFP	enhanced cyan fluorescent protein
EGD	extracellular glucose deprivation
EGFP	enhanced green fluorescent protein
EGTA	ethylene diaminetetraacetic acid
Fig.	figure
FITC	fluorescent isothiocyanate
fPSP	field Post Synaptic Potential
GABA	ɣ-aminobutyric acid
GAD	glutamic acid decarboxylase
GFAP	glial fibrillary acidic protein
GFP	green fluorescent protein
GLAST	glutamate aspartate transporter
GLUT	glutamate transporter
GLS	glutaminase
GS	glutamine synthetase
HEPES	4-(2-hydroxyethyl)-1-piperazineethanesulfonic acid
HC	hippocampus
I	current
ic	internal commissure/capsule

IP3	inositol triphosphate 3
KA	kainic acid
kDa	kilo Dalton
Kir	inwardly-rectifying K^+
ko	knock-out
LDH	lactate dehydrogenase
LSM	laser scanning microscope
LTD	long-term depression
LTP	long-term potentiation
MBP	myelin basic protein
MCT	monocarboxylate transporter
mGluR	metabotropic glutamate receptor
MP	membrane potential
n	number of samples
NADH	nicotinamide adenine dinucleotide
NBQX	2,3-dihydroxy-6-nitro-7-sulfamoyl-benzo[f]quinoxaline-2,3-dione
NDD	non-descanned detector
NG2	nerve/glia antigen 2
NGS	normal goat serum
NMDA	N-methyl-D-aspartic acid
OG	olygodendrocyte glucose
OL	olygodendrocyte lactate
OPC	oligodendrocyte precursor cell
p	postnatal day
PBS	phosphate buffered saline
PCR	polymerase chain reaction
PFA	paraformaldehyde
PLP	proteolipid protein
PMT	photomultiplier tube
Po	posterior thalamic nucleus
PTX	picrotoxin
Rm	membrane resistance
Rs	series resistance
RT	room temperature
RTN	reticular thalamic nuclei
S100ß	S100 calcium binding protein ß
SEM	standard error of the mean
SR101	sulforhodamine 101
TC	thalamo-cortical
TRITC	tetramethylrhodamine isothiocyanate
TTX	tetrodotoxin
V	voltage
VB	ventrobasal
VPL	ventro posterior lateral nucleus
VPM	ventro posterior medial nucleus
v/v	volume per volume

1 Introduction

The role of glial cells in the central nervous system (CNS) has been underestimated and brain studies were restricted to neuronal brain cells for a long time. In the CNS, complex neuronal networks are formed, in which neurons can receive and integrate incoming signals as well as transmit information. Glial cell properties and their interaction with neurons are nowadays known to be essential for proper brain function. Glial cells make up 65% of the mouse brain and there is increasing evidence on their role in brain function, development and more recently in brain metabolism (Barres, 2008; Allen and Barres, 2009). The brain requirements in energy supply are extremely high and glial cells are essential to guarantee proper brain function.

This study focuses on the role of two types of glial cells, astrocytes and oligodendrocytes, and aims to understand their respective role in supporting and providing energy substrates to neurons in a specific region of the brain, the thalamus. This following section gives an overview into this topic.

1.1 The thalamus

The thalamus (from Greek, „inner chamber“) is the largest component of the diencephalon, located in the center of the brain. It is a symmetrical structure and each hemisphere comprises a thalamus. The third ventricle, which is a thin vertical space filled with cerebrospinal fluid, separates the two structures. The thalamus has been described as “the gateway to consciousness” (Crick and Koch, 2003). It plays an essential role as a relay station and only the olfactory sensory pathway is not controlled by the thalamus. The thalamus is now not only believed to be a relay station but it can also process information. There is evidence demonstrating the role of the thalamus in modulation of sensory and motors signals to the neocortex (Sherman and Guillery, 2002).

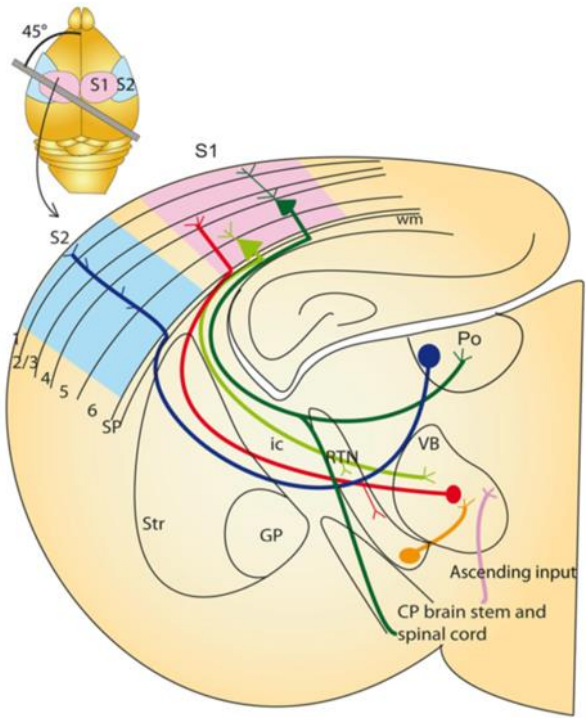

Figure 1.1 Scheme representing thalamocortical projections in the adult mouse brain.
(Inset) Outline of a mouse brain. The thick grey line indicates the cutting angle of the brain section used to obtain thalamocortical slices containing intact thalamocortical projections. (Main illustration) Schematic representation of the connections between the ventrobasal thalamus (VB) and the cortex. The ventrobasal thalamic nucleus receives somatosensory ascending inputs from the brain stem (pink). VB neurons (red) project axons to layer 4 of the primary somatosensory cortex S1 (light pink) and layer 6 neurons signal back to the VB (light green). Axons run across the internal commissure (ic). Thalamo-cortical (TC) as well as cortico-thalamic (CT) neurons form synapses with GABAergic neurons from the reticular thalamic nucleus (RTN), creating an inhibitory feedback loop and an inhibitory feedforward circuit to the VB (orange). Layer 5 axons (dark green) signals from the somatosensory cortex to a higher order nucleus, the posterior thalamic nucleus (Po). This nucleus signals back to a different cortical area, S2 (light blue), that is different from the original input. GP, globus pallidus; Str, striatum; wm, white matter. From Grant et al., 2012.

Sherman and Guillery divided the thalamus into two types of nuclei based on the origin of the information. First order nuclei receive and relay information coming from ascending pathways (visual, sensory, auditory), whereas high order nuclei relay information coming from the cortex itself. Thus, information is transferred between different cortical regions via the thalamus. Glial cells in the ventrobasal nucleus (VB), a first order nucleus, were the focus of this study. The VB consist of the ventral posterior medial (VPM) and the ventral posterior lateral (VPL) nuclei. It is part of the somatosensory system and of the trigeminal pathway, which is transferring information from the brain stem to the thalamus and further to the cerebral cortex (Bosman et al., 2011). The VB receives somatosensory peripheral inputs (Fig. 1.1). Those inputs terminate on glutamatergic synapses. Glutamate receptors are primarily involved in neuronal thalamic firing (Eaton and Salt, 1996). Thalamic relay neurons project axons

mainly to the layer 4 of the primary somatosensory cortex via the thalamo-cortical (TC) pathway (Agmon et al., 1993). Using this pathway, axons cross through the reticular thalamic nucleus (RTN) and the internal capsule. TC neurons from synapses with GABAergic RTN neurons generating an inhibitory feedback loop. Cortico-thalamic (CT) neurons send projections from layer 6 of the somatosensory cortex back to the VB, to form glutamatergic synapses on the distal dendrites of the relay cells (Grant et al., 2012). Following their pathway, CT neurons also form synapses on RTN neurons creating an inhibitory feedforward circuit to the VB (Bourassa et al., 1995; Grant et al., 2012; Pinault 2011).

Nearby GABAergic RTN neurons are also interconnected with each other via gap junctions-mediated electrical synapses that depend mostly on connexin36 (Cx36), throughout thalamic networks development (Landisman et al., 2002; Long et al., 2004; Lee et al., 2014; Zolnik and Connors 2016). Electrical synapses via Cx36 are abundant between VB neurons in one week old animals but decrease in the second week. In fact, they were never observed in VB neurons after postnatal day (p) 12 (Lee et al., 2010).

The thalamus is one of the most heavily interconnected areas in the brain. Therefore thalamic abnormalities have been linked to several disorders. Schizophrenia, absence epilepsy, Alzheimer or fatigue in patients with multiple sclerosis have all been associated with thalamic dysfunctions (Pinault, 2011; Chen et al., 2017; Aggleton et al., 2016; Niepel et al., 2006).

1.2 Thalamic barreloids

The VPM receives input from the whiskers. It contains elongated cellular domains called barreloids, which are the structural basis for the somatotopic organization of vibrissae responses (Van der Loos, 1976; Land et al., 1995). Each barreloid receive sensory input from individual vibrissae and relays those signals to the corresponding cortical module, called a barrel in the layer 4 of the primary somatosensory cortex (Fig 1.2; Ito, 1988; Sugitani et al., 1990; Mosconi et al., 2010; Haidarliu and Ahissar, 2001). Barreloids are whisker-related clusters of neurons that form somatotopically related pathways. Furthermore, adjacent barreloids are closely connected with each other (Lavalée and Deschênes, 2004). In early development one thalamic relay neuron is confined to a single barreloid. The number of primary dendrites does not change from p5 to adulthood. However, during development dendritic arbors extent to adjacent

barreloids. This process is mainly complete by p18 (Zantua et al., 1996). More specifically, thick proximal dendrites of relay cells are restricted to their home barreloids whereas extrabarreloid dendrites can extend to neighbouring barreloids (Varga et al., 2002).

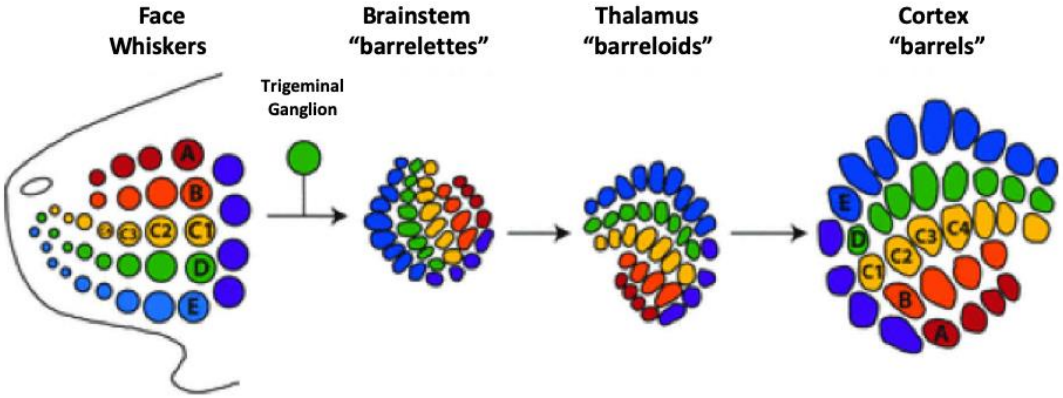

Figure 1.2 Schematic representation of somatotopic whisker organization.
Spatial arrangement of mice whiskers. The somatotopy of face whiskers is maintained in the brain stem as "barrelettes", in the thalamus as "barreloids" and in the cortex as "barrels". From Li and Crair, 2011.

1.3 Glial cells in the brain

Glial cells are at least as abundant as neurons in the human brain but it was only in the middle of the 19th century that Rudolf Virchow, Santiago Ramón y Cajal and Pío del Río-Hortega discovered them. The concept of neuroglia defined those cells as supporting players next to neurons. The name "Nervenkitt", literally "nerve-glue", in ancient Greek was introduced by the German anatomist Virchow in 1856 in his trial to find a "connective tissue" in the brain (Virchow, 1856; Verkhratsky and Nedergaard, 2018).

Pío del Río-Hortega was the first neuroscientist to define the classical view of glial cells by dividing them into the subgroups microglia and macroglia. The latter group consists of astrocytes, oligodendrocytes, NG2 cells and ependymal cells. Today, the role of glia in brain function is progressively recognized. Glial cells have been shown to be involved in physiological processes, like learning, memory and cognition, and they have also been associated with disease development (Barres 2008; Coulter and Steinhäuser, 2015; Elsayed and Magistretti, 2015). In this work, the role of astrocytes and oligodendrocytes in the thalamus will be investigated.

1.3.1 Astrocytes

Astrocytes are the most abundant glial cell type in the adult brain (Kettenmann and Ransom, 2005). Their name was introduced by Michael von Lenhossék and is derived from the Greek *astron*-star and *kutos*-cell, a reference to their star-like morphology (Lenhossék, 1891). They possess numerous ramified processes as firstly described by Ramón y Cajal in 1897 (Fig. 1.3A). Astrocytes play an important role in the gliovascular network. As already suggested by Ramón y Cajal, they are in intimate contact with endothelial cells covering the walls of vascular structures (Fig. 1.3A). Indeed, their endfeet are covering all cerebral blood vessels at the blood-brain-barrier (BBB). This proximity allows for ion, water, amino acid and neurotransmitter transfer and regulation between the two structures (Abbott et al., 2006, Nedergaard et al., 2003). Astrocytes are also perfectly located between blood vessels and neurons to participate in regulating cerebral blood flow (MacVicar and Newman 2015; see section 1.5.2). Consequently, astrocytes are essential in the regulation of brain homeostasis. For this purpose, they express a variety of channels and transporters at their endfeet, such as aquaporins, glucose and lactate transporters as well as K^+ channels (Sofroniew and Vinters, 2010; Wang and Bordey, 2008).

A typical marker for identifying astrocytes is the glial fibrillary acid protein (GFAP). It is an intermediate filament and the most distinctive cytological feature of astrocytes. However, GFAP does not label the entire cell but mostly somata and proximal processes (Wilhelmsson et al., 2004). Only dye filling of individual astrocytes allows the visualization of the entire cell domain. This method demonstrates that astrocyte processes extend around 50 to 100 µm from the somata (Wilhelmsson et al., 2004). Furthermore, most of the astrocyte domains are not overlapping with each other and only few interdigitations are observed between fine processes (Fig. 1.3B; Wilhelmsson et al., 2006; Bushong et al., 2002; Pekny et al., 2014). However, the overlap factor seems age-related as interdigitation of astrocyte territories increases with age in mice (Grosche et al., 2013). In regions where processes are overlapping, neighboring astrocytes are connected together through gap junction channels from early postnatal development, thus forming a network. Astrocyte gap junction coupled networks will be described in section 1.4.1. Another restriction in using GFAP as an astrocyte marker is that it is widely expressed in the hippocampus but not by thalamic astrocytes (Frassoni et al., 2000), whereas the calcium binding protein S100β was found in both

hippocampal and thalamic astrocytes (Matthias et al., 2003; Parri et al., 2010). Another classical astroglial marker, 10-formyl-tetrahydrofolate dehydrogenase (Aldh1L1), is also lacking in thalamic astrocytes and was found to overlap with the oligodendrocyte markers Olig2 and PLP-GFP$^+$ cells in the thalamus (Griemsmann et al., 2015). Glutamine synthetase (GS) is mainly confined to astrocytes in the hippocampus (Coulter and Eid, 2012), but almost all PLP-GFP$^+$ cells expressed GS in the thalamus (Griemsmann et al., 2015). Hence, classical astrocytic markers used in the hippocampus show an overlapping expression profiles in the thalamus and are therefore not reliable tools for cell type identification.

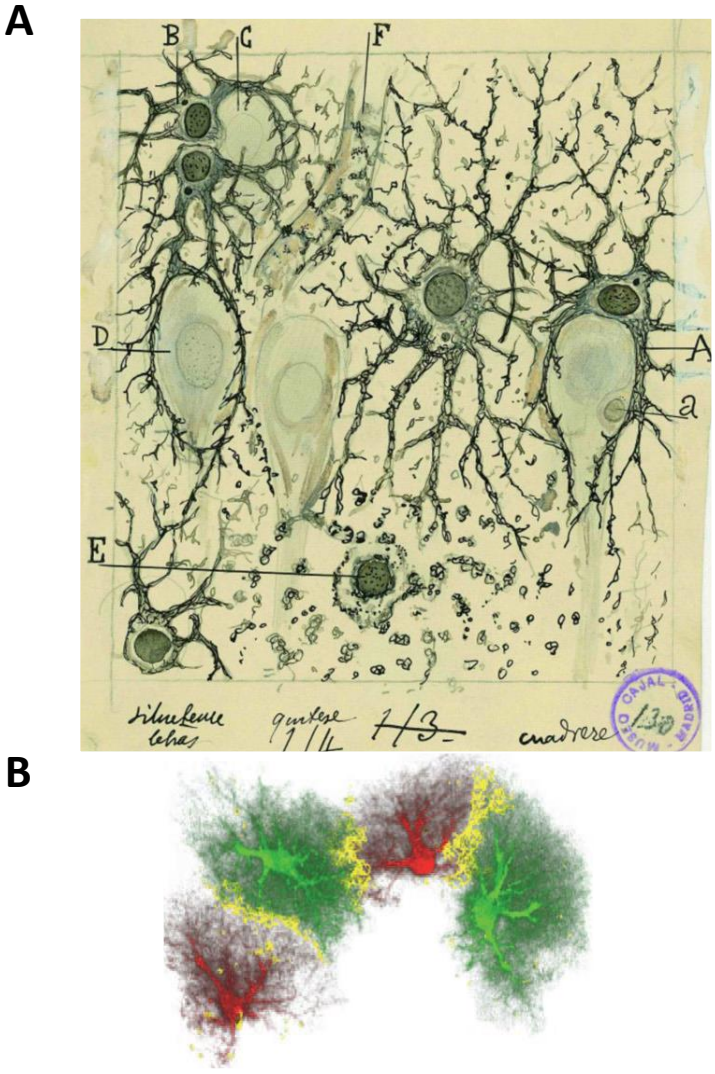

Figure 1.3 Astrocyte morphology and territories.
(A) Santiago Ramon y Cajal's drawing of the pyramidal layer and stratum radiatum of an adult man (3h after his death) showing "neuroglia". He already described and drew astrocytes (dark cells, A, B) as cells with comparatively small soma and numerous thick processes, prolonged with fine distal processes enwrapping adjacent neuronal somata and dendrites. Astrocytes contact neurons (lighter cells, C, D) and blood vessel (F) (Ramon y Cajal, 1897; Navarrete and Araque, 2014). (B) 3D reconstruction of astrocytes in the dentate gyrus. Astrocytes occupy their own domains. Only fine cellular processes (yellow) are overlapping between adjacent astrocytes (red and green; Wilhelmsson et al., 2006).

Astrocytes are electrically non-excitable. Electrophysiological analyses show a passive current pattern in whole-cell mode recordings, reflecting the high density of K^+ channels, inward-rectifying (Kir) and two-pore domain K^+ channels (Wallraff et al., 2004; Djukic et al., 2007; Seifert et al., 2009). Astrocytes are characterized by a high resting permeability for K^+ and a very negative resting potential (around -80 mV) close to the Nernstian equilibrium for K^+ (Somjen, 1975; Nedergaard et al., 2003). Therefore, they are very sensitive to changes in extracellular K^+ concentrations and play a role in spatial K^+ buffering. Astrocytes can take up the excess of extracellular K^+ occurring during neuronal excitabitiliy and this process is mainly mediated via Na^+/K^+ pumps and $Na^+/K^+/Cl^-$ cotransporter 1 (Balestrino and Somjen, 1986; Ransom et al., 2000; D'Ambrosio et al., 2002). Spatial buffering is another mechanism involved in regulating K^+ concentrations. It is based on the fact that astrocytes are connected with each other via gap junction channels to form coupled networks. Astrocytes are taking up K^+ from high concentrated regions, and redistribute it through their network into areas with low concentration of K^+, via weakly rectifying Kir4.1 channels. This mechanism occurs due to the more negative resting membrane potential than the K^+ equilibrium potential leading to an K^+ influx in astrocytes (Orkand, 1986). An intact gap junction network is essential for efficient K^+ buffering, as an impaired K^+ buffering was observed in mice lacking connexin43 and connexin30 (Wallraff et al., 2006). There is now increasing evidence that astrocytes play important roles in modulation of neuronal activity and synaptic transmission. At the synapses, they are enwrapping neurons with their processes and are therefore active players in the concept of the "tripartite synapse" (Araque et al., 1999), which will be described further in section 1.5.1.

1.3.2 Oligodendrocytes

Oligodendrocytes are considered to be the second major group of glial cells in the CNS. They were first discovered by Pío del Río-Hortega in 1928. He introduced the term of *oligodendroglia* to describe these neuroglia cells with few processes arriving from the cell somata (Del Río Hortega, 1921). Oligodendrocytes originate from oligodendrocyte progenitor cells (OPCs), also called NG2 glial cells as they express the NG2 chondroitin sulfate proteoglycan on their surface (Nishiyama et al., 2009). NG2 glia is widely considered to be the third major glial cell type in the CNS.

First studies focused on oligodendrocytes' myelinating function. In the CNS, once OPCs differentiate in oligodendrocytes, they extend multiple exploratory processes to enwrap neuronal axons with an insulating multilamellar lipid structure called myelin (Sherman and Brophy, 2005). This process ensures accurate saltatory conduction of action potentials from one node of Ranvier to another. Myelination is a continuous process that starts during early development. It is region dependent and crucial for the signaling capacity of the brain (Fuss et al., 2000). In the adult brain, oligodendrocytes have been shown to contribute to myelination modeling (Young et al., 2013). While there is heterogeneity across brain regions, white matter areas are mostly composed of oligodendrocytes which form myelin around long-range axons. The optic nerve contains almost exclusively myelinated axons, whereas more than 70% of the axons are unmyelinated in the corpus callosum (Young et al., 2013). Oligodendrocytes are nevertheless also present in grey matter. The start of the myelination process in the thalamus is characterized by light myelin protein formation in thalamic nuclei around p8, which continues until 4 weeks after birth in rats (Downes and Mullins, 2014). However, myelination is not the only function of oligodendrocytes. In grey matter, so called satellite or perineuronal oligodendrocytes are found whose function is not well understood (Simons and Nave, 2016). Recent studies have put forward that oligodendrocytes in white matter also provide metabolic support to neurons. They do so via myelin sheaths, which are crucial to secure proper axonal function (Simons and Nave, 2016). This will be further described in section 1.5.4.

Like astrocytes, oligodendrocytes also express connexins. However, they express other connexin isoforms than astrocytes. Oligodendrocyte gap junction coupled networks will be described in section 1.4.2.

1.4 Connexin gap junction channels

Gap junction channels are intercellular channels providing a direct pathway for intercellular connection and communication. The cytoplasm of connected cells is linked, therefore allowing the exchange of small molecules up to around 1 to 1.2 kDa (Giaume and Naus, 2013). In vertebrates, gap junctions are formed by membrane proteins called connexins (Cx). 21 different genes encoding connexins have been identified in humans and 20 in mice. Cx are usually named according to their predicted molecular weight (Willecke et al., 2002; Söhl and Willecke, 2003).

A single gap junction channel consists of 2 connexons. One connexon is composed of 6 connexin molecules, which are transmembrane proteins. Connexins have four transmembrane domains, two extracellular loops, one intracellular loop and N- and C-terminal tails (Fig. 1.4). The length of the C-terminal tail mostly determines the connexin size. In mice, the molecular weight ranges from 23 to 57 kDa (Willecke et al., 2002; Giaume et al., 2010; Söhl and Willecke, 2003). A gap junction channel can be homotypic, formed by identical connexons, or heterotypic, formed by 2 different connexon types. Connexons of uniform connexins are called homomeric whereas heteromeric connexons contain different connexins (Willecke et al., 2002; Goldberg et al., 2004). The molecular weight, as well as the net charge and the shape, influence the permeability properties of gap junction channels (Goldberg et al., 2004; Giaume et al., 2010). Several studies have shown that gap junction channels are permeable to numerous molecules, as for example ions (K^+, Na^+, Ca^{2+}), second messengers (cAMP, IP_3), metabolites (glucose, lactate) or water (Niermann et al., 2001; Rouach et al., 2002; Bedner et al., 2006; Wallraff et al., 2006; Rouach et al., 2008; Giaume et al., 2010). Different sets of connexins are expressed depending on the cell type, the developmental stage or the brain region (Goodenough et al., 1996; Willecke et al., 2002; Nagy et al., 2004; Schools et al., 2006; Bedner et al., 2012).

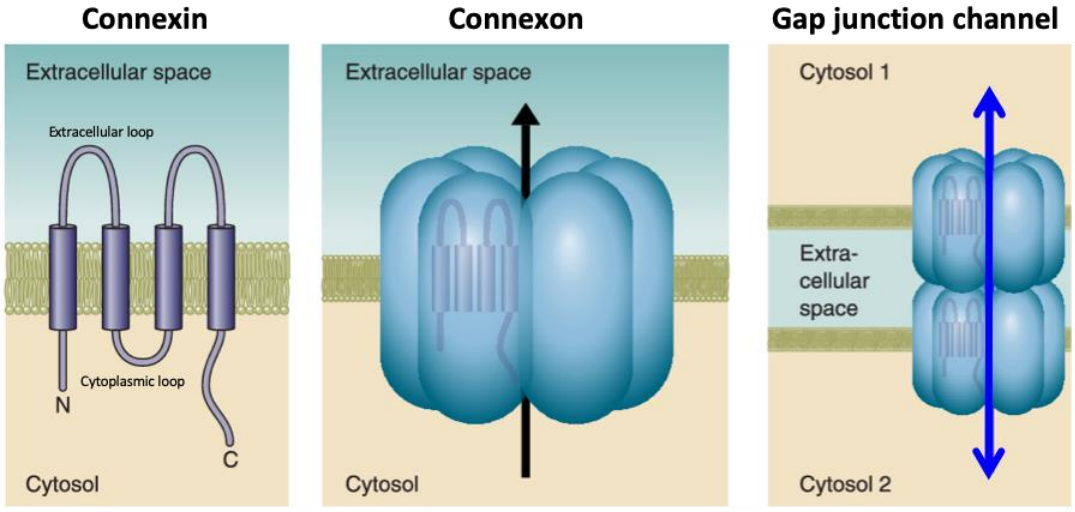

Figure 1.4 Structure of a gap junction channel
A connexin is composed of 4 transmembrane domains, two extracellular loops, one cytoplasmic loop, and an N- and C-terminal. A hexamer of connexin subunits forms a connexon, also referred to as a hemichannel. A gap junction channel is formed when two connexons of two adjacent cells connect with each other (Adapted from Bosco et al., 2011).

28 human genetic diseases have been associated with connexin mutations or connexin expression alterations (Giaume et al., 2010; Giaume and Naus, 2013; Srinivas et al., 2018). For example, in humans a mutation of Cx32 leads to a demyelination disorder, the X-linked Charcot Marie Tooth Disease (Bergoffen et al., 1993). Mutations in the Cx47 gene are associated with the Pelizaeus-Merzbacher-like disease, a hypomyelinating leukodystrophie characterized by progressive spasticity and ataxia (Uhlenberg et al., 2004). Thus, connexins and gap junction channels are important for proper brain function.

1.4.1 Astrocyte connexins

Astrocytes express the highest levels of Cx in the brain. The main cell specific astrocytic gap junction proteins are Cx43 (gene name *Gja1*) and Cx30 (*Gjb6*) while Cx26 (*Gjb2*) is expressed by a small population of grey matter astrocytes (Nagy et al., 2003; Nagy and Rash, 2003; Nagy et al., 2011). Astrocytic connexins can form intra-astroglial connections (Wallraff et al., 2006). Using antibodies and immunoreactivity, Cx43 has been well recognized as the major constituent of gap junctions in astrocytes in the neocortex or in the hippocampus but not in the thalamus (see below). Expression of Cx43 starts early during embryonic stage in white and grey matter of the CNS and remains high throughout postnatal development (Dermietzel et al., 1989; Yamamoto et al., 1990). Loss of Cx43 in the hippocampus leads to partial inhibition of up to 50% of astrocyte coupled networks and increases velocity in hippocampal spreading depression (Theis et al., 2003). Cx43 is an important element in brain development and physiology, such as in K^+ spatial buffering, inter-astroglial Na^+ waves, Ca^{2+} waves, metabolite transport and glutamate clearance (Wallraff et al., 2006; Scemes and Giaume, 2006; Langer et al., 2012; Rouach et al., 2008; Theis et al., 2003; Pannasch et al., 2011). Modulation of glial networks and metabolism will be described in section 1.5.

In mice lacking Cx43, an upregulation of Cx30 expression was observed (Theis et al., 2003; Wallraff et al., 2006). Cx30 is expressed later than Cx43, starting at postnatal day 10 and is dominant in grey matter (Dahl et al., 1996; Kunzelmann et al., 1999; Nagy et al., 1999). Cx30 has been shown to control excitatory synaptic transmission in the hippocampus through modulation of astrocytic glutamate transport, mediated by changes in synaptic location of astroglial processes. Therefore, Cx30 sets synaptic strength and is involved in long-term synaptic plasticity and memory (Pannasch et al.,

2014). Cx30 is also upregulated in mice, which are exposed to cages with a rich environment, and is thus linked to cognitive processes (Rampon et al., 2000). Interestingly, in the olfactory bulb, neuronal activity regulates astroglial networks through Cx30, suggesting Cx30 as a molecular target for activity-dependence of gap junction channels (Roux et al., 2011).

Cx43 and Cx30 are both enriched at perivascular astrocytic endfeets and along blood vessel walls (Pannasch and Rouach, 2013). Loss of both Cx43 and Cx30 leads to dysmyelination, vacuolization and complete loss of astrocyte coupling, as well as reduced astrocyte/oligodendrocyte coupling in the CNS of these mice (Wallraff et al., 2006; Lutz et al., 2009; Maglione et al., 2010; Pannasch et al., 2011; Griemsmann et al., 2015). The distribution of astrocytic connexins is broad but heterogeneous among different brain regions. In the hippocampus, astrocytic coupling is dominated by Cx43, whereas in the thalamus many astrocytes even lack Cx43 (Griemsmann et al., 2015). In the thalamus, Griemsmann et al. (2015) have shown that Cx30 is the dominant connexin.

While an abundant expression of Cx26 was observed in the thalamus using immunostaining (Nagy et al., 2001, 2011), deletion of Cx26 did not impact gap junction coupling (Griemsmann et al., 2015). This indicates that there is no major functional role of this specific connexin in thalamic coupling networks (Griemsmann et al., 2015). In conclusion, astroglial connexins are crucial for the regulation and maintenance of proper brain homeostasis and neuronal activity (Rouach et al., 2008; Giaume et al., 2010; Roux et al., 2011).

1.4.2 Oligodendrocyte connexins

Oligodendrocytes express Cx29 (gene name Gjc3), Cx32 (*Gjb1*) and Cx47 (Gjc2) (Dermietzel et al., 1997; Kunzelmann et al., 1997; Altevogt et al., 2002; Nagy and Rash, 2003). Connexins are critical for CNS myelination through electrical and metabolic coupling (Menichella et al., 2006; Giaume and Naus, 2013). Oligodendrocytic connexins can form intra-oligodendroglial connections (Maglione et al., 2010; Wasseff and Scherer, 2011). Cx29 is localized at the adaxonal membrane of the myelin sheaths and also at the cell body of oligodendrocytes (Altevogt et al., 2002; Li et al., 2004; Nagy et al., 2003). However, this connexin does not form functional gap junction

channels (Kleopa et al., 2004). Deletion of Cx29 alone did not impact the coupled network size in the corpus callosum (Maglione et al., 2010).

Gap junction plaques in oligodendrocytes are composed of Cx32 and Cx47 and are localized at oligodendrocytic cell bodies (Kleopa et al., 2004). Cx32 is also localized at the outer membrane of large myelin sheaths (Kleopa et al., 2004; Kamasawa et al., 2005). In mice, deletion of Cx32 did not show neurological abnormalities (Nelles et al., 1996) and the deletion of Cx32 alone did not significantly reduce glial network size in the corpus callosum (Maglione et al., 2010). Cx47 is localized in oligodendrocyte somata and is widely present at astrocyte-oligodendrocyte gap junctions (Nagy et al., 2003). Mice lacking only Cx47 did not show obvious abnormal behaviour, and only sporadic vacuoles (Odermatt et al., 2003; Menichella et al., 2003). However, functional studies have shown that the deletion of Cx47 reduces the coupled network by about 80% and completely abolishes coupling of oligodendrocytes to astrocytes (Maglione et al., 2010). Furthermore, the loss of Cx47 in mice was associated with the loss of other connexins located in oligodendrocyte somata (Li et al., 2008). Mice lacking both Cx47 and Cx32 showed severe vacuolation, died early after birth (6 weeks) and coupling was completely absent in white matter (Odermatt et al., 2003; Maglione et al., 2010). In conclusion, oligodendroglial connexins are crucial for proper myelination and regulation of brain homeostasis (Kamasawa et al., 2005; Maglione et al., 2010; Giaume and Nave, 2013).

1.4.3 Panglial gap junction coupling

As astrocytic and oligodendrocytic connexins are different, astrocyte/oligodendrocyte gap junctions are therefore heterotypic. Recent findings suggest that astrocytic and oligodendrocytic connexins can form inter-astro-oligodendroglial connections, called panglial coupling, *in vivo* (Maglione et al., 2010; Wasseff and Scherer, 2011; Tress et al., 2012; Griemsmann et al., 2015). In grey matter, immunohistochemical studies have demonstrated that oligodendrocytic Cx47 and astrocytic Cx43 colocolize at oligodendrocyte-to-astrocyte gap junctions, while oligodendrocytic Cx32 colocalizes with astrocytic Cx30 (Nagy et al., 2003; Altevogt and Paul, 2004). Electrophysiological studies have identified that some couplings pairs are functional and permeable to molecules, like the Cx30/Cx32, Cx47/Cx43 and Cx47/Cx30 pairs, whereas other pairs are not functional, like the Cx43/Cx32 pair (White and Bruzzone, 1996; Orthmann-

Murphy et al., 2007; Magnotti et al., 2011). Panglial gap junction networks have been shown to be essential for maintenance of myelin in the CNS. Using mice lacking one astrocytic (Cx30) and one oligodendrocytic (Cx47) connexin, a complete loss of functional oligodendrocyte to astrocyte gap junction coupling was observed in the corpus callosum (Tress et al., 2012). Another study has shown that Cx47 expression and phosphorylation in oligodendrocytes is dependent on astrocytic Cx43 expression in astrocytes (May et al., 2013), thus, explaining the similarities observed in mice lacking Cx43/Cx32 or Cx32/Cx47. Biocytin filling of either one astrocyte or oligodendrocyte in the corpus callosum resulted in panglial coupled networks (Maglione et al., 2010; Meyer et al., 2018). In the thalamus, biocytin filling of glial cells showed abundant panglial coupling, with more than 50% of the coupled cells being oligodendrocytes. In contrast, panglial coupling is much less prevalent in other brain regions, e.g. the hippocampus and neocortex (Griemsmann et al., 2015).

1.5 Neuron-glia interactions and metabolism

1.5.1 Tripartite synapse and calcium waves

Astrocytes and neurons are closely interacting. Astrocyte processes are enwrapping neuronal presynaptic and postynaptic terminals at the synapse. This observation led to the concept of the tripartite synapse, which is based on the existence of a bidirectional communication between astrocytes and neurons (Fig. 1.5; Araque et al., 1999; Halassa et al., 2007).

Neurons release neurotransmitters like GABA or glutamate at the synaptic cleft. Specifically, glutamate activates astrocytic G-protein coupled receptors, like mGluR5 in the VB thalamus (Nedergaard et al., 2003; Matthias et al., 2003; Parri et al., 2010). This increases astrocytic intracellular Ca^{2+} concentration, which leads to astrocytic release of gliotransmitters like glutamate, D-serine and ATP (Bezzi et al., 2004; Perea et al., 2009; Henneberger et al., 2010; Navarrete et al., 2012). Moreover, astrocytes can covert glutamate to glutamine through the glutamine synthetase, which can in return be taken up by neurons to resynthesize glutamate and GABA (Parpura et al., 1994; Bergles et al., 1999; Matsui et al., 2005; Allaman et al., 2011; Amaral et al., 2013). This concept, called the glutamate shuttle, was introduced by Van den Berg and Garfinkel in 1971, while glutamine synthetase was first observed in glia by Martinez-Hernandez et al. in 1977.

The glutamate-induced increase of intracellular Ca^{2+} has been shown to propagate as waves within the cytoplasm of one astrocyte to adjacent astrocytes, first in cell cultures and then *in vivo*, in most brain regions and also in human brain tissue (Cornell-Bell et al., 1990; Navarrete et al., 2013). Intracellular Ca^{2+} waves can occur spontaneously (Nimmerjahn et al., 2009) or be evoked (Sun et al., 2013). They involve mGluRs, the activation of the phospholipase C, IP_3 production and subsequent release of Ca^{2+} from the endoplasmic reticulum (Scemes and Giaume, 2006). It has been shown that intercellular Ca^{2+} waves are dependent on Cx channels (Blomstrand et al., 1999; Enkvist and McCarthy, 1992; Scemes and Giaume, 2006; Giaume et al., 2010), *in vivo* (Hoogland et al., 2009) and in pathological conditions (Kuchibhotla et al., 2009). However, whether Ca^{2+} waves propagate through astrocyte gap junction networks, or extracellular signaling pathways through the extracellular release of ATP and activation of P2 receptors at neighboring astrocytes, is still unclear (Nedergaard et al., 2003; Haydon and Carmignoto, 2006; Giaume et al., 2010; Pirttimaki and Parri, 2012). In conclusion, astrocytes can integrate and regulate synaptic information, influence synaptic transmission and plasticity.

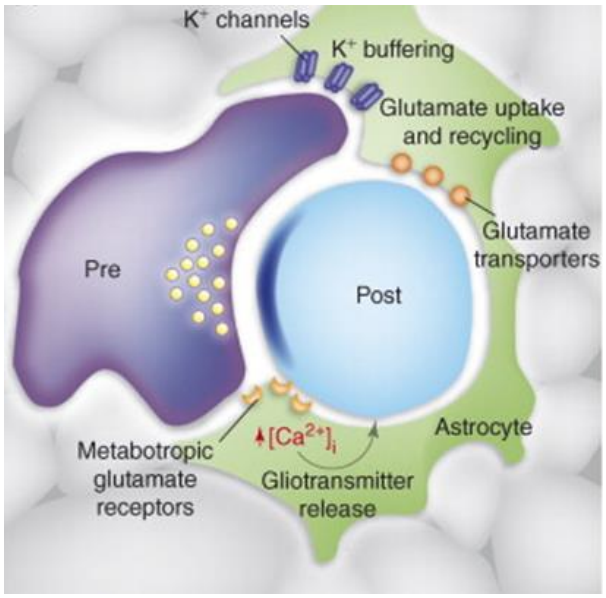

Figure 1.5 Scheme of the tripartite synapse.
Astrocytic processes (green) are in close interaction with the presynaptic (Pre, purple) and postsynaptic (Post, blue) terminals. After neuronal activity, K^+ accumulates and astrocyte processes have an important role in K^+ clearance. Astrocytes are also essential in glutamate uptake from the synaptic cleft. Additionally, neurotransmitter release from neurons activates astrocytic metabotropic receptors, which leads to an increase in astrocytic Ca^{2+} concentration. In a Ca^{2+}-dependent process, they then release gliotransmitters, which then modulate neuronal activity (Halassa et al., 2007).

1.5.2 Astrocytes and neurovascular coupling

In 1886 Camillo Golgi already hypothesized that astrocytes, thanks to their cytological features, would be involved in delivery of energy substrates to neurons and in cerebrovascular regulation (Fig. 1.6; Golgi 1886; Magistretti and Pellerin, 1999; Nedergaard et al., 2003; Iadecola and Nedergaard, 2007). Astrocytes are involved as intermediaries in modulating neurovascular coupling (Magistretti et al., 1994; Attwell et al., 2010). Together with endothelial cells and pericytes, they tightly wrap blood vessels, and although astrocytes do not form the BBB, they contribute to its healthy development (Kacem et al., 1998; Nedergaard et al., 2003; Abbott et al., 2006; Mathiisen et al., 2010). Astrocytes are therefore in the strategic position to take up glucose from the blood using their endfeet, which are particular structures closely apposed to blood vessels (Belanger et al., 2011; Mergenthaler et al., 2013). They do so through the glucose transporter GLUT1, expressed on astrocytes enfeet (Morgello et al., 1995). The specific proteins aquaporin 4 and Cx43 are also strongly express at astrocytic endfeet (Simard et al., 2003). Astrocytes can influence the diameter of capillaries and arterioles, thereby adapting blood flow to neuronal activity (Attwell et al., 2010). As astrocyte endfeet express high levels of Cx, they enhance gap junction communication between astrocytes located close to the blood vessels (Nagy et al., 1999; Rouach et al., 2008). As outlined above, astrocyte gap junction channels participate in the propagation of Ca^{2+} waves *in vivo* and in pathological conditions (Hoogland et al., 2009; Kuchibhotla et al., 2009). Consequently, it was proposed that they might contribute to blood flow modulation by increasing the number of endfeet processes involved in the response, as the regulation and production of vasoactive molecules is Ca^{2+}-dependent (Scemes and Giaume, 2006; Giaume et al., 2010).

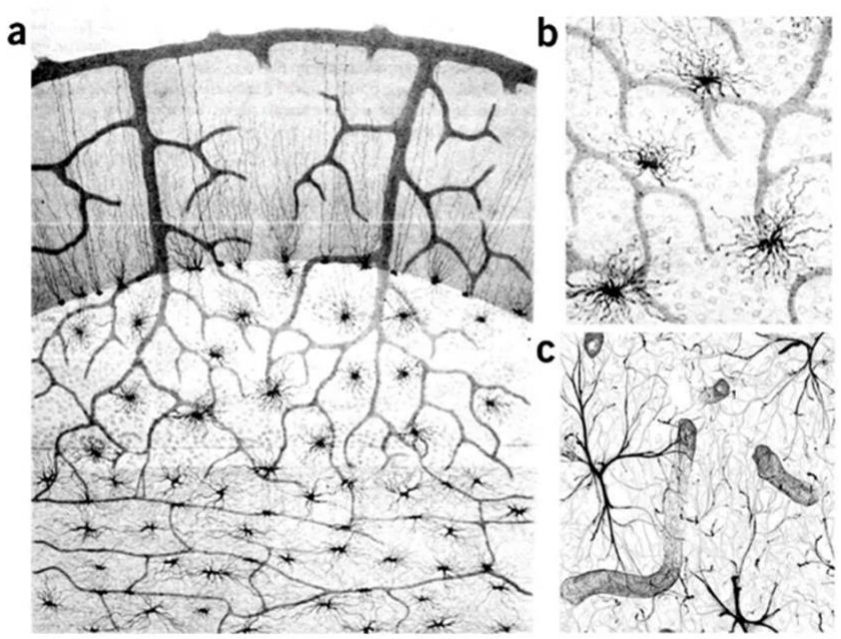

Figure 1.6 Astrocytes and neurovascular interactions.
Astrocyte endfeet are in close contact with blood vessels. (a) Drawing of astrocytes and blood vessels from a human cerebellum, from table XII of Golgi's book. (b) Zoom in of the drawing in a, which emphasizes the close spatial relationship between astrocytes and blood vessels. (c) Confocal image of astrocytes, which were double-labeled with aquaporin 4 and GFAP. It is striking that this picture taken with a confocal microscope is really similar to Golgi's drawings from 100 years earlier. (Golgi, 1886; Iadecola and Nedergaard, 2007).

1.5.3 Astrocyte Neuron Lactate Shuttle hypothesis

Glial cells are now recognized as active players that do not merely react to neuronal activity but also perceive metabolic changes and accordingly support and influence neuronal energy metabolism (Barros et al., 2018). Astrocytes and neurons are preferentially using different metabolic mechanisms. Although different, their metabolic profiles are actually complementary (Belanger et al., 2011). Neurons depend on oxidative metabolism to satisfy their high energy consumption whereas astrocytes rely on aerobic glycolysis and lactate production (Magistretti, 2006; Pellerin, 2003). Studies have shown that astrocytes can take up large amounts of glucose, more than needed for their own metabolism. *In vivo* experiments in rats suggested that half of the glucose uptake in the brain is done by astrocytes, and this uptake quickly accelerates in astrocytes, but not in neurons during intense neuronal activity triggered by whisker stimulation (Chuquet et al., 2010).

Therefore, although neurons express GLUT3 and can also take up glucose from the extracellular space, astrocytes have the highest energy uptake. Findings suggest that astrocytes are a major source of neuronal energy supply. The current hypothesis in the

field of neuron-glia metabolism is called the Astrocyte Neuron Lactate Shuttle (ANLS; Fig. 1.7) hypothesis and was introduced 25 years ago by Pellerin and Magistretti (1994). It has been shown that upon increase in neuronal activity, astrocytes can take part in the clearance of extracellular glutamate around the synaptic cleft of glutamatergic synapses. Glutamate is taken up by excitatory amino acid transporters (EAATs), which in astrocytes are GLUT1 and GLAST. It is cotransported with Na^+, leading to an increase in intracellular Na^+ (three Na^+ are cotransported with one glutamate molecule). The cotransported Na^+ led to the activation of the astrocytic Na^+/K^+-ATPase pump, which in turn promotes glycolysis (Magistretti and Chatton, 2005). This mechanism is associated with an increase in glycolytic flux, resulting in the stimulation of glucose uptake from blood vessels through the GLUT1 transporter located on astrocytes and capillary endothelial cells (Magistretti and Pellerin, 1999; Pellerin and Magistretti, 2012). Through glycolysis, glucose is converted to two molecules of pyruvate, and ATP and NADH are produced. Pyruvate is then transformed into lactate using lactate dehydrogenase 5, located mainly in astrocytes. Once lactate is released to the extracellular space through the monocarboxylate transporter MCT4 in astrocytes, neurons can take it up using the monocarboxylate transporter MCT2. Neurons can then consume lactate as an energy substrate and convert it to pyruvate through the neuron specific lactate dehydrogenase 1 for oxidative ATP production (Pellerin et al., 2007; Belanger et al., 2011). Another consequence of glutamate uptake in astrocytes is its conversion into glutamine through an astrocyte-specific enzyme, glutamine synthetase (Martinez-Hernandez et al., 1977). Glutamine can then be taken up by neurons to be resynthesized into glutamate by glutaminase. Several studies are now supporting the ANLS hypothesis (Pellerin and Magistretti, 2012).

Gap junction networks and energy metabolites trafficking might therefore be crucial in pathological conditions like hypoglycemia or ischemia, to ensure neuronal survival (Giaume et al., 2010). Additionally, during hypoglycemia or ischemia, astrocytes can break down glycogen and produce lactate, which is released to the extracellular space and can be taken up by neurons to fuel their energy needs. Glycogen is the only source of energy reserve in the brain and is almost exclusively localized in astrocytes (Dringen et al., 1993; Magistretti et al., 1993; Brown et al., 2005; Brown and Ransom, 2007; Belanger et al., 2011; Barros, 2013). Astrocytic glycogen breakdown and lactate release to the extracellular space through the ANLS pathway is essential for long-term memory formation and plasticity (Suzuki et al., 2011). Additionally, in the hippocampus,

delivery of glucose or lactate from astrocytes has been demonstrated to be essential to maintain neuronal synaptic transmission during extracellular glucose deprivation. Astrocyte gap junction networks are necessary for this protective effect (Rouach et al., 2008).

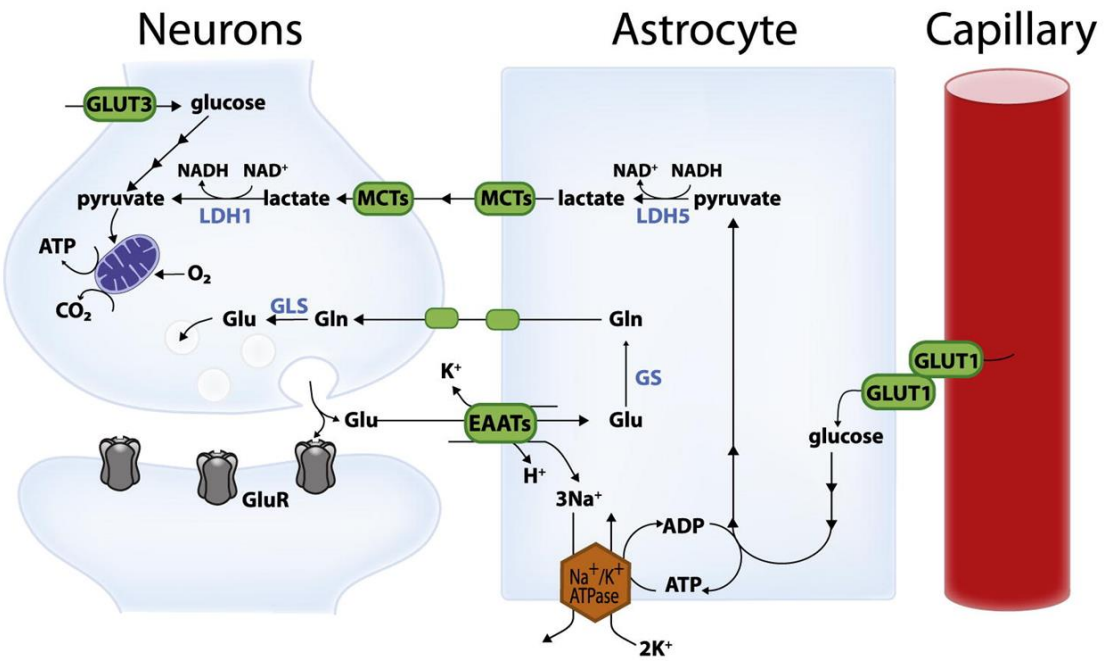

Figure 1.7 Representation of the Astrocyte-Neuron Lactate Shuttle (ANLS)
Glutamate (Glu) is released at the synaptic cleft and can activate glutamatergic receptors (GluR). The majority of the glutamate released at the synapse is taken up by astrocytes through excitatory amino acid transporters (EAATs), mainly GLUT1 and GLAST. Thereby, astrocytes are taking up 3 Na^+ ions and activate the Na^+/K^+-ATPase, consuming ATP. Non oxidative glucose utilization is activated, as well as glucose uptake from the blood vessels via the glucose transporter GLUT1 (located on astrocytes and capillary endothelial cells). Through glycolysis, glucose is converted to two molecules of pyruvate and ATP and NADH are produced. Pyruvate is converted to lactate through lactate dehydrogenase 5 (LDH5; located mainly in astrocytes). Lactate is finally transported to neurons by monocarboxylate transporters (mainly MCT4 on astrocytes and MCT2 in neurons). Lactate can then be used by neurons as an energy substrate after being converted back to pyruvate by LDH1, expressed by neurons. Alternatively, neurons can take up glucose directly via GLUT3. The glutamate-glutamine cycle is also shown. Astrocytes can clear up glutamate from the synaptic cleft to then convert it to glutamine through the glutamine synthetase (GS), which can then be taken up by neurons to resynthesize glutamate by the glutaminase (GLS) (Belanger et al., 2011).

1.5.4 Oligodendrocytes and metabolic support to axons

In white matter, oligodendrocytes have been recently identified as key player in fueling axonal activity. Most studies have been done in the optic nerve (Morrison et al., 2013). In this specific region, oligodendrocytes have been identified as crucial partners in maintaining axonal function by supplying lactate as an energy metabolite (Brown et al.,

2003, 2005). Oligodendrocytes are in close contact with axons as they are enwrapping neuronal axons. The first studies suggesting a role for oligodendrocytes in neuronal metabolic support were done in mice with a specific knockout for myelin proteins, either myelin proteolipid protein (PLP), myelin basic protein (MBP), or myelin-associated enzyme 2',3'-Cyclic-nucleotide 3'-phosphodiesteras (CNP). The loss of those oligodendrocyte proteins leads respectively either to axonal degeneration with intact myelin, to dysmyelination with intact neurons, or to more compact myelin than normal leading to severe axonal degeneration (Griffiths et al., 1998; Klugmann et al., 1997; Loers et al., 2004; Lappe-Siefke et al., 2003). These observations revealed differential effects of myelin in axonal degeneration and action potential propagation. Thus, oligodendrocytes appear as essential partners in neuronal metabolic support (Philips and Rothstein, 2017). Metabolites need to be shuttled from oligodendrocytes to axons and it has been shown that oligodendrocytes are expressing transporters to guarantee that energy metabolites are delivered to axons to meet neuronal metabolic needs (Fig. 1.8). The first two studies available on the metabolic role of oligodendrocytes in the CNS were performed less than a decade ago. Oligodendrocytes were first found to express a transporter for monocarboxylate metabolites (such as lactate, pyruvate or ketone bodies), the monocarboxylate transporter MCT1. MCT1 has been shown to allow the transfer of metabolites to support neurons and a specific inhibition of MCT1 leads to severe axon injury and neuronal death (Lee et al., 2012). Lactate can therefore be shuttled through MCT1 into the periaxonal space, where neurons can take it up via MCT2. Neurons can then convert lactate to pyruvate by lactate dehydrogenase to meet their energy needs (Lee et al., 2012). Another study in white matter has confirmed oligodendrocytes as a source of lactate for neurons through aerobic glycolysis (Fünfschilling et al., 2012). As axons can use lactate during aglycemia (Tekkök et al., 2005), Fünfschilling et al. suggested a physiological function to the axon-oligodendrocyte metabolic coupling model. A recent study by Meyer et al. (2018) in the corpus callosum has shown that networks of coupled oligodendrocytes provide energy to sustain axonal function through delivery of energy metabolites. Grey matter has higher metabolic needs than white matter areas (Amaral et al., 2013). Thus, it is likely that the ANLS mechanism is operative to deliver energy substrates to glutamatergic synapses in grey matter, while the axon-oligodendrocyte signalling assures supplying myelinated axons with energy metabolites (Morrison et al., 2013; Philips and Rothstein, 2017).

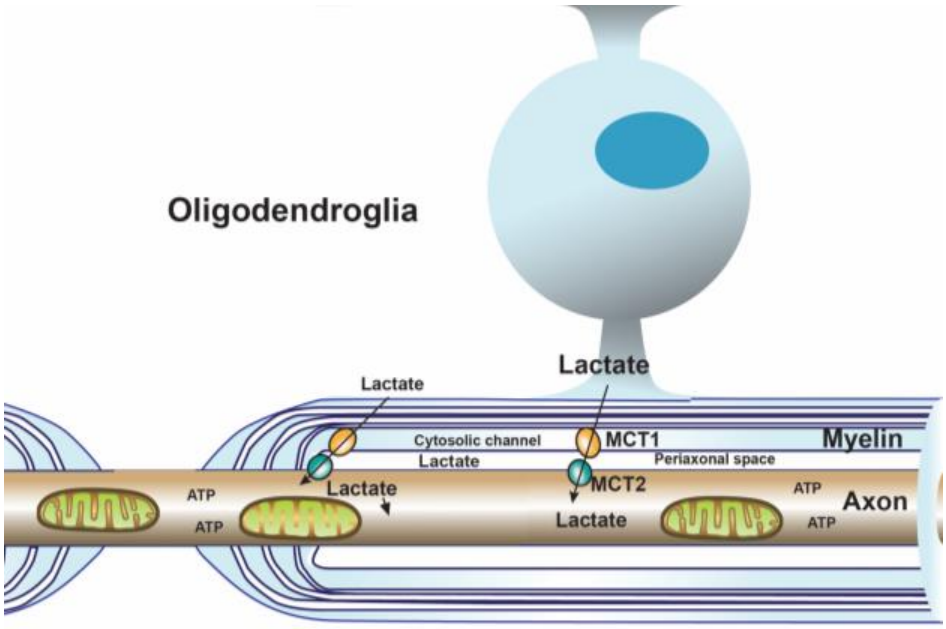

Figure 1.8 Representation of axon-oligodendrocyte metabolic coupling
Lactate is transported from oligodendrocytes to the periaxonal space through the monocarboxylate transporter MCT1. Myelinated axons can then take up lactate from this space through the monocarboxylate transporter MCT2. Axons are then converting lactate to pyruvate by lactate dehydrogenase. Pyruvate is then shuttled into mitochondria for oxidative phosphorylation and production of ATP (Morrison et al., 2013).

2 Aim of the Study

Over the past decades, growing evidence has revealed the importance of glial cells in maintaining physiological brain function by providing proper metabolic energy supply to neighboring neurons. Recent studies demonstrate extensive astrocyte and oligodendrocyte heterogeneity between brain regions. The thalamus has been refereed as the „gateway to consciousness" and plays an essential role in relay and modulation of sensory and motors signals to the cortex. The present study aimed to understand the functional effect of astrocyte-oligodendrocyte coupling and more precisely the role of oligodendrocytes in energy metabolism and neuron-glia signaling in the thalamus. To this end, the two following aspects were investigated in detail.

(i) Analysis of glial network properties in thalamic barreloids.

Astrocytes and oligodendrocytes are connected with each other to form large coupled networks via gap junction channels. In contrast to other brain areas, an abundant astrocyte/oligodendrocyte coupling called panglial coupling has been found in the thalamus (Griemsmann et al., 2015). The ventral posterior nucleus of the thalamus is part of the somatosensory system and contains an area forming whisker-related domains called barreloids (Van Der Loos., 1976). Interestingly thalamic barreloids are mainly formed by oligodendrocytes and have been shown to shape coupled networks (Claus et al., 2018). The first part of the study aimed to analyze the properties of those oligodendrocytes located on barreloid borders and to provide the first structure-function analyses of gap junction networks in thalamic barreloids.

(ii) What is the specific role of oligodendrocytes in neuron-glia signaling and energy metabolism in the thalamus?

As explained, astrocytes and oligodendrocytes express gap junction channels which allow diffusional exchanges of small molecules under 1 kDa like energy metabolites including glucose and lactate (Giaume et al. 2010). Thalamic oligodendrocytes make up for more than 50% of coupled cells (Griemsmann et al., 2015; Claus et al., 2018; Höft et

al., 2014) whereas hippocampal networks are mainly formed by astrocytes (Griemsmann et al., 2015). An intact and extensive astrocytic coupling network has been shown to be essential to sustain synaptic activity in the hippocampus (Rouach et al., 2008), whereas in white matter oligodendrocytes support axonal function by transport of metabolites (Lee et al., 2012; Meyer et al., 2018). The functional impact of astrocyte/oligodendrocyte coupling in grey matter is still unclear. Studying corticothalamic field potential recordings combined with the patch-clamp technique, this part of the study aimed to unravel the functional impact of abundant panglial thalamic networks on energy metabolism. Since oligodendrocytes do not directly contact blood vessels, the panglial network is a possible route of transport for energy metabolites from blood vessels to the oligodendrocytes. This study aimed to investigate whether and through which mechanism oligodendrocytes in the thalamus contribute in the energy delivery to neurons.

3 Materials

3.1 Chemicals

Product	Company
2-NBDG	Thermo Fisher Scientific, Carlsbad, USA
Biocytin	Sigma-Aldrich, Munich, Germany
$CaCl_2.6H_2O$	AppliChem GmbH, Darmstadt, Germany
Carbogen	Linde, Pullach, Germany
EGTA	Sigma-Aldrich, Munich, Germany
Ethanol 99%	AppliChem GmbH, Darmstadt, Germany
Ethanol absolut pa.	AppliChem GmbH, Darmstadt, Germany
Glucose	AppliChem GmbH, Darmstadt, Germany
Glue	Superglue, Uhu, Bühl, Germany
HEPES	AppliChem GmbH, Darmstadt, Germany
Hoechst 33342	Thermo Fisher Scientific, Carlsbad, USA
Isoflurane	Piramal Healthcare, Morpeth, UK
L-Lactate	Sigma-Aldrich, Munich, Germany
$MgSO_4.7H_2O$	AppliChem GmbH, Darmstadt, Germany
KCl	AppliChem GmbH, Darmstadt, Germany
K-Gluconate	AppliChem GmbH, Darmstadt, Germany
KH_2PO_4	AppliChem GmbH, Darmstadt, Germany
KOH	Merck Millipore, Darmstadt, Germany
$MgCl_2$	AppliChem GmbH, Darmstadt, Germany
$MgSO_4$	AppliChem GmbH, Darmstadt, Germany
Na_2-ATP	Sigma-Aldrich, Munich, Germany
NaCl	AppliChem GmbH, Darmstadt, Germany
NaH_2PO_4	AppliChem GmbH, Darmstadt, Germany
$NaHCO_3$	AppliChem GmbH, Darmstadt, Germany
NGS	Merck Millipore, Darmstadt, Germany
Mounting Medium	Aqua-Poly/Mount, Polyscience, Warrington, USA
Paraformaldehyde	AppliChem GmbH, Darmstadt, Germany
Picrotoxin	Abcam, Cambridge, UK
Pyruvate	Sigma-Aldrich, Munich, Germany
Sulforhodamine B	Sigma-Aldrich, Munich, Germany
SR101	Sigma-Aldrich, Munich, Germany
Sucrose	AppliChem GmbH, Darmstadt, Germany
TritonX-100	Sigma-Aldrich, Munich, Germany
TTX	Abcam, Cambridge, UK

3.2 General materials

Materials	Company
Borosilicate glass	Science Products, Hofheim, Germany
Coverslips, object slides	Engelbrecht, Edermünde, Germany
Gloves	Ansell, Staffordshire, UK
Kimtech	Kimberley Clark
Needles and syringes	BD, Franklin Lakes, USA
Parafilm	Pechiney Plastic Packaging, Chicago, USA
Plastic Pasteur pipettes	Carl-Roth, Karlsruhe, Germany
Razor blade	Wilkinson, Bucks, UK
Well plates	Sarstedt, Nümbrecht, Germany
Surgical instruments	Fine Science Tools, Heildeberg, Germany
Syringe filters 4 mm	Thermo Fisher Scientific, Waltham, USA
Tips, tubes	Greiner GmBH, Frickenhausen, Germany
Whatman paper	Whatman International, Maidstone, UK
Bipolar stimulation electrode,WE3ST31.0A10	MicroProbes for Life Science, Gaithersburg, USA

3.3 Software

Software	Company
Igor Pro	Wave Metrics, Portland, USA
ImageJ	NIH, Maryland, USA
LAS AF	Leica Microsystems, Wetzlar, Germany
Matlab	The MathWorks, Natick, USA
MC Stimulus II	Multi Channel Systems, Reutlingen, Germany
Tida	Heka, Lambrecht, Germany

3.4 Equipment

Device	Company
Axiophot	Carl Zeiss, Göttingen, Germany
Centrifuges	Eppendorf, Wesseling, Germany
DMZ Zeitz-Puller	Zeitz, Martinsried, Germany
Eclipse E600FN microscope	Nikon, Tokyo, Japan
DIC camera	Cohu, Poway, USA
EPC-7	Heka, Lambrecht, Germany
EPC-800	Heka, Lambrecht, Germany
Fluorescemt lamp	Leica Microsystems, Wetzlar, Germany
IPC pump	Ismatec, Wertheim, Germany

Leica SP5 LSM	Leica Microsystems, Wetzlar, Germany
Leica SP8 LSM	Leica Microsystems, Wetzlar, Germany
Leica TCS NT confocal	Leica Microsystems, Wetzlar, Germany
LIH 1600	Heka, Lambrecht, Germany
MaiTai	Newport Spectra-Physics, Darmstadt, Germany
Micromanipulator, electric	Luigs und Neumann, Ratingen, Germany
MC Stimulus II	Multi Channel Systems, Reutlingen, Germany
Oscilloscope HM 507	Hameg, Maihausen, Germany
pH meter	Mettler Toledo, Giessen, Germany
DMZ Zeitz-Puller	Zeitz, Martinsried, Germany
STG-2004	Multi Channel Systems, Reutlingen, Germany
Vibration isolation platform LW 3036B-OPT	Newport, Irvine, USA
Vibratome VT1200S	Leica, Nussloch, Germany
Vortexer	VWR, Darmstadt, Germany
Weight balance	Sartorius group, Göttingen, Germany

3.5 Antibodies

Primary Antibodies

Epitope	Species	Type	Dilution	Company
GFP	chicken	polyclonal	1:500	Abcam

Secondary Antibodies

Epitope	Species	Dilution	Company
Anti-chicken-A488	goat	1:500	Invitrogen

Streptavidin Conjugate

Streptavidin-Alexa Fluor 647	1:600	Thermo Fisher Scientific

3.6 Solutions and buffers

3.6.1 Solutions for electrophysiology

Preparation solution

NaH_2PO_4	1.25 mM
NaCl	87 mM
KCl	2.5 mM
$MgCl_2.6H_2O$	7 mM
$CaCl_2.6H_2O$	0.5 mM
Glucose	25 mM
$NaHCO_3$	25 mM
Sucrose	75 mM

And pH 7.4 adjusted with carbogen (95% O_2/5% CO_2)

Artificial cerebrospinal fluid 1 (for barreloids and coupling experiments)

NaH_2PO_4	1.25 mM
NaCl	126 mM
KCl	3 mM
$MgSO_4.7H_2O$	2 mM
$CaCl_2.6H_2O$	2 mM
Glucose	10 mM
$NaHCO_3$	26 mM

And pH 7.4 adjusted with carbogen (95% O_2/ 5% CO_2)

Artificial cerebrospinal fluid 2 (for glucose deprivation experiments)

NaCl	119 mM
KCl	2.5 mM
$CaCl_2.6H_2O$	2.5 mM
$MgSO_4.7H_2O$	1.3 mM
NaH_2PO_4	1 mM
$NaHCO_3$	26.2 mM
Glucose	11 mM

And pH 7.4 adjusted with carbogen (95% O_2/ 5% CO_2)

Intracellular standard solution (for oligodendrocyte patching on barreloid borders and coupling experiments)

K-gluconate	130 mM
$MgCl_2.6H_2O$	2 mM
EGTA	10 mM
Hepes	10 mM
Na_2-ATP	3 mM

pH 7.28

Supplemented with 0.5% biocytin or 0.5% biocytin and 0.1% Texas Red Dextran

Intracellular K-gluconate solution (for glucose diffusion in barreloids experiments)

K-gluconate	105 mM
$MgCl_2.6H_2O$	1 mM
$CaCl_2.6H_2O$	0.5 mM
HEPES	10 mM
EGTA	5 mM
KCl	30 mM
Na_2-ATP	3 mM

pH 7.2
Supplemented with 0.5% biocytin, 0.1% Texas Red Dextran and 14.6 mM 2-NBDG

Intracellular K-gluconate solution (for extracellular glucose deprivation experiments)

K-gluconate	100 mM
$MgCl_2.6H_2O$	1 mM
$CaCl_2.6H_2O$	0.5 mM
HEPES	10 mM
EGTA	5 mM
KCl	30 mM
KOH	20 mM
Na_2-ATP	3 mM
Glucose	20 mM or L-Lactate 40mM

pH 7.2
Supplemented with sulforhodamine B (10 µg/ml)

3.6.2 Solutions and buffers for immunohistochemistry

Phosphate buffered saline (PBS 10x)

NaCl	1.5 mM
Na_2HPO_4	83 mM
NaH_2PO_4	17 mM

Dissolved in dH_2O, pH 7.4

Paraformaldehyde solution
Paraformaldehyde 4% (w/v) dissolved in PBS and dH_2O, pH 7.4

Blocking solution

NGS	10% (v/v)
TritonX-100	0.5-2% (v/v)

Diluted in PBS, pH 7.4

1st antibody solution

NGS	2-5% (v/v)
TritonX-100	0.5-2% (v/v)

Diluted in PBS, pH 7.4

2nd antibody solution

NGS	2-5% (v/v)
TritonX-100	0.1% (v/v)

Diluted in PBS, pH 7.4

Hoechst nuclei staining solution

Hoechst	1% (v/v)

Diluted in dH_2O

3.7 Animals

Mice used in this study were kept under standard housing conditions with 12h/12h dark-light cycle, food and water ad libitum. All experiments were carried out in accordance with local state and European regulations. All measures were designed to minimize the number of animals used.

3.7.1 C57BL/6J mice

This inbred strain C57BL was developed by C.C Little (Founder of The Jackson Laboratory) in 1921 at the Bussey Institue for Research in Applied Scielnce. C57BL/6J was isolated in 1937 and maintained in Jackson Laboratories. They are one of the oldest and most widely used strains in research (Bryant et al., 2008). Wild-type mice C57BL/6J of either sex, aged between postnal days p14-17 were purchased from Charles River and used to perform barreloid experiments.

3.7.2 hGFAP-EGFP mice

In this transgenic mouse line, astrocytes are labelled with the enhanced green fluorescent protein (EGFP), which is expressed under the control of the human glial fibrillary protein (hGFAP) promoter. This mouse line has an FVB/N background and was generated by micro-injecting oocytes with a plasmid construct of 2.2kb DNA fragment of the hGFAP promoter (Nolte et al., 2001). In this mouse line, in all regions of the CNS such as the hippocampus, cortex or corpus callosum, EGFP-positive cells with morphological properties of astrocytes are labeled (Nolte et al., 2001). Moreover, EGFP expression was also revealed in NG2 cells (Wallraff et al., 2004). In many regions, a good overlap of GFAP and EGFP-positive cells was observed. However, in the thalamus GFAP immunoreactivity is only weak, despite a strong EGFP expression

(Nolte et al., 2001; Frassoni at al., 2000). Animals aged p28-40 were used to perform our glucose experiments.

3.7.3 PLP-GFP mice

In the PLP-GFP mouse line with a C57BL/6J background, mature oligodendrocytes can easily be visualized in live and fixed tissue. The green fluorescent protein is expressed under the control of a PLP promoter (Fuss et al., 2000). The proteolipid protein is the major protein component of CNS myelin and has been shown to be expressed specifically in differentiating and myelinating oligodendrocytes. Indeed, immunocytochemical studies of GFP fluorescence confirmed that GFP expression in this mouse line is restricted to terminally differentiated oligodendrocytes (Fuss et al., 2000). Additionally, GFP fluorescence is limited to cell somata and nuclei (Fuss et al., 2000).

3.7.4 Cx32/Cx47 dko mice

The Cx47-null mouse line was generated by replacing the Cx47 (Gjc2) coding DNA with an enhanced green fluorescent protein (EGFP) reporter gene. This reporter is under the control of the endogenous Cx47 promoter (Odermatt et al., 2003). Homozygous mutant mice are fertile and show sporadic vacuolation of nerve fibers but no obvious morphological or behavioral abnormalities (Odermatt et al., 2003). The Cx32 deficient mice have a constitutive deletion of Cx32 (Gjb1) (Nelles et al., 1996). The Cx32 gene is located on the X chromosome. $Cx47^{EGFP(-/-)}$ male mice were intercrossed with $Cx32^{-/-}$ female mice and the F1 generation was intercrossed again to obtain Cx32/Cx47 (dko) mice (Odermatt et al., 2003). Mice lacking both Cx47 and Cx32 die by postnatal week 5 to 10 and develop severe abnormalities such as thin or absent myelin sheaths, vacuolation, enlarged periaxonal collars, oligodendrocyte cell death, axonal loss, tonic seizures and sporadic convulsions (Menichella et al., 2003; Odermatt et al., 2003). The Cx47 and Cx32 genotypes were tested by tail-tipPCR by PD Dr. Gerald Seifert and Thomas Erdmann.

4 Methods

4.1 Electrophysiology

4.1.1 Preparation of acute brain slices

Acute brain slices were prepared from p14-17 days old mice for visualization of thalamic barreloids or from p28-40 days old mice for field potential recordings. Animals were anaesthetized with isoflurane and decapitated. The brain was quickly removed, put into ice-cold slicing solution, and a cut was made along the midline. The midline of each hemisphere was laid on a plastic homemade block with a 30° angle and a small piece of the dorsal part of the brain was cut off. For field potential recording, the hemispheres were glued dorsally on a specimen holder and 300 µm thick slices were made. To visualize thalamic barreloids in acute brain slices, the cutting plane was additionally tilted up 5° anteriorly from the horizontal plane and 200 µm thick slices were made (Claus et al., 2018).

The brains were placed in ice-cold preparation solution constantly bubbled with carbogen (95% O_2/ 5% CO_2) and cut with a vibrotome (VT1200S) at a speed of 0.12 mm/s and an amplitude of 1.2 mm. Horizontal slices containing the thalamic ventrobasal nuclei were obtained. Slices were allowed recovering in a sucrose solution constantly bubbled with carbogen at 35°C for 20 min. Sections were then transferred into bubbled ACSF and cooled down to room temperature. Slices were kept resting before use for at least 20 min for tracer filling experiments or 1 h for field potential recording. In some experiments, prior to transfer into ACSF at room temperature, slices were stained with 1 µM sulforhodamine 101 (SR101) supplemented ACSF at 35°C for 20 min.

4.1.2 Electrophysiological set up

The tracer diffusion experiments were performed in a recording chamber of an electrophysiological setup. The microscope was located in a Faraday cage to reduce electrical noise and placed on a vibration isolated board (Newport) to guarantee stable

recording conditions. A slice was placed in the chamber and held in place under a U-shaped platinum wire where nylon strings were glued. Brains sections were perfused continuously with carbogenized ACSF at room temperature by a peristaltic pump at 1-2 ml/min. Patch-clamp pipettes were pulled from borosilicate glass by a horizontal puller and had a resistance of 3-6 MΩ when filled with internal solution (see chapter 3.6.1). A Teflon-coated silver wire with a chlorinated tip was connected to the preamplifier to record electrical signals. The reference electrode, also connected with the head stage of the preamplifier, was made of a silver/silver chloride pellet. The patch pipette was controlled by an electrically-driven micromanipulator. To visualize the tissue, slices were transferred to a Leica TCS SP5 confocal microscope equipped with a Leica HCX APO L 20x 1.0 water immersion objective and differential interference contrast (DIC) optics were used. The LAS AF software was required to perform the experiments (see chapter 4.3.4 for detailed list of equipment). To identify astrocytes or oligodendrocytes, fluorescence was emitted after applying light of the respective wavelength. An EPC-7 or EPC-800 patch clamp amplifier was used to record currents in voltage clamp mode. Currents were monitored by the TIDA software (Heka). Data were filtered at 3-10 kHz and sampled at 6-30 kHz.

4.1.3 Whole-cell patch-clamp recording

The patch-clamp technique was first introduced by Erwin Neher and Bert Sakmann (Neher and Sakmann, 1976). This technique allows for electricals recordings and characterization of single ion channels. Astrocyte and oligodendrocytes were identified either by their endogenous fluorescence and morphologies. In some experiments, SR101 was used to mark astrocytes (Nimmerjahn et al., 2004; Kafitz et al., 2008). All cells were analyzed in the whole-cell voltage clamp mode. Briefly, a patch pipette was filled with internal solution and placed above the slice. The cell was then approached while using overpressure to keep the tip of the pipette clean of potential tissue debris. Once the cell was reached, the overpressure was released and low pressure was applied to establish a close contact between the pipette tip and the cell membrane. This is called the “cell-attached” mode and it is characterized by a high resistance above 1 GΩ, known as a “Gigaseal”. During this process, the cell was continuously clamped at -80 mV. Next, to disrupt the cell membrane, short pulses of negative pressure were applied in order to get in the whole-cell configuration.

Currents were recorded in the whole cell mode. In this mode, the amplifier compares the command potential of our patched cell to the actual resting membrane potential. If the resting membrane potential differs from the test potential, small currents are injected into the cell to keep it at the test potential. Analysis of input and series resistance (R_s) was determined every 10 min by applying 10 repetitive steps of 10 mV over 50 ms (ΔV = 10 mV). Analysis was done with the Igor Pro tool written by PD Dr. Ronald Jabs (average of 10 traces). R_s was calculated from the current at the beginning of the recordings $I(t_0)$, according to the Ohm's law $Rs=\Delta V/I(t_0)$. Recordings with R_s > 20 MΩ were discarded. The membrane resistance (R_m) was determined from the constant current after the decline of the capacitive current $I(t_1)$ and calculated based on the equation $R_m==\Delta U/I(t_1)-R_s$ (Fig. 4.1A). Recordings with Rm > 10 MΩ were discarded.

To characterize the membrane parameters, de- and hyperpolarization steps of 10 mV from +20 mV to -160 mV were applied, starting from the holding potential at -80 mV, as shown in Fig. 4.1B. Cells with a resting potential above -60 mV were discarded.

All intracellular solutions were based on K-gluconate, causing a liquid junction potential which was compensated accordingly online during the measurement by adjusting the holding potential. For biocytin experiments, after 20 min of filling, slices were fixed in 4% PFA overnight at 4°C and stored the next day in PBS at 4°C until used for immunohistochemistry.

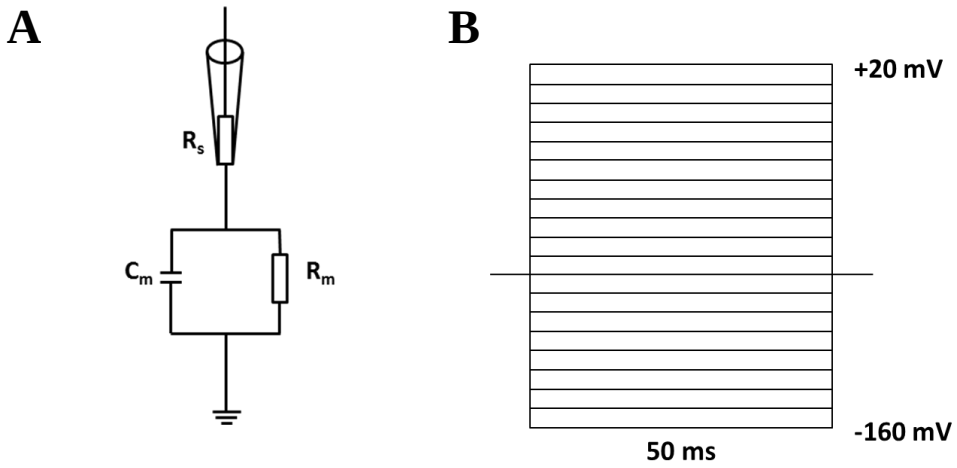

Figure 4.1 Electrical circuit and analysis of the whole-cell patch clamp configuration.
(A) Equivalent circuit of the whole cell mode. Series resistance (Rs) originates at the transition between the pipette and the cell cytoplasm. R_s is in series with the membrane capacitance (C_m) and the membrane resistance (R_m) of the cell. R_m depends on the membrane properties whereas C_m is generated by the lipid bilayer. (B) To record the electrophysiological properties of the patched cell, 10 mV pulses were applied for 50 ms each, every 10 min.

4.1.4 Recording of thalamic field potentials and data analysis

Slices containing the VB thalamus were prepared and transferred to a recording chamber. To stimulate the cortico-thalamic (CT) pathway, a bipolar stimulation electrode was placed in the internal capsule (Fig. 4.2 A). Electrical stimulation was achieved with a computer-controlled constant current isolated stimulator (STG2004). The bipolar stimulation electrode (WE3ST31.0A10) had an outer diameter of 0.61 mm, a tip separation of 250 µm and an impedance of 1.0 MΩ. A field recording electrode, made from borosilicate glass capillaries with an outside diameter of 2 mm and a resistance of 3-6 MΩ, was located in the VB thalamus and field potentials were recorded with a recording pipette connected to a bridge amplifier SEC05-LX. Both electrodes were separated by about 700 µm. (Fig 4.2 B). The depth of the recording electrode was adjusted in the tissue to evoke maximal responses.

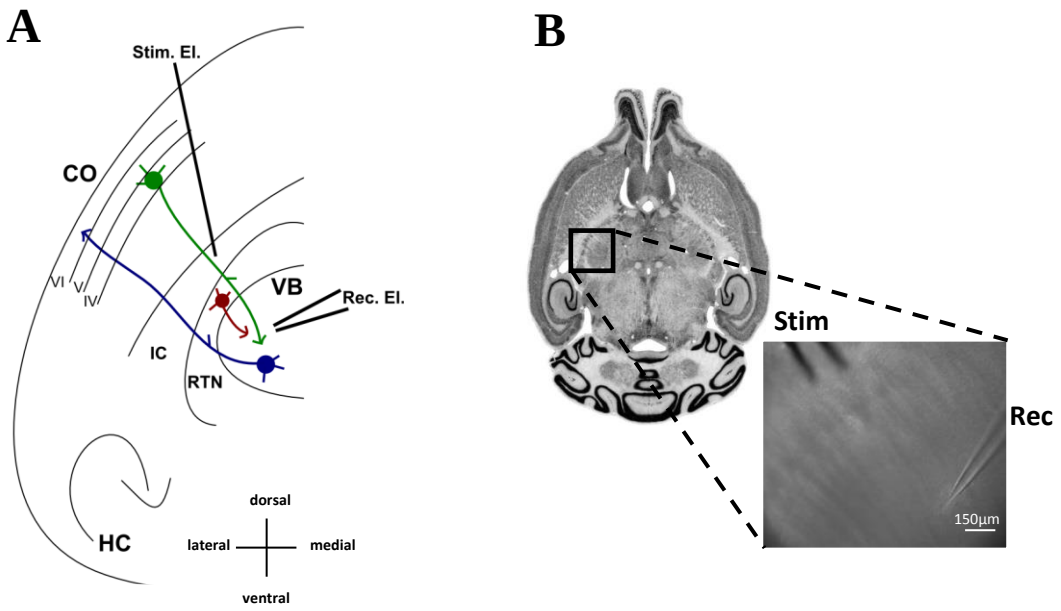

Figure 4.2 Recording of field potentials in the thalamus.
(A) Scheme of a coronal slice, obtained after a cut at a 30° angle from the horizontal plane. The plane contains the cortex (CO), the internal capsule (IC), the reticular thalamic nucleus (RTN), the ventrobasal thalamus (VB) and the hippocampus (HC). The orientation is indicated at the bottom by a cross. The cortico-thalamic pathway is displayed with a green neuron whereas the thalamocortical pathway is shown in blue. Additionally, GABAergic neurons of the RTN are presented in brown. From Stephanie Griemsmann, thesis (2015) and modified from Grant et al. (2012). (B) Example of a thalamic brain slice used for electrophysiology. In the inset, the stimulation electrode (Stim) and the recording electrode (Rec) are displayed.

Field potentials were recorded by applying trains of stimuli (duration 100 µs, 5 stimuli at 20 Hz, from 50 µA to 200 µA, every 15 s) in the presence of picrotoxin (100 µM) to block GABAregic neurons present in the reticular thalamic nucleus (RTN). Ten traces were averaged and used for the analysis, therefore giving one data point every 150 s. To ensure stable responses over time (> 1 h) without inducing LTP or LTD, the stimulation intensity was set to 80% of the maximal peak amplitude. The response after the third stimulus was later analyzed in all experiments (FIG. 4.3 A-B).

Stephanie Griemsmann established a protocol in our lab to analyze field potentials. fPSPs were isolated by subtracting responses evoked in the presence of either picrotoxin, D-2-amino-5-phosphonopentanoate (D-AP5) to blocked NMDA receptors and 2,3-dihydroxy-6-nitro-7-sulfamoyl-benzo[f]quinoxaline-2,3-dione (NBQX) to block AMPA/KA, from responses recorded in normal ACSF (Fig. 4.3C-D). At the end of each experiments, thalamic field potentials were completely blocked by adding the Na^+ channel blocker tetrodotoxin (TTX) (0.5 µM) tot the bath solution (Fig. 4.3D, bottom).

Data analysis was achieved using a custom made Igor Pro tool written by PD Dr. Ronald Jabs. Recordings were averaged (10 traces). A TTX protocol was recorded at the end of each experiment, and was then subtracted from the corresponding experiment recording before analysis, to remove stimulation artefacts. Three measuring points were manually positioned (grey circles in Fig. 4. 3E). The first one represents the highest amplitude after the second peak, the second one was placed just before the descending slope went back to baseline level. Those two points defined a slope that was extrapolated (dotted blue line in Fig. 4.3E). A third point was placed at the minimum level of the second peak. Thus, fPSP amplitudes were calculated as the distance between the second peak of the field potential and the intersection of the extrapolated slope (dotted blue line in Fig. 4. 3E).

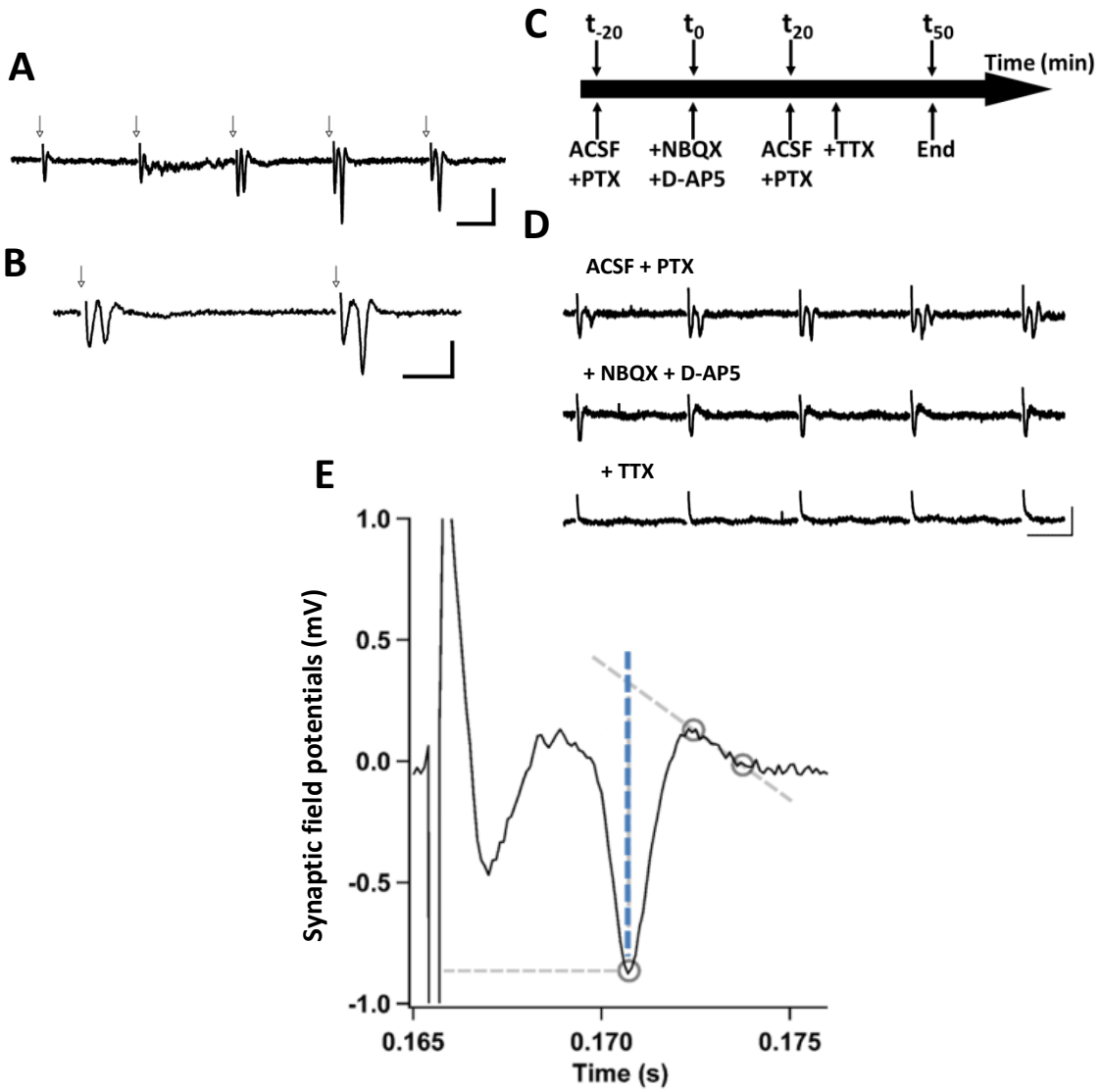

Figure 4.3 Analysis of field potentials in the thalamus.
(A) Average of 10 recording in which every 15 s, stimulation trains of 5 pulses (black arrows) were applied. The synaptic field potentials increased over the 5 stimuli. (B) Enlargement of the third and fourth response displayed in (A). Scale bar, 10 ms, 0.5 mV. (C) Time line of the recording protocol used to isolated fPSPs via application of blockers. (D) Synaptic field potentials were sensitive to blockers of glutamate receptors. The upper trace was recorded in the presence of ACSF supplemented with picrotoxin. D-AP5 and NBQX were added to the bath solution in the second recording, were post synaptic activity is inhibited. Finally, the bottom trace was recorded after TTX application which blocks action potentials. (E) Example of fPSP analysis with a custom made Igor Pro tool. Three measuring points (grey circles) were positioned manually and the amplitude of the fPSPs was measure (blue dotted line). Modified from Stephanie Griemsmann, thesis (2015).

4.2 Confocal and 2-photon microscopy

For glucose diffusion experiments in thalamic barreloids, the glucose analogue 2-NBDG (2-(N-(7-Nitrobenz-2-oxa-1,3-diazol-4-yl)Amino)-2-Deoxyglucose) was applied. Using a Leica SP5 laser scanning microscope, we could image the spread of 2-NBDG between two barreloid borders, after filling an SR101+ astrocyte. Taking advantage of a pulsed infrared laser, we could separate the 2-NBDG fluorescence from the GFP signal of the PLP-GFP mice. 2 photon imaging was realized by excitation of the fluorophores with femtosecond pulses of infrared light at a repetition rate of 80 MHz. Imaging was done with a MaiTai femtosecond laser (Spectra Physics). Excitation wavelength and laser power were adjusted to 710 nm and 1.15 W for optimized signal-to-noise ratio of the GFP/SR101 signals. The emitted light of GFP/SR101 was separated with an FITC-TRITC filter cube. Spatial resolution was of 1024x1024x30-70 pixels. The spread of 2-NBDG was captured online 20 min after patching an astrocyte and the quantification of the number of coupled cells was analyzed offline with Fiji software. The 2-NBDG signal was isolated at 465-540 nm using the 2-photon laser. Continuous wave laser signals (SR101 and PLP-GFP; also GFAP-EGFP in some experiments) were detected with photomultiplier tubes (PMTs). The 2-photon signal (2-NBDG) was acquired with a non-descanned detector (NDD).

$SR101^+$ cells were imaged at 586/605 nm (absorption and emission), PLP-GFP^+ cells at 488/509 nm using conventional continuous wave lasers (Leica SP5, Argon 488 nm and HeNe 543 nm).

4.3 Immunohistochemistry

4.3.1 Immunofluorescence staining

After patch-clamp experiments, each 200 µm thick slice was fixed overnight using a 24-well plate containing 4% PFA. Each slice could float freely during the staining procedure. Slices were first incubated for 4 h at room temperature (RT), in a blocking solution (PBS containing 0.5-2% TritonX-100 and 10% normal goat serum (NGS)). This step intended to prevent unspecific binding of antibodies. Slices were incubated with the first antibodies, diluted in PBS containing 0.1%TritonX-100 and 2% NGS, and stored overnight at 4°C on a shaker. The following day, each slice was washed 3 times for 10 min in PBS and subsequently incubated with a solution containing the secondary

antibodies for 2 h at RT on a shaker. A second washing step of 3 times 10 min each was performed. A nucleus staining was then applied; slices were incubated with Hoechst (1:100 in dH_2O) for 10 min at RT. After a final washing step, slices were mounted on object slides with Aqua-Poly/Mount and lastly covered with cover slips. We allowed slices to rest at 4°C overnight for optimal final fixation before confocal imaging.

4.3.2 Microscopy of fixed slices

Images of our immunofluorescence stainings were acquired at a 1 µm interval with a confocal laser scanning microscope, Leica SP8. A resolution of 1024x1024 pixels and a scan speed during acquisition of 400 Hz were chosen. Hybrid detectors were used to detect all stainings with the exception of Hoechst, were a photo-multiplier tube was sufficient for detection. Depending on the samples, 20x or 40x immersion objectives were used to visualize tracer filled networks.

4.3.3 Data analysis

Images were analyzed using Fiji software. Panglial networks were analyzed by counting manually all biocytin filled cells using the plugin Cell-Counter created in Fiji by Kurt De Vos (URL https://imagej.nih.gov/ij/plugins/cell-counter.html).

4.4 Statistics

All statistical analyses were done with Excel (Microsoft Excel 2010, US) and the software R (R Development Core Team, URL http://www.R-project.org). Data are given as mean ± standard error of the mean (SEM); n refers to the number of brains slices investigated and N to the number of animals. Normality was tested using the Shapiro-Wilk test. Data were tested with Student's t-test or analysis of variance (ANOVA) followed by Tukey's post-hoc test. For non-normal distributions, the non-parametric Kruskal-Wallis test followed by Dunn´s test was used. Differences were regarded as significant at $*p < 0.05$, $**p < 0.01$.

5 Results

5.1 Thalamic barreloids

The ventrobasal nucleus of the thalamus containing the VPL and VPM plays an essential role in relay and modulation of information to the cortex (Shermann and Guillery, 2002). The VPM is part of the somatosensory system and contains elongated cellular domains called barreloids. Those domains offer a basic structure for the representation of vibrissae (Van Der Loos, 1976). In the first part of the present study, patch-clamp recordings and immunohistochemistry were combined to further study functional properties of glial cells in thalamic barreloids and their impact on neuron signaling.

5.1.1 Properties of oligodendrocytes localized on barreloid borders

The shape of panglial networks in the VPM of the thalamus has been shown to follow the barreloid structure. Interestingly oligodendrocytes were preferentially located along the borders (Claus et al., 2018). This observation led to the question whether those oligodendrocytes were part of the panglial network. Taking advantage of PLP-GFP mice in which oligodendrocytes are labeled by the green fluorescent protein (Fuss et al., 2000), a single oligodendrocyte located on the border was identified and patched. All patched cells were electrophysiologically characterized and displayed typical current patterns during the voltage steps and large symmetrical tail currents (Berger et al., 1991). Initial cells were filled during 20 min using a pipette solution supplemented with biocytin and Texas Red Dextran. Biocytin is small enough to efficiently diffuse through gap junction networks (Rouach at el., 2008) while Texas Red Dextran is bigger and consequently restricted to the initial cell. Tracer diffusion through glial networks was analyzed and network sizes were evaluated. Out of 8 filled oligodendrocytes, 2 were totally uncoupled (2 slices from 2 mice) (Fig. 5.1). Additionally, a significantly reduced spread of biocytin in glial networks (39.8 ± 4.8 cells, with 51.5% of oligodendrocytes,

and 48.5% of astrocytes) was found in the other 6 slices (6 slices from 6 mice). Those results can be compared with filling an oligodendrocyte outside the barreloid area (86 ± 13.9 cells, with 66.5 ± 8% of oligodendrocytes, see Griemsmann et al., 2015). Interestingly, as described by Claus et al. (2018) after filling an astrocyte, many PLP-GFP positive cells located within the biocytin-filled networks were actually not biocytin-positive (39%, i.e., 13.3 ± 2.2 out of 33.7 ± 3.8 cells). In conclusion, oligodendrocytes located on barreloid borders show no or low coupling.

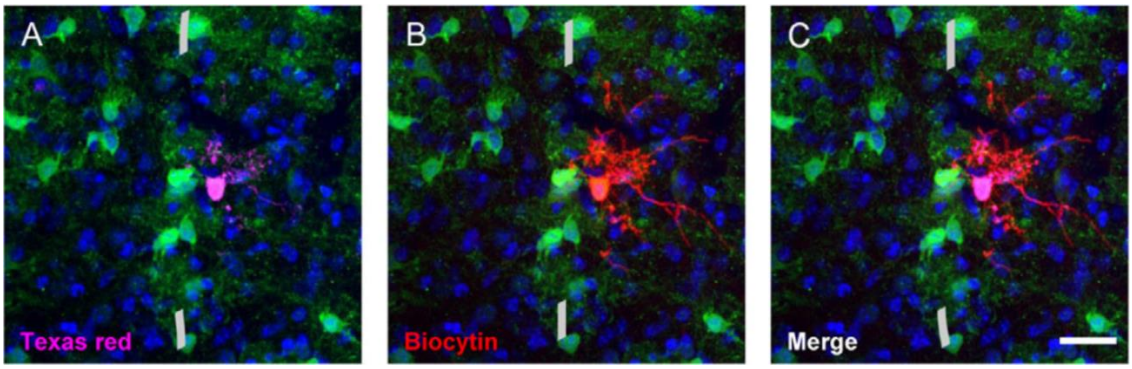

Figure 5.1 Tracer diffusion in oligodendrocytes located on barreloid borders show no or low coupling.
Brain slices of p14-17 PLP-GFP mice were prepared to obtain slices containing thalamic barreloids. (A) One oligodendrocyte positioned on a barreloid border (indicated by a grey line) was recognized thanks to its intrinsic GFP fluorescence (green) and therefore patch-clamped for 20 min with a solution containing Texas Red Dextran (pink). (B) Biocytin (red) was added to observe coupled networks. This example shows that the biocytin signal colocalizes with the Texas Red Dextran signal (merge). Thus, this oligodendrocyte is not coupled to any other cell. The image shows that the initial patch cell is slightly shifted to the right side of the border. Originally this patched oligodendrocyte was located on the border. It was shifted due to a technical issue inherent to the patch technique when removing the pipette after the experiment. Scale bar 25 µm. See also Claus et al. (2018).

5.1.2 Functional impact of neuronal activity on glial coupling in thalamic barreloids

In other brain areas, like the hippocampus and the olfactory bulb, astrocyte coupling is controlled by and needed for neuronal activity (Rouach et al., 2008, Roux et al., 2011). Thus, the question next addressed was whether astrocyte/oligodendrocyte coupling in thalamic barreloids is controlled by neuronal activity. Brain slices from p14-p17 C57BL/6J mice were used. Thalamic slices were incubated for 3-4 h with TTX (0.5 µM) and ω-conotoxin GVIA (0.5 µM) to block voltage–gated Na^+ channels and N-type Ca^{2+} channels. Individual astrocytes were filled with a patch pipette containing Texas Red Dextran, biocytin and the fluorescent metabolizable glucose analog, 2-NBDG. Astrocytes were identified by the efficient, specific but non-fixable red fluorescent dye sulforhodamine 101 (SR101) labeling after incubating the tissue before recording (Nimmerjahn et al., 2004; Kafitz et al., 2008). In the thalamus, it has been shown that only a few, weakly $SR101^+$ cells were also GFP^+ in PLP-GFP mice which were not visible using conventional epifluorescence microscopy (Griemsmann et al., 2015). Thus, SR101 is a reliable marker to identify astrocytes in the thalamus. Additionally, this dye has been described to affect neuronal activity in the hippocampus (Kang et al., 2010) but later on has been proven to have no influence on coupled network sizes (Griemsmann et al., 2015). The same time of incubation, either with blockers or in ACSF without blockers, was applied. Tracer diffusion through glial networks and network sizes was quantified (Fig. 5.2). 2-NBDG analysis was done online. 2-NBDG spread into 50.3 ± 1.7 cells (5 slices from 4 mice) under control condition whereas the spread was significantly reduced to 26.6 ± 1.0 cells after inhibition of neuronal activity by TTX and ω-conotoxin GVIA (5 slices from 4 mice).

Using the same technique as described by Claus et al., 2018, the shape of the coupled network after neuronal inhibition was analyzed. A spherical shape of the coupling was observed with 2-NBDG (y/x-ratio 0.96 ± 0.02, see also Claus et al. 2018). Immunohistochemistry was performed after fixation of the tissue and biocytin filled cells were visualized. Under control condition biocytin spread into 88.2 ± 4.6 cells (5 slices from 4 mice). Number of biocytin filled cells after neuronal inhibition was significantly lower (54.1 ± 3.5 cells, 5 slices from 4 mice). As observed with 2-NBDG, biocytin spread was also spherical (y/x-ratio 0.99 ± 0.06). Furthermore, as the 2-NBDG spread analysis was done online, it was possible to test whether there were also

uncoupled astrocytes within the volume covered by the dye spread. The strong fluorescence intensity of the 2-NBDG-filled patch pipette, covering part of the region of interest, hampered steady online analysis of the whole panglial coupled network. Nonetheless, several uncoupled astrocytes, i.e. 2-NBDG-negative/SR101-positive cells, were observed. Beside the region covered by the pipette fluorescence, those cells added up to about 40% of the SR101-positive astrocytes in this area, both control conditions and after incubation with TTX and ω-conotoxin GVIA (5 slices from 4 mice, see also Claus et al., 2018). Taken together, these results indicate that within the barreloids numerous astrocytes and oligodendrocytes were not part of the coupling network. Furthermore, those observations confirm that, as shown previously in other brains areas for astrocytic networks, modulation of neuronal activity can disturb 2-NBDG and biocytin diffusion, i.e. panglial coupling in thalamic barreloids.

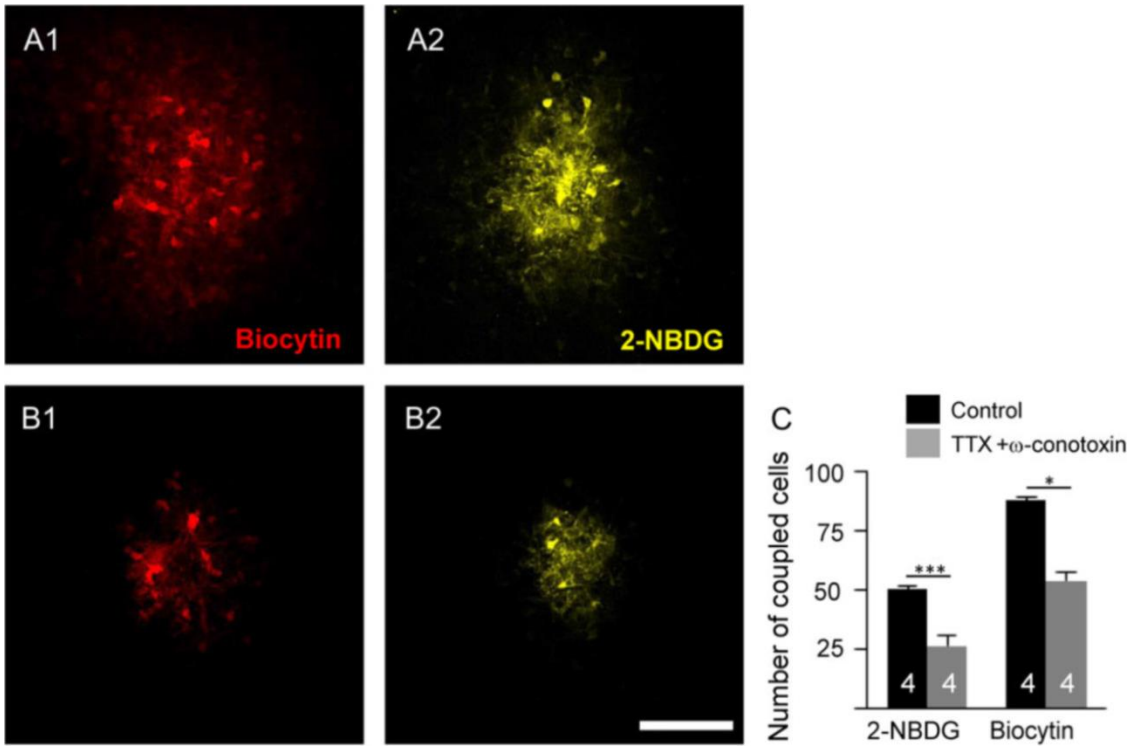

Figure 5.2 Inhibition of neuronal activity modulates panglial coupling in thalamic barreloids.
Thalamic slices containing barreloids were obtained from young C57BL/6J mice. SR101 was used to identify astrocytes. One individual astrocyte was patched and filled for 20 min with Texas Red Dextran, biocytin (A1, B1 red) and the glucose analog 2-NBDG (A2, B2 yellow). Those experiments were done under control conditions (A1, A2) or after preincubation of the slices with TTX (0.5 µM) and ω-conotoxin GVIA (0.5 µM) for 3–4 h. Scale bar, 100 µm. (C) Quantification of the spread of 2-NBDG and biocytin after inhibition of neuronal activity. Number of coupled cells was significantly reduced (grey bars, 5 slices from 4 mice) after incubation with blockers compared to control experiments (black bars, 5 slices from 4 mice). Number of mice is given in bar graphs. Student's t-test, $p = 0.0047$ and $p = 0.013$ for 2-NBDG and biocytin respectively.

5.2 Effect of extracellular glucose deprivation on post synaptic field potentials in the thalamus

The first part of the present study revealed how neuronal activity shapes panglial coupling in thalamic barreloids. The next experiments aimed at finding a reliable protocol to analyze changes in synaptic activity in the thalamus.

5.2.2 Analyses at physiological temperature

To study neuronal networks in the thalamus the cortico-thalamic pathway was stimulated. To investigate neuronal activity and the role of oligodendrocytes in the thalamus, extracellular glucose deprivation (EGD) was used in the following experiments as previously described in the corpus callosum, the optic nerve or the hippocampus (Meyer al et., 2018; Wender et al., 2000; Brown et al., 2001; Rouach et al., 2008).

Acute thalamic slices were placed in a bath chamber with continuously gassed (95% O_2, 5% CO_2) ACSF containing 11 mM glucose. Next, the corticothalamic pathway was stimulated and synaptic activity was monitored with a field electrode (as described in chapter 4.1.4). Stable field potentials were recorded for over 40 min (Fig. 5.3 A, black line). Synaptic activity was reduced by applying EGD (Fig. 5.3, gluc-).

fPSPs were isolated and quantified (as described in chapter 4.1.4). After a 10 min control baseline recording, EGD was induced by applying ASCF without glucose (gluc-) and subsequently changing back to ACSF containing glucose (Fig. 5.3 A,B). Following 5 min (purple line) or 10 min (red line) of EGD, a total drop of the fPSPs to 0 was observed (Fig. 5.3 A). More importantly, in almost all recordings, no recovery of the synaptic activity was observed after reperfusion with ACSF containing glucose. Therefore, experiments with only 2.5 min of EGD were performed (Fig. 5.3 B). Here, no decline in fPSPs was observed in 5 experiments out of 8 (blue lines). In the other 3 (red lines), only 1 showed a recovery above 80% of the control value.

In summary, even if doing experiments at 35°C is more physiological, the following experiments were done at room temperature to have a reliable model to study the effect of glucose deprivation on synaptic activity in the thalamus.

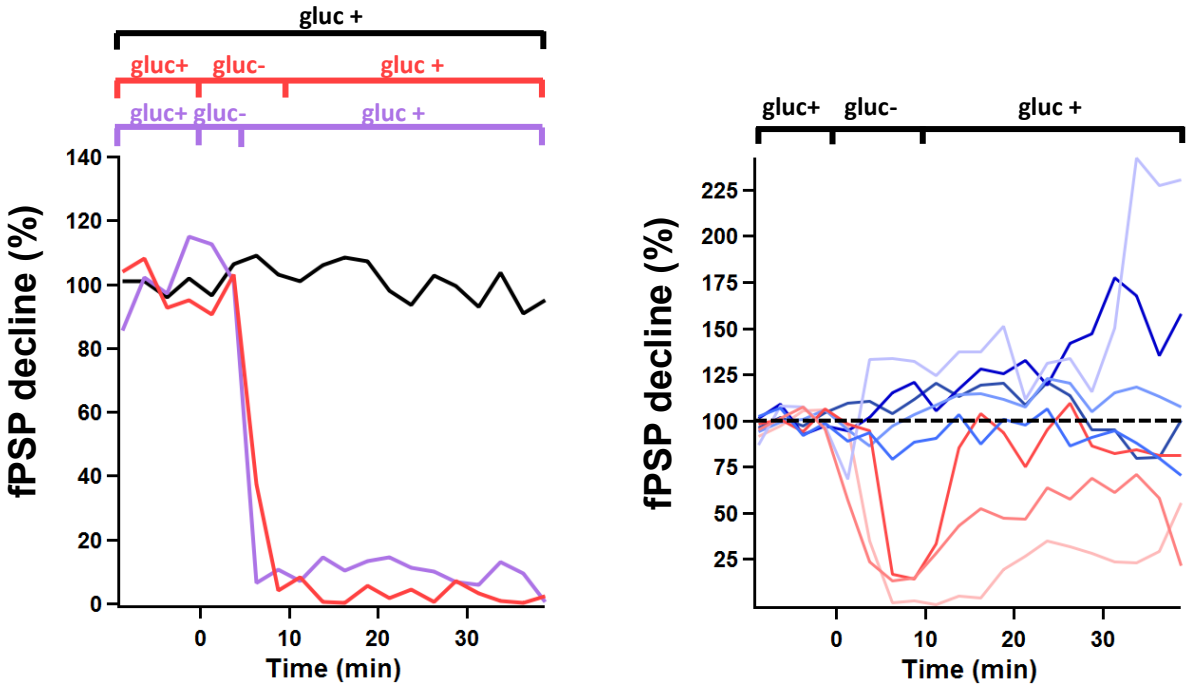

Figure 5.3 Effect of temperature on EGD experiments to study fPSPs in the thalamus.
Thalamic field potentials were recorded at 35°C. (A) Normalized fPSPS under control conditions (gluc+,black line; n = 5; N = 5), during 5 min of EGD (purple line) and 10 min of EGD (red line). fPSPs were stable under control conditions. They declined to zero after a 10 or a 5 min EGD, and did not recover after glucose reperfusion in most cases. (B) Examples traces of the normalized fPSPs after 2.5 min of EGD. A decline in fPSPs was only observed in 3 out of 8 experiments (red lines) whereas no decline was observed in the other 5 experiments (blue lines).

5.2.1 Analyses at room temperature

Previous experiments were done at physiological temperature. Recordings at room temperature were next performed. Stable field potentials were recorded for over >40 min (Fig. 5.4 A, B, black line). Control fPSPs were first recorded in ACSF for 10 min. Next, EGD was induced by removing glucose from the bath (10 min; gluc-) and subsequently ACSF containing glucose was re-perfused (Fig. 5.4 A,B, orange line). A decline in fPSPs was observed during EGD, follow by a recovery after reperfusion with ACSF containing glucose (12 slices from 10 animals). In conclusion, the effect of EGD on synaptic activity in acute thalamic slices can reliably be study at room temperature with this protocol.

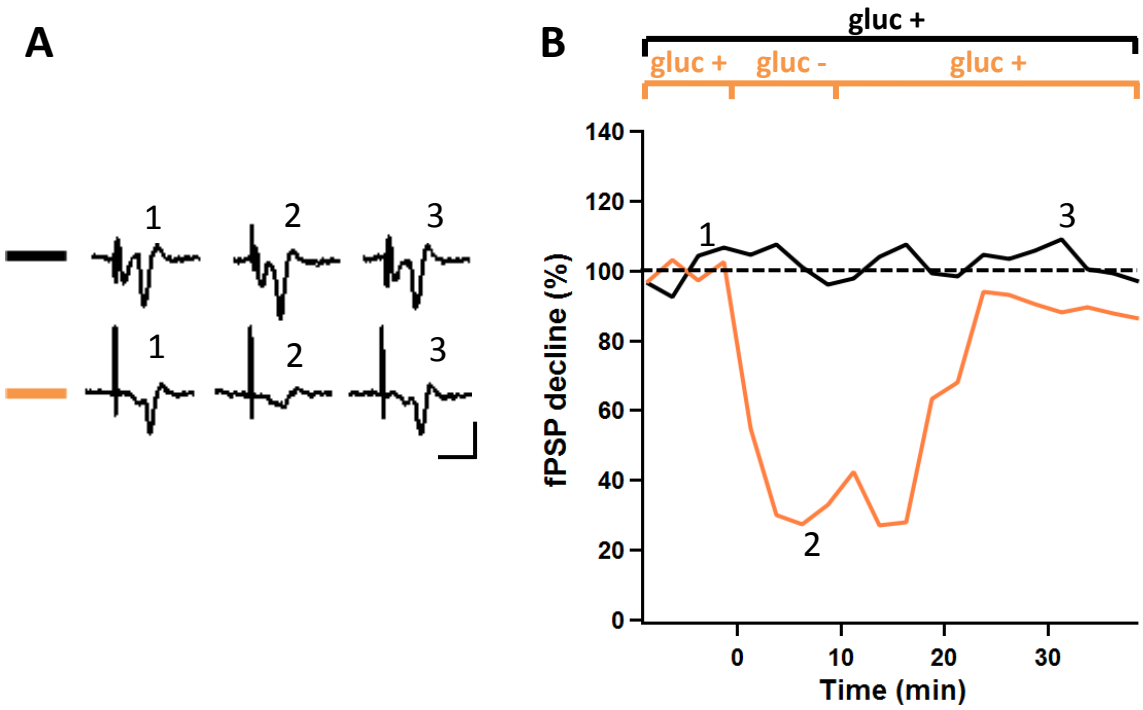

Figure 5.4 EGD leads to a fast decrease of thalamic synaptic activity.
Synaptic field potentials were monitored in thalamic slices containing the VPM of the thalamus. (A) Example traces of thalamic field potentials were recorded under control conditions over 40 min (indicated by black line in B, numbers correspond to times points specified in B) or under 10 min control recording (1), during EGD (2) and after reperfusion with ACSF containing glucose (3) (indicated in orange line in B Scale bars, 0.5 ms, 0.5 mV. (B) Normalized fPSPs under control conditions in ACSF over 40 min shown in black (gluc+, n = 4, N = 4), and of a 10 min extracellular glucose deprivation (gluc-) shown in orange (n = 10, N = 12).

5.3 Decline of fPSPs during EGD cannot be rescued by extracellular bath application of lactate or pyruvate

Lactate and pyruvate have been shown to be able to replace glucose to sustain axonal activity in the optic nerve (Brown et al., 2001) but not in the corpus callosum (Meyer et al., 2018). During EGD, fPSPs declined to around 45% of the initial amplitude (EGD, orange line and bar graph, 44.83 ± 5.47%, n = 12, N=10, Fig. 5. 5 B) and a recovery was observed upon reperfusion with ACSF containing glucose. In the following experiments, 11 mM glucose was first replaced by 22 mM L-lactate (L-lact+). We used 22 mM to have an equimolar amount of L-lactate and glucose. When extracellular lactate was applied fPSPs dropped to around 60% of the control value (red line and bar graph, EGD + lactate, 61.25 ± 3.50%, n = 5, N = 5). Thus, similar to the corpus callosum, lactate was not able to compensate the lack of glucose (ANOVA followed by Tukey's post-hoc test, p = 0.13). Next 11 mM glucose was also replaced by 22 mM pyruvate and recorded comparable results as with L-lactate with a decline to around

60% of the control value (pink line and bar graph, EGD + pyruvate, 61.52 ± 4.47%, n = 6, N = 6, p = 0.10). In both lactate and pyruvate experiments, a recovery in post synaptic activity was observed after reperfusion with ACSF containing glucose, similar to the one observed in EGD experiments without lactate or pyruvate (Fig. 5.5 A, red and pink lines).

In summary, these findings indicate that extracellular glucose, rather than extracellular lactate or pyruvate, is specifically needed to sustain post synaptic activity in the thalamus.

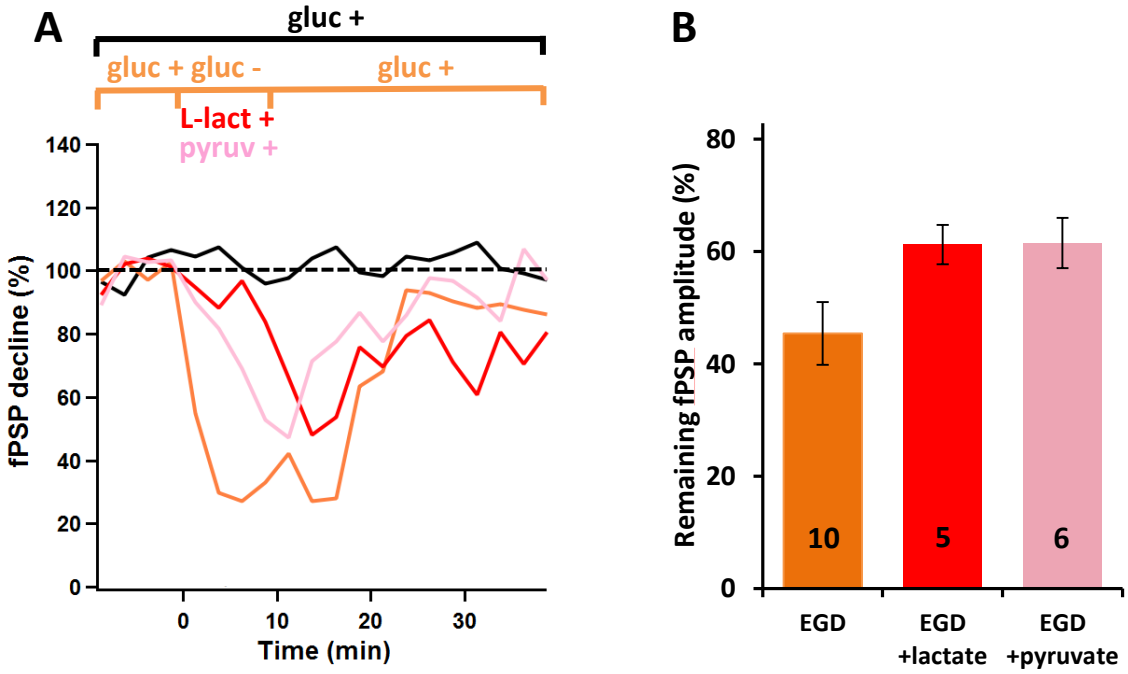

Figure 5.5 EGD suppresses fPSPs in the thalamus and is not rescued by extracellular lactate or pyruvate application.

(A) Normalized fPSPs during 10 min EGD, follow by reperfusion (orange line). Experiments were done at room temperature. Additionally, normalized fPSPs in which extracellular glucose was replaced by either 22 mM L-lactate (red line) or 22 mM pyruvate (pink line) during 10 min of EGD, are shown. (B) Bar graphs represent the mean of the remaining fPSP amplitudes, normalized to the respective conditions during control recording prior to EGD. Perfusing extracellular lactate or pyruvate did not significantly attenuate the decline in fPSPs induced by EGD (EGD, orange, n = 12, N = 12; EGD + lactate, red, N = 5, N = 5, EGD + pyruvate, pink, N = 6, N = 6; ANOVA followed by Tukey's post-hoc test p = 0.13 and 0.10 for L-lactate and pyruvate respectively). Number of mice is given in bar graphs.

5.4 Effect of filling glial cells with energy metabolites during EGD on neuronal activity

5.4.1 Effect of filling an astrocyte

In the hippocampus, astrocytic networks help maintaining synaptic activity (Rouach et al., 2008). In the corpus callosum, glial networks consist mainly of oligodendrocytes. They form a pathway to provide energy substrates to axons, sustaining axonal activity (Meyer et al., 2018). There are abundant panglial coupling networks in the thalamus. Indeed, coupled networks contain more than 50% of oligodendrocytes (Griemsmann et al., 2015; Claus et al., 2018). Hence, this observation led to the question whether panglial coupling networks in the thalamus can provide energy to sustain synaptic activity and therefore rescue the decline of fPSPs observed during EGD.

We investigated whether loading glial cells with metabolites could rescue the loss of fPSP amplitudes mediated by EGD. Astrocytes were identified in the VPM of acute thalamic slices of hGFAP-GFAP mice by their bright fluorescence. A single astrocyte was patched and dialyzed with an intracellular solution containing a high concentration of glucose (20 mM) for 20 min. Then 10 min of EGD was applied, followed by a reperfusion step with ACSF containing glucose. To control the successful spread of biocytin into the coupled network, the pipette solution also contained the gap junction permeable dye sulforhodamine-B. The initial, patched hGFAP-EGFP^{+} cell displayed a passive current pattern typical of astrocytes, an average resting membrane potential (MP) of -70.25 ± 1.89 mV and a very low input resistance (Rm) of 3.45 ± 0.60 MΩ (n = 8, N = 7 animals). Glucose filling of an astrocyte significantly reduced the decline in fPSPs induced by EGD (to around 71%, EGD, orange line and bar graph, 44.83 ± 5.47 , n = 12, N=10; after astrocyte filling: EGD+ AG, dark green line and bar graph, 71.21 ± 3.19, n = 8, N = 7) (Fig. 5.6 B, ANOVA followed by Tukey's post-hoc test, p = 0.004).

Filling a single astrocyte (MP = -74.85 ± 1.58 mV; Rm = 2.37 ± 0.38 MΩ; n = 7, N = 7) with a high concentration of lactate (40 mM L-lactate) was performed to test if it could also rescue fPSPs. A concentration of 40 mM L-Lactate was used because during lactic fermentation, 1 molecule of glucose generates 2 molecules of lactate. A significant rescue of the EGD-induced drop of fPSPs was observed when filling an astrocyte with lactate (EGD+ AL, light green line and bar graph, 66.55 ± 3.27%, n = 7, N = 6, Fig. 5.6 B, ANOVA followed by Tukey's post-hoc test, p = 0.014). In conclusion, high

intracellular glucose concentration as well as high L-lactate loading of astrocytes can rescue the decline of fPSP amplitudes in the thalamus during EGD.

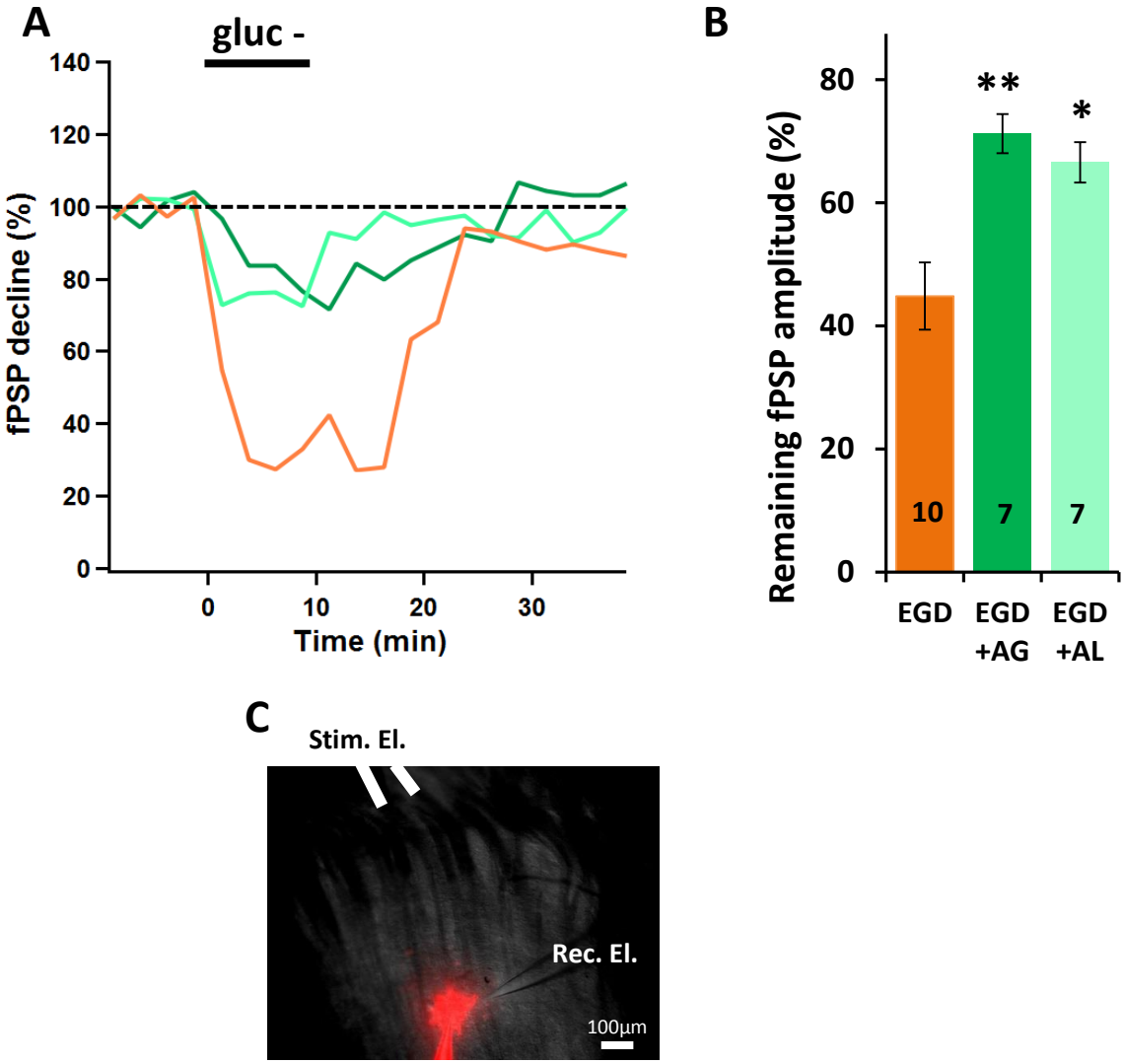

Figure 5.6 Glucose and lactate filling of astrocytes can rescue synaptic activity in the thalamus during EGD.

Thalamic astrocytes of hGFAP-EGFP mice were loaded with metabolites before recording synaptic activity. (A) Normalized fPSPs during a 10 min EGD (orange line), after dialyzing an astrocyte with 20 mM glucose (dark green line) or dialyzing an astrocyte with 40 mM L-lactate (light green line). (B) Bar graphs represent the mean of the remaining fPSPs amplitude, normalized to the respective conditions during control basal recording prior to EGD. Filling an astrocyte with glucose or L-lactate led to a significant rescue of fPSP amplitudes during EGD. ANOVA followed by Tukey's post-hoc test p = 0.004 and 0.014 for glucose and L-lactate respectively. (C) Overview of a thalamic brain slice used for electrophysiological recordings. Close to the recording electrode (Rec. El.), one astrocyte was loaded with an energy metabolite and sulforhodamine B (red dye, 10 µg/ml) to visualize online its spread in the coupling cloud. Number of mice is given in bar graphs. Asterisks indicate statistical significance (*p<0.05, **p<0.01).

5.4.2 Effect of filling an oligodendrocyte

In the corpus callosum, filling an oligodendrocyte with energy metabolites was shown to be more efficient than astrocyte filling in rescuing the decline of axonal activity during EGD (Meyer et al., 2018). In the thalamus, astrocytes and oligodendrocytes form abundant panglial coupling networks (Griemsmann et al., 2015; Claus et al., 2018). More than half of the thalamic coupled cells are oligodendrocytes, irrespective of whether an astrocyte or an oligodendrocyte was initially filled with the tracer (Griemsmann et al., 2015).

Thus, to test if oligodendrocytes also protect synaptic activity in the thalamus, a single oligodendrocyte was loaded with a high glucose concentration (20 mM, for 20 min) using the same experimental strategy as mentioned before. Oligodendrocytes were identified by their GFP fluorescence and patched in the VPM of acute brain slices form PLP-GFP mice. On average they had a MP of -73.57 ± 1.27 mV and an R_m 6.63 ± 1.16 MΩ (n = 7, N =7 animals). Similar to loading an astrocyte, dialyzing oligodendrocytes with glucose significantly reduced the decline of fPSP amplitudes (to around 68%), during EGD (EGD, orange line and bar graph, 44.83 ± 5.47% , n = 12, N = 10; EGD+OG, dark blue line and bar graph 67.80 ± 2.82%, n = 7, N = 7 (Fig. 5.7 A, B, ANOVA followed by Tukey's post-hoc test, p = 0.01). Loading an oligodendrocyte with a high concentration of lactate (40 mM) led to a similar effect. The remaining fPSPs amplitude during EGD was on average about 66% (EGD+OL, light blue line and bar graph, 66.09 ± 3.65%, n = 5, N = 5, fig. 5.7 B, ANOVA followed by Tukey's post-hoc test, p = 0.031).

Summarizing, dialyzing glucose or lactate into a patched oligodendrocyte can rescue the decline in fPSP amplitude during EGD. This rescue was as efficient as filling an astrocyte with energy metabolites.

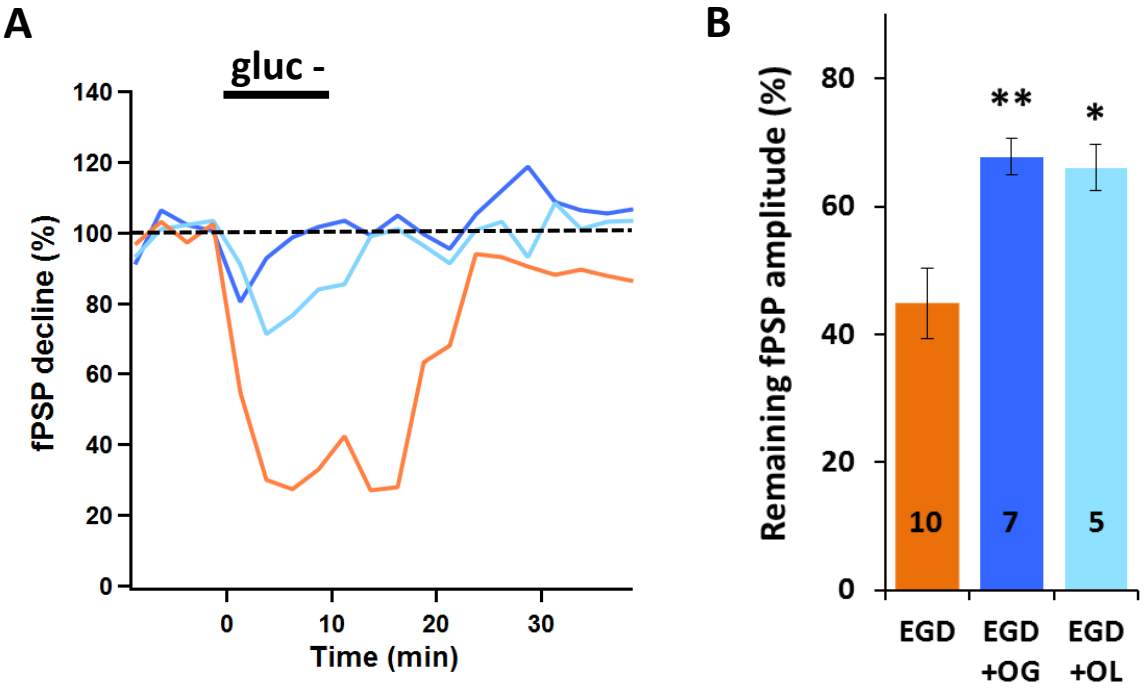

Figure 5.7 Glucose and lactate filling of oligodendrocytes can attenuate fPSP amplitude decline mediated by EGD.

(A) Normalized fPSPs during 10 min EGD (orange line), while dialyzing an oligodendrocyte with 20 mM glucose (dark blue line) or with 40 mM L-lactate (light blue line). (B) Bar graphs illustrate the mean of the remaining fPSP amplitudes, normalized to the respective control recording prior to EGD for each condition. Loading of oligodendrocytes with 20 mM glucose or 40 mM L-lactate can partially rescue fPSP amplitudes during EGD (control EGD, orange line and bar graph n = 12, N = 10; 20 mM glucose, EGD+OG, dark blue line and bar graph n = 7, N = 7; 40 mM L-lactate, EGD+OL, light blue line and bar graph, n = 5, N = 5). ANOVA followed by Tukey's post-hoc test p = 0.01 and 0.031 for glucose and lactate, respectively. Number of mice is given in bar graphs. Asterisks indicate statistical significance (*p<0.05, **p<0.01).

5.5 The impact of Cx32 and Cx47

5.5.1 Impact on panglial networks

White matter oligodendrocytes contribute to sustain axonal activity by transport of metabolites in the corpus callosum and the optic nerve (Lee et al., 2012; Meyer et al., 2018). Oligodendrocytes express Cx32 and Cx47. Cx30 is the dominant astrocytic connexin in the thalamus (Griemsmann et al., 2015). Heterotypic Cx30:Cx32 gap junction channels have been proposed to mainly mediate thalamic panglial coupling (Claus et al. 2018). Hence, the impact of oligodendrocyte connexins on thalamic panglial networks was first investigated.

Panglial coupling efficiency was quantified after injecting biocytin (for 20 min of patch clamp recording) in a single astrocyte of $Cx32^{-/-}$;$Cx47^{EGFP(-/-)}$ (dko) mice (n = 10, N = 3), $Cx32^{-/-}$;$Cx47^{EGFP(+/-)}$ mice (n = 11, N = 4) and $Cx32^{-/-}$;$Cx47^{EGFP(+/+)}$ mice (n = 15, N = 4). Astrocytes were identified in those mice by SR101 labelling in acute thalamic brain slices. Coupling efficiency was significantly reduced in dko mice (36 ± 8 cells, n = 10 slices) compared to $Cx32^{-/-}$;$Cx47^{EGFP(+/-)}$ mice (69 ± 11 cells, n = 11 slices, p = 0.048) and to control mice (110 ± 20 cells, n = 8 slices, p = 0.0028; Griemsmann et al., 2015) (Fig. 5.9, Kruskal–Wallis test followed by Dunn´s test).

Interestingly, when looking at the proportion of oligodendrocytes which were still part of tracer-coupled networks, among those biocytin-coupled cells, 27% were GFP^+, i.e. oligodendrocytes in $Cx32^{-/-}$;$Cx47^{EGFP(+/-)}$ mice, compared to 55% in control mice. In $Cx32^{-/-}$;$Cx47^{EGFP(-/-)}$ dko mice, the remaining small networks completely lacked oligodendrocytes, as no $EGFP^+$ cells were observed. Thus, we next investigated whether oligodendrocytes in the thalamus contribute to the maintenance of synaptic activity by providing metabolites through the coupled network by using $Cx32^{-/-}$;$Cx47^{EGFP(-/-)}$ dko mice, where no oligodendrocytes are part of the biocytin-coupled network anymore.

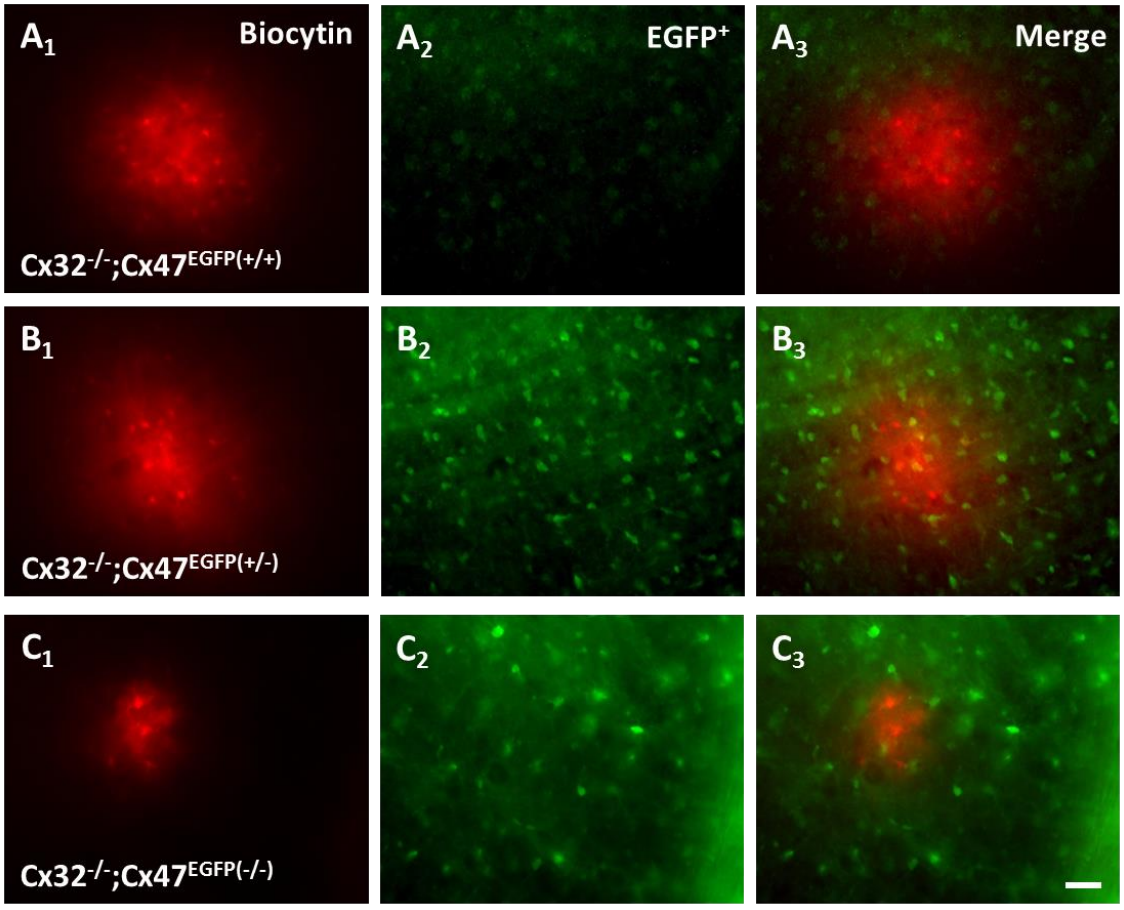

Figure 5.8 Biocytin diffusion in Cx32/Cx47 mice.
(A_1-C_1) $SR101^+$ astrocytes were filled with biocytin for 20 min in the thalamus of 3 different genotypes $Cx32^{-/-}$;$Cx47^{EGFP(+/+)}$ (A), $Cx32^{-/-}$;$Cx47^{EGFP(+/-)}$ (B) and $Cx32^{-/-}$;$Cx47^{EGFP(-/-)}$ (C). Cx47-$EGFP^+$ oligodendrocytes are displayed in green (A_2-C_2) and the merge images are shown (A_3-C_3). Notice that EGFP is not expressed in $Cx32^{-/-}$;$Cx47^{EGFP(+/+)}$ mice (A_2). Immunostaining for GFP (B_1-B_3) revealed that biocytin spread into Cx47-$EGFP^+$ oligodendrocytes in $Cx32^{-/-}$; $Cx47^{+/-}$mice as revealed by the colocalization of both markers (yellow cells, B_3). Scale bar 40 µm.

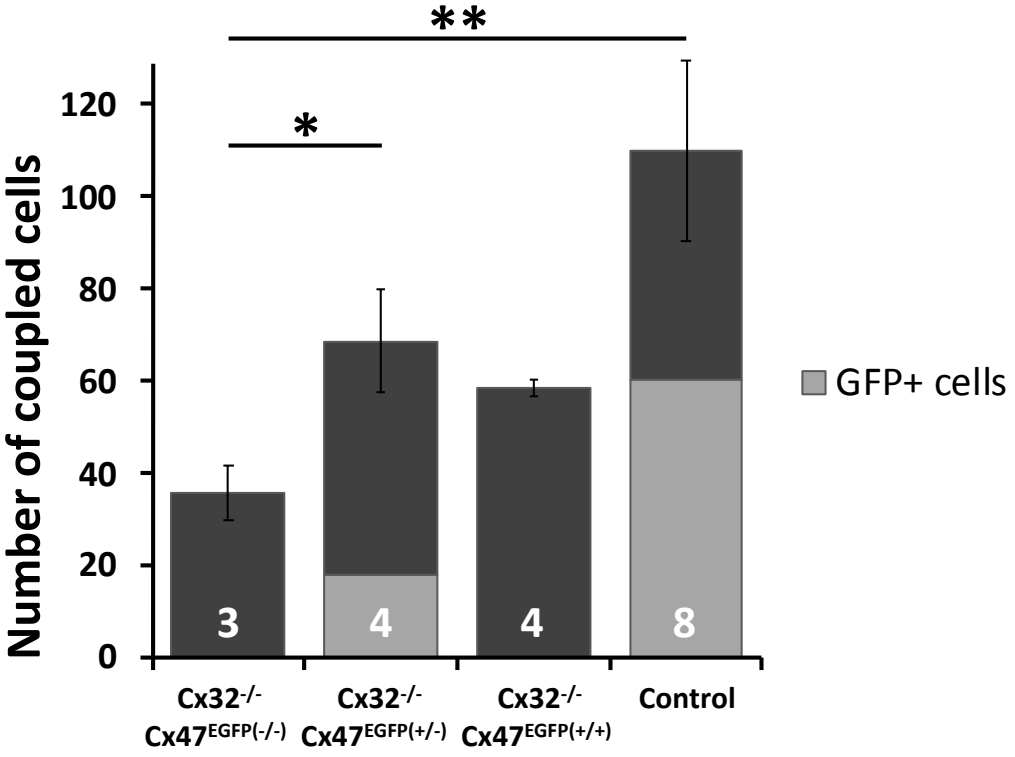

Figure 5.9 Quantification of panglial network size in Cx32/Cx47 dko mice.
Graph summarizing the coupling efficiency after injecting astrocytes with biocytin (20 min) in the thalamus of Cx32/Cx47 dko mice. Total numbers of coupled cells (black bars) and number of GFP+ cells (light grey bars), which were part of biocytin-coupled networks, were compared. Coupling efficiency was reduced in In $Cx32^{-/-}$;$Cx47^{EGFP(-/-)}$ dko mice (n = 10, N = 3), compared to $Cx32^{-/-}$;$Cx47^{EGFP(+/-)}$ mice (n = 11, N = 4) and in control mice (n = 14, N = 8). Moreover, in $Cx32^{-/-}$;$Cx47^{EGFP(+/-)}$ mice, biocytin-filled networks still contained around 27% of GFP^+ cells (i.e. oligodendrocytes) whereas 55% were GFP^+ cells in control mice. No GFP^+ cells were found in coupled networks of $Cx32^{-/-}$;$Cx47^{EGFP(-/-)}$ dko mice. As oligodendrocytes were completely lacking in those networks, those mice were used for further experiments. In $Cx32^{-/-}$;$Cx47^{EGFP(+/+)}$ mice, Cx47 was not fluorescent. Therefore, the proportion of oligodendrocytes that were part of the coupled networks could not be estimated (n = 15, N = 4). Number of mice is given in bar graphs. Asterisks indicate statistical significance (*$p<0.05$, **$p<0.01$). Kruskal–Wallis test followed by Dunn´s test.

5.5.2 Impact on neuronal activity

Oligodendrocytes support axonal function by transport of metabolites in white matter areas (Lee et al., 2012; Meyer et al., 2018). In $Cx32^{-/-}$;$Cx47^{EGFP(-/-)}$ dko mice, the remaining small networks completely lacked oligodendrocytes (see section 5.5.1). In this part of the study, the protection of fPSP activity during EGD through glucose filling of astrocytes was investigated in $Cx32^{-/-}$;$Cx47^{EGFP(-/-)}$ dko mice. Incubation of acute thalamic brain slices of $Cx32^{-/-}$;$Cx47^{EGFP(-/-)}$ dko mice with the astrocytic marker SR101 confirmed that green fluorescent $Cx47^+$ cells never colocalized with the astrocytic marker SR101 (Fig. 5.10, N = 4 mice, n = 12 regions of interest).

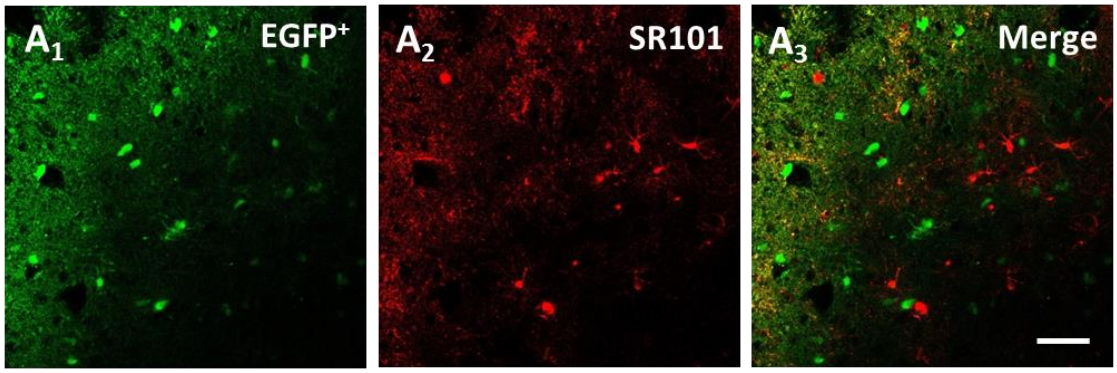

Figure 5.10 EGFP$^+$ cells do not colocalize with the astrocytic marker SR101 in Cx32$^{-/-}$;Cx47$^{EGFP(-/-)}$ mice.
Employing the astrocytic marker SR101 (red, center A_2), online visualization of EGFP$^+$ oligodendrocytes (green, left A_1) did not colocalize with astrocytes (merge, right A_3) Cx32$^{-/-}$;Cx47$^{EGFP(-/-)}$ mice. Scale bar, 50 µm.

Astrocytes were therefore identified as Cx47$^-$ cells, their low input resistance (1.8 ± 0.27 MΩ) and a negative resting MP (-84.57 ± 2.28 mV, n = 6, N = 6). To visualize online that our initial patched cell was an astrocyte and was coupled, sulforhodamine B (10 µg/ml) was added to the pipette solution. The fPSP decline during EGD in Cx32$^{-/-}$;Cx47$^{-/-}$ mice (dark grey, EGD dko, 46.61 ± 5.12%, n = 5, N = 5) did not differ significantly from the fPSP decline during EGD in hGFAP-EGFP mice (orange, EGD, 44.83 ± 5.47%, n = 12, N = 10; Fig. 5.11 B, ANOVA followed by Tukey's post-hoc test, p = 0.99).

In Cx32$^{-/-}$;Cx47$^{EGFP(-/-)}$ mice, filling an astrocyte with 20 mM glucose (for 20 min) did not rescue fPSP amplitudes during 10 min of EGD (light grey, EGD dko + AG, 53.76 ± 6.42%, n = 6, N = 6) compared to control experiments (dark grey, EGD dko, 46.61 ± 5.12%, n = 5, N = 5, ANOVA followed by Tukey's post-hoc test, p = 0.87, Fig. 5. 11 B).

In conclusion, these experiments demonstrate that dialyzing an astrocyte with glucose in Cx32$^{-/-}$;Cx47$^{EGFP(+/-)}$ mice, where oligodendrocyte are not part of the coupled network, showed no rescue in neuronal activity, during EGD. Therefore, in the thalamus coupled oligodendrocytes participate in neuronal provision of metabolite substrates.

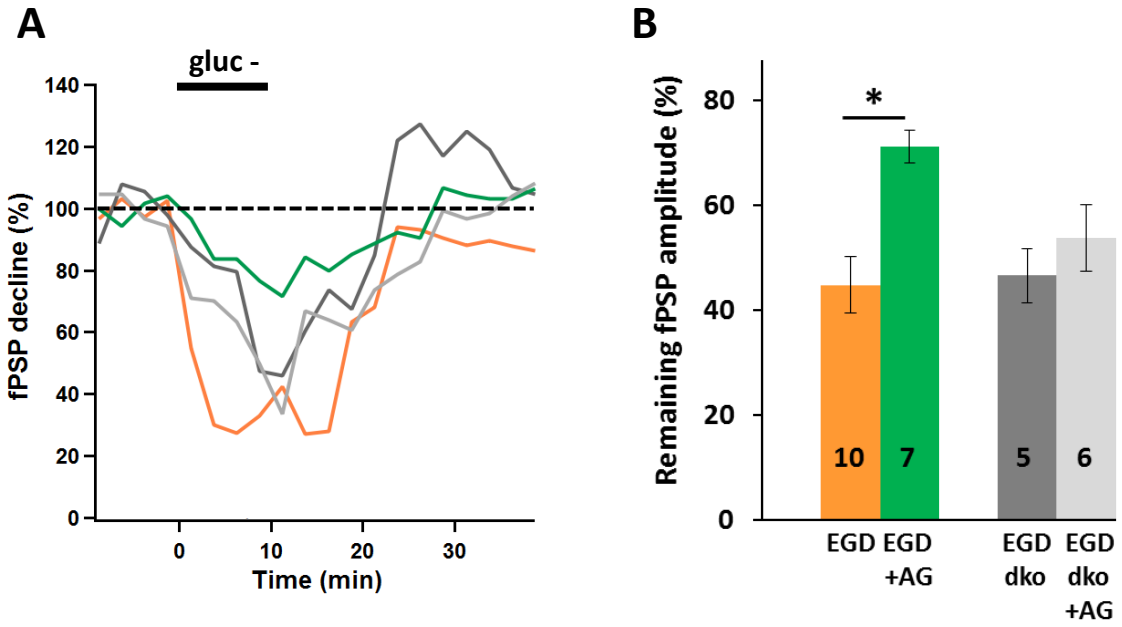

Figure 5.11 Filling an astrocyte with glucose cannot rescue thalamic fPSPs during EGD in Cx32$^{-/-}$;Cx47$^{EGFP(-/-)}$ dko mice.

(A) Normalized fPSPs during 10 min of EGD (orange line, n =12, N =10) and while dialyzing an astrocyte with 20 mM glucose (dark green line, n = 7, N = 6) in hGFAP-EGFP mice. Furthermore normalized fPSPs during 10 min of EGD (dark grey line, n =5, N = 5) and while dialyzing an astrocyte with 20 mM glucose (light grey line, n = 6, N = 6) in Cx32$^{-/-}$;Cx47$^{EGFP(-/-)}$ mice are shown. (B) Bar graphs illustrate the mean of the remaining fPSPs amplitude, normalized to the respective conditions during control recording prior to EGD for each condition. Filling an astrocyte with a high glucose concentration in Cx32$^{-/-}$;Cx47$^{EGFP(-/-)}$ mice did not rescue fPSP amplitudes during EGD. Number of mice is given in bar graphs. ANOVA followed by Tukey's post-hoc test. Asterisks indicate statistical significance (*p<0.05).

5.6 Effect of glucose and monocarboxylate transporters on neuronal activity

To further characterize the mechanisms involved in the rescue of fPSPs while loading an astrocyte with glucose during EGD, the effect of glucose and monocarboxylate transporter inhibitors was tested. First, a combination of blockers was employed. AR-C155858 (1 µM) specifically inhibits the monocarboxylate transporters MCT1 and MCT2, which are isoform expressed by oligodendrocytes and by neurons, respectively. Stf31 (5 µM) specifically blocks the glucose transporter GLUT1, which is expressed by oligodendrocytes as well as by astrocytes. An astrocyte was patched and loaded with 20 mM glucose before applying the cocktail of blockers during 10 min of EGD. After loading an astrocyte with glucose, the combined application of AR-C155858 and Stf31, prohibited the rescue of fPSP amplitudes during EGD as fPSPs still declined to around 45% (dark green, EGD+AG+Stf/AR-C applic., 45.49 ± 7.98%, n = 6, N = 6), which is similar to the decline observed without glucose filling of astrocytes (orange, EGD,

44.83 ± 5.47%, n = 12, N = 10; Fig. 5.11 B, ANOVA followed by Tukey's post-hoc test, p = 0.99, Fig. 5.12 B). Next, SR13800 (0.01 µM), an MCT1 specific inhibitor, was used. After dialyzing an astrocyte with glucose, application of SR13800 alone did not have a significant effect on fPSP amplitudes during EGD (purple, EGD+AG+SR13800, 59.28 ± 3.63%, n = 6, N = 6) compared to EGD only (p = 0.36, ANOVA followed by Tukey's post-hoc test, Fig. 5.12 B) or to applying both blockers (p = 0.50, ANOVA followed by Tukey's post-hoc test, Fig. 5.12 B). Taken together, these results show that in the thalamus, the protective effect of providing glucose through the panglial network on thalamic synaptic activity during EGD is dependent on both MCT1/2 and GLUT1 transporter activity.

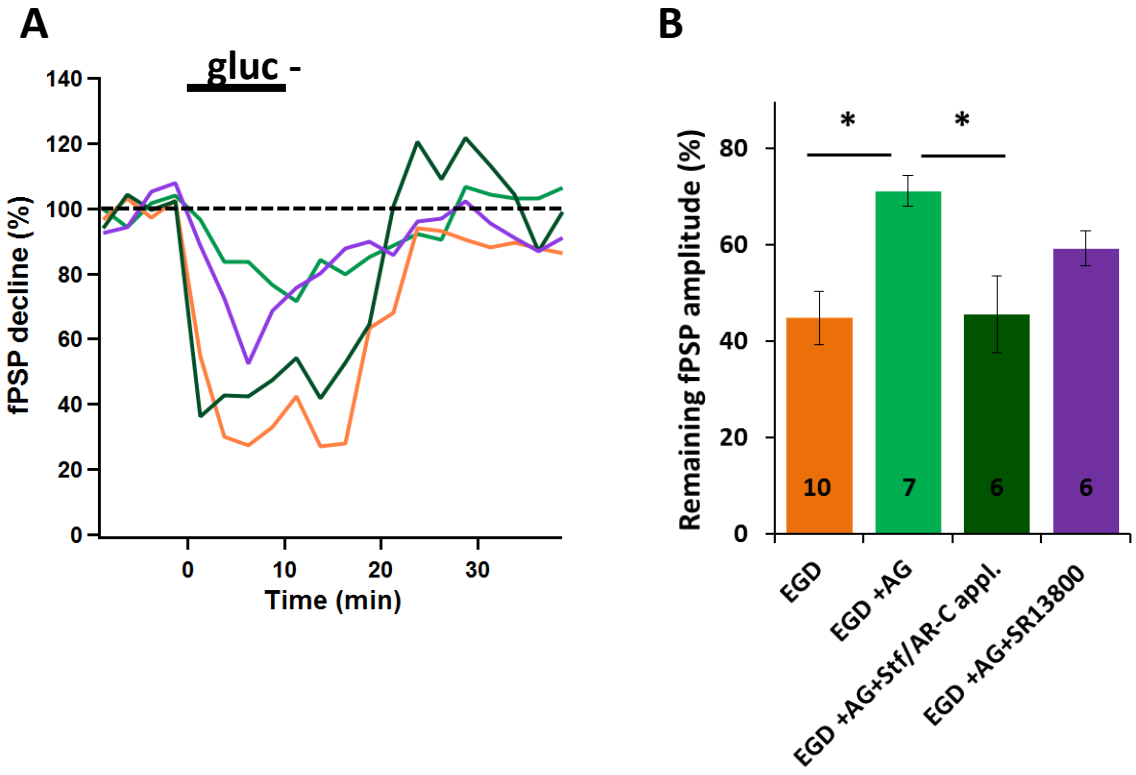

Figure 5.12 Simultaneous disruption of both glucose and monocarboxylate transport inhibits the rescue of fPSPs after glucose filling of astrocytes.

(A) Normalized fPSPs during 10 min of EGD (orange line, n =12, N =10), while dialyzing an astrocyte with 20 mM glucose (green line, n = 7, N = 6), with application of the blockers Stf31 (5 µM) to block the glucose transporter GLUT1 and AR-C155858 (1 µM) to block monocarboxylate transporters MCT1 and MCT2 (dark green line, n = 6, N =6) and with application of the specific MCT1 blocker SR13800 (0.01 µM) (purple line, n = 6, N = 6). (B) Bar graphs illustrate the mean of the remaining fPSP amplitudes, normalized to the respective conditions during control recording prior to EGD for each condition. fPSPs amplitude do not rescue after filling an astrocyte with glucose during EGD while applying both AR-C155858 and Stf31. (EGD+AG+Stf/AR-C appl., dark green bar graph, ANOVA followed by Tukey's post-hoc test p = 0.99). Applying SR13800 (0.01 µM) alone did not impact fPSP amplitudes during EGD while an astrocyte was loaded with glucose (EGD+AG+SR13800, purple bar graph, n = 6, N = 6, ANOVA followed by Tukey's post-hoc test, p = 0.36 and p = 0.50 compared to EGD only and to applying both blockers, respectively).

6 Discussion

Glial cells in the CNS, and in particular astrocytes, are interconnected via gap junction channels, forming coupled networks. These glial networks are essential for several functions such as brain homeostasis and brain metabolism. In contrast to other brain areas, in the thalamus not only astrocytes are coupled to each other. Oligodendrocytes are making up for more than half of the coupled cells within a network (Griemsmann et al., 2015; Claus et al., 2018). While the human brain represents only 2% of the total body volume, 20% of whole-body glucose consumption is allocated to meet the brain's energy demands (Magistretti and Allaman, 2015; Mink et al., 1981), suggesting high energy requirements for the nervous system. Consequently, over the last two decades, brain energy metabolism and the most recent term "neuroenergetics" have been a research focus. Recent studies have started to unravel the key role of glial cells in brain energy metabolism. However, little is known about glial cells in the thalamus, a grey matter region with long myelinated fibers projecting to and from the cortex. It is described as the gate to consciousness as it receives somatosensory inputs (Crick and Koch, 2003). In grey matter, astrocyte coupling networks have emerged as active players in sustaining neuronal energy requirements (Rouach et al., 2008), whereas in white matter, coupled oligodendrocytes are key elements in supporting axonal function (Meyer et al., 2018). The functional impact of oligodendrocytes on neuronal activity in grey matter remains unclear. Thus, thalamic panglial networks with their abundant astrocyte-oligodendrocyte coupling might influence brain energy metabolism. To this end, the characteristics and the specific role of oligodendrocytes in the panglial thalamic network and in energy metabolism were investigated in this project.

6.1 Barreloid borders are mostly shaped by weakly coupled oligodendrocytes

As part of the somatosensory system, the VPM of the thalamus contains elongated domains called barreloids. Barreloids in rat and mice reflect the spatial arrangement of whiskers (Haidarliu and Ahissar, 2011). In our study by Claus et al. (2018), thalamic barreloid borders were shown to restrict panglial coupling networks. Furthermore, analysis in PLP-GFP mice showed that barreloid borders are mainly formed by oligodendrocytes. This information initiated a first set of experiments to ask whether those oligodendrocytes located on barreloid borders were part of the panglial network. Using PLP-GFP mice, selected oligodendrocytes positioned on the barreloid borders were patched and filled with biocytin. I could show that barreloid borders are mainly formed by weakly coupled or uncoupled oligodendrocytes (Fig. 5.1), thus giving an explanation to why biocytin diffusion was asymmetrical and restricted to an individual barreloid field after filling a single astrocyte in between barreloids borders (Claus et al., 2018). Furthermore, several PLP-GFP-positive cells within the volume of the biocytin-filled networks were biocytin-negative. We also detected some astrocytes as biocytin-negative within the volume occupied by biocytin-filled networks (Claus et al., 2018). In the juvenile hippocampus, it has been reported that not all astrocytes located in a coupling domain are coupled with each other (Houades et al., 2006). However, this observation was actually due to the immature functional stage of those cells (Wallraff et al., 2004; Schools et al., 2006; Strohschein et al., 2011). Noteworthy, in the thalamus the number of biocytin coupled cells reached maximum coupling capacity already at an earlier development stage (Griemsmann et al., 2015). Therefore, the immature stage is not responsible for the observed uncoupled cells in thalamic barreloids. However, it still remains to be determined whether those non-filled cells are really uncoupled or if they are actually part of another coupled network or if they are just temporarily not part of the network. These results are contributing to the concept of glial heterogeneity within thalamic glial cells. Two sub-populations of astrocytes from the VB thalamus were described in a previous study, using acuted isolated astrocytes to study their expression of glutamate receptors. Those thalamic astrocytes were either expressing or lacking AMPA/KA receptors (Höft et al., 2014). Other studies have also shown heterogeneity in thalamic astrocytes regarding their response to sensory or corticothalamic inputs in the VB thalamus (Parri et al., 2010; Pirttimaki and Parri, 2012). It remains elusive whether

biocytin-negative and -positive astrocytes have different functional features. Further analyses are also required to determine if uncoupled astrocytes may be involved in specific signaling pathways in respect to neurons in thalamic barreloids.

6.2 Neuronal activity shapes panglial networks in thalamic barreloids

Only a handful of studies have covered neuronal activity effects on astrocyte networks. The first investigations were done in cell cultures. Mouse co-culture of astrocytes with cerebellar neurons increases the amount of dye-coupled astrocytes (Fischer and Kettenmann, 1985). Those results were confirmed in another study in which astrocyte gap junction coupling was upregulated by neurons in rat astrocyte-neuron co-cultures (Rouach et al., 2000). Marrero and Orkand (1996) were the first to report an activity-dependent regulation of glial networks by neurons. They demonstrated that in the frog optic nerve, nerve stimulation increases glial coupling. The mechanisms mediating this process are mainly unknown. An increase in extracellular K^+ concentration leads to the depolarization of astrocytes which then modulates gap junction permeability of glial cells (Enkvist and McCarthy, 1994; see also review by Giaume et al., 2010). Phosphorylation of the C-terminus of Cx43 by Ca^{2+}-calmoduline protein kinase II has been proposed to play a role in this K^+-induced increased glial coupling (De Pina-Benabou et al., 2001). Astrocytic coupling is dominated by Cx43 in the hippocampus (Griemsmann et al., 2015). Furthermore, modulation of hippocampal neuronal activity shapes the spread of energy metabolites like 2-NBDG, while gap junction permeability to biocytin was not impacted (Rouach et al., 2008). Interestingly, in contrast to the hippocampus, astroglial gap junction coupling is reduced in olfactory glomeruli when neural network activity is inhibited by TTX or after early sensory deprivation (Roux et al., 2011). This study also suggested that Cx30 is the molecular target for the activity-dependence of gap junction channels in astroglial glomerular networks. Indeed, in Cx30 KO mice, dye coupling was affected neither by TTX treatments nor by early olfactory deprivation, whereas astroglial coupling was reduced when doing experiments in Cx43 KO mice. To strengthen this point, the same results were confirmed in juvenile mice, at a development stage in which Cx30 is not yet expressed by astrocytes (Roux et al., 2011).

I have analyzed glial networks in thalamic barreloids after treatments with TTX and ω-conotoxin GVIA. Inhibition of neuronal activity significantly reduced the spread of both

2-NBDG and biocytin in glial networks to the same extent (Fig. 5.2). As Cx30 is the dominant astrocytic Cx in coupled thalamic network (Griemsmann et al., 2015), our results are consistent with the findings from Roux et al. (2011). Taking together the literature and these neuronal activity dependent coupling networks, panglial coupling in thalamic barreloids of young mice is likely mediated by heterotypic Cx30/Cx32 channels.

In addition, Roux et al. (2011) have speculated that in olfactory glomeruli, changes in extracellular K^+ generated by neuronal activity can modulate astrocytic Cx30-mediated gap junction channels through a mechanism including their K_{ir} channels. Astrocyte properties have been reported to be heterogeneous between different brain areas (Xin and Bonci, 2018; Zhang and Barres, 2010). Indeed, as mentioned earlier, two sub-populations of astrocytes were defined in the VB thalamus (Höft et al., 2014). AMPA receptor-bearing astrocytes displayed a lower K_{ir} current density than astrocytes lacking this receptor. Therefore, taking those data together, biocytin-negative astrocytes observed in our experiments might be part of the astrocytic population expressing AMPA receptors.

What might be the advantage of having an anatomofunctional compartmentalization of panglial coupling networks for each barreloid? Houades et al. (2008) have shown that in the somatosensory cortex, glial networks are limited to a single barrel. Thus, they speculated that this compartmentalization could be necessary to restrict the activation of a single whisker to a single cortical barrel. In future studies, it would be interesting to investigate if a comparable concept can be observed in thalamic barreloids. Analyses of changes in panglial networks after whisker trimming could be studied. In case network formation is altered, Cx30 deficient mice could be employed to identify molecular targets of activity-dependent panglial coupling in thalamic barreloids. How panglial networks can perceive and modulate neuronal output in the thalamus is not well known. But, one can speculate that separation of glial networks by thalamic barreloid borders can limit neuronal interaction to one specific barreloid and therefore prevent any irregular neuronal activity. In addition, barreloid borders separation might be a requirement for high energy supply within the barreloid rather than in between barreloids. These limited gap junction networks in thalamic barreloids might also lead to metabolic pathway signaling, which is restricted to a single corresponding vibrissae. Using GAD (the synthetic enzyme for GABA) stainings as an indicator of thalamic metabolism, Land and Akhtar (1987) have shown that depriving adult rat of tactile input

via chronic whisker trimming leads to reduced metabolic activity and GAD immunoreactivity in corresponding barreloids in the VB thalamus. Future studies should aim at understanding the role of each glial cell type in sustaining and modulating neuronal activity in thalamic barreloids, in the healthy and diseased brain.

6.3 Thalamic fPSPs are sensitive to EGD and extracellular lactate or pyruvate cannot replace glucose to maintain fPSPs

What might be the link between neuronal activity and panglial networks in the thalamus? Thalamic oligodendrocytes make up for more than 50% of coupled cells (Griemsmann et al., 2015; Claus et al., 2018; Höft et al., 2014). In contrast, in the hippocampus panglial networks are mainly formed by astrocytes (Griemsmann et al., 2015), while oligodendrocytes are predominant in the corpus callosum (Meyer et al., 2018). This add to the evidence of different glial features and properties between brain regions (Matyash and Kettenmann, 2010; Xin and Bonci, 2018). Thus, what is the specific role of oligodendrocytes in energy metabolism? In the hippocampus, astrocytic networks provide metabolic substrates to neurons to sustain glutamatergic synaptic transmission (Rouach et al., 2008). Furthermore, recent studies have reported that in white matter, oligodendrocytes are metabolically highly active cells (Amaral et al., 2016). Hence, oligodendroglial networks are expected to participate significantly to brain metabolism activity. Additionally, oligodendrocytes are essential for sustaining the function of myelinated axons via transport of metabolites (Fünfschilling et al., 2012; Lee et al., 2012; Morrison et al., 2013; Meyer et al., 2018). Since oligodendrocytes are not in direct contact to blood vessels, brain metabolism might make use of the panglial coupling network to transport energy metabolites from the circulation, via astrocytic endfeets to synapses and via oligodendrocytes to axons. The thalamus has been described as a region of high energy consumption in accordance with its functional role as a gateway, in relaying and modulating sensory information to the cortex (Gordji-Nejad et al., 2018). From an anatomical organization point of view, high energy levels are probably needed to support long-range myelinated axons projecting from the cortex to the VB thalamus and vice versa.

A protocol to record thalamic field potentials from acute brain slices was established in our lab by Stephanie Griemsmann (PhD thesis, 2015). The corticothalamic pathway was stimulated and field potentials were recorded in the VB thalamus. A method to analyze

and quantify fPSP, representative of postsynaptic activity, was developed (also see chapter 4.1.4). Unfortunately, due to the experimental protocol parameters, analyzes of the pre-synaptic component of thalamic field potentials was not possible, as the axonal signals were merged with artefact recordings, even after TTX subtraction.

After 10 min of glucose deprivation, a decline by 55% in fPSP amplitudes was observed, followed by a recovery after reperfusion with ACSF containing glucose (Fig. 5.4). Next, extracellular glucose was replaced by lactate or pyruvate. Several studies have recently shown that lactate or pyruvate delivery by oligodendrocytes in white matter, mainly in the optic nerve and the spinal cord, is essential for proper axonal function (Hirrlinger and Nave, 2014; Funfschilling et al., 2012; Brown et al., 2003; Lee et al., 2012). On the other hand, astrocytes have been shown to deliver lactate as the main energy substrate to neurons, through the astrocyte-neuron lactate shuttle (ANLS) (Pellerin and Magistretti, 2012). Hence, oligodendrocytes in panglial thalamic networks might contribute to sustain presynaptic (axonal) function while astrocytes might sustain postsynaptic activity by delivering energy metabolites through the ANLS model. This hypothesis has been tested in the present study.

Applying extracellular lactate or extracellular pyruvate did not prevent the decline in fPSP amplitudes during EGD (Fig. 5.5). These results are in line with a recent report from the corpus callosum (Meyer et al., 2018) but in contrast with data from another white matter region, the optic nerve, were lactate could replace glucose in maintaining axonal activity (Brown et al., 2003). Another characteristic of thalamic fPSPs is their really fast decline during EGD compared to another grey matter region, the hippocampus (Rouach et al., 2008). Notably, initial experiments were performed at physiological temperature. However, after 5 or 10 min of glucose deprivation, field potentials irreversibly declined to zero while shorter duration of EGD (2.5 min) did not induce a reduction of the field potential (Fig. 5.3). These changes in energy dynamics might be caused by organizational differences in the thalamus, resulting in higher energy consumption in the VB thalamus than in the hippocampus. Indeed, as already mentioned above, corticothalamic neurons have long-range myelinated axons compared to shorter Schaffer collateral axons in the hippocampus, and are therefore in need of higher energy supply.

Another explanation for these changes in energy dynamics might be lower glycogen storage in thalamic astrocytes, compared to other brain areas. During metabolic challenges, astrocytic glycogen may be transformed to lactate (Pellerin and Magistretti,

2012) and therefore lower glycogen storage would result in a faster decline of energy metabolites available to fuel neuronal activity. Some reports have shown heterogeneity in metabolic activity between brain regions. A few decades ago, Yamamoto et al. (1989) have already described certain regionalization in the role of astrocytes in glutamate metabolism. Inhibition of glutamine synthetase generated a substantial glycogen accumulation in hippocampal, as well as in neocortical astrocytes but not in thalamic astrocytes. More recent evidence by Oe et al. (2016) has shown direct confirmation of regional differences in glycogen storage. Indeed, glycogen immunoreactivity was high in the hippocampus and the neocortex compared to the thalamus, which was only labeled sparsely. Accordingly, lower glycogen storages in the thalamus might cause the faster decrease in fPSP amplitudes observed during EGD.

6.4 Loading an astrocyte with energy metabolites can rescue the EGD-induced decline of thalamic fPSPs

Upon filling an astrocyte with the fluorescent glucose analog 2-NBDG, its spread reaches neighboring oligodendrocytes and myelin sheaths (Claus et al., 2018; Stephanie Griemsmann, thesis, 2015). On the other hand, loading astrocyte networks with energy metabolites can sustain synaptic activity in the hippocampus (Rouach et al., 2008). Hence, filling glial cells with metabolic substrates in the thalamus might rescue the decline in fPSP amplitudes observed during EGD. Glucose was first loaded in a single astrocyte. A high concentration of 20 mM, much higher than in physiological conditions (0.5-1 mM; Lerchundi et al., 2015), was used. However, due to the diffusion resistance, a much lower concentration is expected to be found in the coupled network, as the glucose spreads. Filling an astrocyte with glucose was sufficient to significantly attenuate the EGD-induced drop of post synaptic activity (Fig. 5.6). In the ANLS model, glucose is metabolized to lactate by astrocyte glycolysis, and then used by neurons (Magistretti and Allaman, 2018; Pellerin and Magistretti, 1994). Therefore, a single astrocyte was also loaded with high lactate. Lactate could also rescue the decline in thalamic synaptic activity. Those results suggest that in contrast to extracellular supply, delivery of intracellular lactate and glucose, which is likely metabolized to lactate and pyruvate, was able to sustain synaptic transmission in the thalamus.

6.5 Oligodendrocytes in gap junction networks are essential to maintain fPSP activity in the thalamus

As oligodendrocytes constitute a large part of thalamic panglial networks, further analyzes were conducted to unravel their role in thalamic energy supply. Loading an oligodendrocyte with glucose or lactate had a similar effect as filling an astrocyte in preventing the decline of thalamic synaptic activity (Fig. 5.7). Those results suggest that both astrocytes and oligodendrocytes are engaged by the thalamic panglial network to transport energy metabolites from blood vessels to neurons. To provide additional insight into the specific role of oligodendrocytes in sustaining synaptic activity, genetically modified mice were used. Cx32 and Cx47 are oligodendrocytic connexins. Mice lacking these connexins showed severe vacuolation, thin or absent myelin sheaths, axonal loss and died between 5 and 10 weeks after birth (Menichella et al., 2003; Odermatt et al., 2003). Additionally, those connexins are essential for oligodendrocyte coupling (Maglione et al., 2010; Griemsmann et al., 2015). As anticipated, mice lacking both Cx32 and Cx47 showed significantly reduced coupling compared to control mice (Fig. 5.8 and 5.9). Moreover, oligodendrocytes were completely lacking in glial networks from those double-deficient mice. Next, after confirmation that green fluorescent $Cx47^{+}$ cells never colocalized with the astrocytic marker SR101 (Fig. 5.10), an $SR101^{+}$ astrocyte was patched and filled with glucose in those double-deficient mice. No rescue of fPSP amplitudes was observed during EGD (Fig. 5.11). Consequently, we can conclude that oligodendrocytes are crucial elements of thalamic panglial networks for proper energy metabolite supply to the neuronal network.

A recent study by Saab et al. (2016) provided new insights in oligodendrocyte regulation of glucose utilization in the optic nerve. Oligodendrocytes use NMDA receptor signals as an indicator of axonal activity, leading to an increased trafficking of GLUT1 transporters to the oligodendrocyte membrane, which in turn increases glucose uptake. This mechanism does not require gap junction coupling (Saab et al., 2016). In the present study, experiments in connexin deficient mice showed that oligodendrocyte networks are necessary to sustain neuronal activity in the thalamus. Therefore, despite the fact that it is still unclear whether thalamic oligodendrocytes possess GLUT1 and NMDA receptors and at which extent, these data contribute to demonstrating heterogeneity in glial cells between the thalamus and other brain areas (Claus et al., 2018; Griemsmann et al., 2015). Oligodendrocytes in the optic nerve are weakly

coupled (Butt and Ransom, 1989) compared to the thalamus (Claus et al., 2018; Griemsmann et al., 2015) and have noticeably established other strategies to support neuronal activity.

Interestingly, when taking together findings from all different regions, including the hippocampus, the optic nerve and the corpus callosum, it is tempting to speculate that in the thalamus, astrocytes support neuronal activity at the synapse while oligodendrocytes primarily sustain axonal energy metabolism.

6.6 Glucose and monocarboxylate transporters are involved in providing energy substrates through thalamic panglial networks to sustain neuronal activity

Next, this study aimed to further challenge the later hypothesis by investigating, which metabolic pathways are involved in the energy supply from the panglial network to neurons. Glucose and monocarboxylate transporters are integral membrane proteins which mediate the fueling of neurons with energy metabolites (Barros and Deitmer, 2010). According to the current ANLS hypothesis, glucose can be taken up by astrocytes from the blood vessels via the glucose transporter GLUT1 (Belanger et al., 2011). Astrocyte glycolysis converts glucose into lactate, which is exported via MCT4, a specific astrocyte transporter (Rafiki et al., 2003; Rinholm et al., 2011). Lactate can then be taken up by MCT2, a neuron specific transporter, whereas MCT1 is expressed by oligodendrocytes and predominantly localized at the myelin sheaths around axons (Pierre and Pellerin, 2005; Rinholm et al., 2011; Morrison et al., 2013; Lee at al., 2012). Meyer at al. (2018) recently reported that lactate, rather than glucose, derived from oligodendrocytes could contribute to support axonal metabolic support in the corpus callosum. To further characterize the mechanisms involved in the prevention of EGD-induced decline in thalamic fPSPs, glucose and monocarboxylate transport blockers were used. GLUT1 and MCT1/2 blockers were applied to the bath solution while an astrocyte was filled with glucose. Simultaneous disruption of MCTs and GLUT1 completely inhibited the protective effect of astrocyte glucose loading (Fig. 5.12). Next, EGD experiments were performed under application of an MCT1 specific blocker (Fig. 5.12). The remaining fPSP amplitude was neither different from the control experiments (EGD) nor from experiments where blockers for MCT1/2 and GLUT1 were applied

(EGD +AG + AR-C155858 + Stf31). Thus, the conclusion of these results is difficult to explain, and the metabolite route used by oligodendrocytes to fuel neurons remains elusive.

In conclusion, as speculated in a review by Morrison et al. (2013), energy metabolites are transported between astrocytes and oligodendrocytes through gap junction networks prior to being used to fuel neurons/axons. Indeed, in the thalamus, astrocytes and oligodendrocytes are jointly involved in sustaining neuronal synaptic activity by delivery of energy substrates like glucose and lactate through the panglial network. Additionally, these data confirm the increasing evidence of glial heterogeneity throughout different brain regions. Glial heterogeneity occurs between the hippocampus and the thalamus, as well as between grey and white matter regions. However, further work needs to be carried out as it remains unclear whether oligodendrocytes in the thalamus modulate neuronal activity either by supporting axons or by supporting astrocytes in promoting energy metabolite transport at the synapse, or both.

7 Summary

Glia is now recognized as a key element in brain metabolism. In the thalamus, astrocytes and oligodendrocytes are coupled via gap junction channels and form extensive panglial networks. Interestingly and in contrast to other brain regions, thalamic panglial networks are equally composed of astrocytes and oligodendrocytes. The functional impact of astrocyte-oligodendrocyte coupling in grey matter is still unclear. Thus, thalamic glia properties and their role in brain energy metabolism and neuron-glia signaling were investigated.

The ventral posterior nucleus of the thalamus is part of the somatosensory system and contains elongated cellular domains called barreloids, which are the basic structure for the representation of vibrissae. In the first part of the present study, electrophysiological recordings and immunohistochemistry revealed new features of glial cells in thalamic barreloids. It could be shown that barreloid borders were formed by uncoupled or weakly coupled oligodendrocytes. Furthermore, it could be demonstrated that thalamic panglial networks were dependent on neuronal activity and limited by the barreloid borders.

Oligodendrocytes make up for more than 50% of coupled cells in the thalamus. However, their functional impact remains elusive. The role of thalamic oligodendrocytes in brain energy metabolism was investigated in this study. In acute brain slices, the cortico-thalamic pathway was stimulated and extracellular glucose deprivation (EGD) suppressed thalamic postsynaptic field potentials (fPSPs). This EGD-induced decline could not be rescued by extracellular lactate or pyruvate bath application. However, filling an astrocyte with glucose or lactate was sufficient to rescue the decline of fPSP amplitudes during EGD. Interestingly, loading a single oligodendrocyte with energy metabolites also rescued thalamic fPSP amplitudes during EGD. Next, connexin 32/47 double-deficient mice lacking oligodendroglial coupling

were used. Filling an astrocyte with glucose in those mice did not rescue the decline in fPSP amplitudes during EGD. Moreover, employing pharmacological blockers it could be shown that the prevention of the decline of fPSP amplitudes during EGD required glucose and monocarboxylate transporters.

In conclusion, the present study demonstrates that thalamic astrocytes and oligodendrocytes are jointly engaged in maintaining neuronal activity by supplying energy metabolites like glucose and lactate through the panglial network. In addition, these results enhance our understanding of glial network functional dissimilarities between different grey matter and white matter areas.

8 Perspective

The current study highlights new specific features of thalamic oligodendrocytes in and outside thalamic barreloids. Excitingly, a new essential role for thalamic glial cells in sustaining synaptic activity via delivery of energy substrates was unraveled. The importance of oligodendrocytes in thalamic energy metabolism could be demonstrated.

Uncoupled or weakly coupled oligodendrocytes are the cellular element restricting neuronal communication to a single barreloid. As thalamic panglial networks were dependent on neuronal activity it would be interesting to determine whether this characteristic might be important to guarantee energy support along the metabolite route from individual vibrissae to the corresponding neuronal network within a barreloid. In this study, TTX incubation reduced thalamic panglial coupling. There is evidence that connexin 30 is predominant in the thalamus and is the molecular target for the activity-dependence of coupled networks in another brain region. Therefore, studying which connexin mediates the activity-dependence of coupling and starting with Cx30-defficient mice would be interesting. Moreover, it would be of interest to test whether neuronal activity modulates coupling not only in slices but also in vivo. Thus, the impact of the reduction of sensory inputs to the barreloids through whisker trimming, which leads to long term reorganization of the thalamus, could be investigated.

Excitingly, the present study provides new insights into the physiological relevance of oligodendrocytes within thalamic panglial networks. Astrocytes and oligodendrocytes were identified as being conjointly engaged in sustaining synaptic activity through the delivery of metabolites. However, it still remains to be investigated whether oligodendrocytes apply their effect by supporting axonal/presynaptic function and/or rather by assisting astrocyte metabolite transport to the postsynapse. Obviously, basic thalamic mechanisms regarding brain energy metabolism differ from other brain regions. Thus, exploring panglial networks in other yet unstudied brain areas would be of great interest for the field of brain metabolism.

References

Abbott NJ, Rönnbäck L and Hansson E (2006) Astrocyte-endothelial interactions at the blood-brain barrier. Nat Rev Neurosci 7:41-53.

Aggleton JP, Pralus A, Nelson AJD, Hornberger M (2016) Thalamic pathology and memory loss in early Alzheimer's disease: moving the focus from the medial temporal lobe to Papez circuit. 139:1877-1890.

Agmon A, Yang LT, O'Dowd DK, Jones EG (1993) Organized growth of thalamocortical axons from the deep tier of terminations into layer IV of developing mouse barrel cortex. J Neurosci 12:5365-5382.

Allaman I, Bélanger M and Magistretti PJ (2011) Astrocyte-neuron metabolic relationships: for better and for worse. Trends Neurosci 34:76-87.

Allen NJ and Barres BA (2009) Neuroscience: Glia - more than just brain glue. Nature 457:675-677.

Altevogt BM, Kleopa KA, Postma FR, Scherer SS, Paul DL (2002) Connexin29 is uniquely distributed within myelinating glial cells of the central and peripheral nervous systems. J Neurosci 22:6458-6470.

Altevogt BM and Paul DL (2004) Four classes of intercellular channels between glial cells in the CNS. J Neurosci 24:4313-4323.

Amaral AI, Hadera MG, Tavares JM, Kotter MR, Sonnewald U (2016) Characterization of glucose-related metabolic pathways in differentiated rat oligodendrocyte lineage cells. Glia 64:21-34.

Araque A, Parpura V, Sanzgiri RP, Haydon PG (1999) Tripartite synapses: glia, the unacknowledged partner. Trends Neurosci 22:208–215.

Attwell D, Buchan AM, Charpak S, Lauritzen M, Macvicar BA, Newman EA (2010) Glial and neuronal control of brain blood flow. Nature 468:232-243.

Balestrino M and Somjen GG (1986) Chlorpromazine protects brain tissue in hypoxia by delaying spreading depression-mediated calcium influx. Brain Res 385:219–226.

Barres BA (2008) The mystery and magic of glia: a perspective on their roles in health and disease. Neuron 60:430-440.

Barres BA (2013) Metabolic signaling by lactate in the brain. Trends Neurosci 36:396-404.

Barros LF, Brown A and Swanson RA (2018) Glia in brain energy metabolism: a perspective. Glia 66:1134-1137.

Barros LF and Deitme JW (2010) Glucose and lactate supply to the synapse. Brain Res Rev 63:149-159.

Bedner P, Niessen H, Odermatt B, Kretz M, Willecke K, Harz H (2006) Selective permeability of different connexin channels to the second messenger cyclic AMP. J Biol Chem 281:6673-6681.

Bedner P, Steinhäuser C and Theis M (2012) Functional redundancy and compensation among members of gap junction protein families? Biochim Biophys Acta 1818:1971-1984.

Belanger M, Allaman I, and Magistretti PJ (2011) Brain energy metabolism: focus on astrocyte-neuron metabolic cooperation. Cell Metab 14:724-738.

Berger T, Schnitzer J, Kettenmann H (1991) Developmental changes in the membrane current pattern, K+ buffer capacity, and morphology of glial cells in the corpus callosum slice. J Neurosci 11:3008–3024

Bergles DE, Diamond JS and Jahr CE (1999) Clearance of glutamate inside the synapse and beyond. Curr Opin Neurobiol 9:293-298.

Bergoffen J, Scherer SS, Wang S, Scott MO, Bone LJ, Paul DL, Chen K, Lensch MW, Chance PF, Fischbeck KH (1993) Connexin mutations in X-linked Charcot-Marie-Tooth disease. Science 262:2039-2042.

Bezzi P, Gundersen V, Galbete JL, Seifert G, Steinhäuser C, Pilati E, Volterra A (2004) Astrocytes contain a vesicular compartment that is competent for regulated exocytosis of glutamate. Nat Neurosci 7:613-620.

Blomstrand F, Aberg ND, Eriksson PS, Hansson E, Rönnbäck L (1999) Extent of intercellular calcium wave propagation is related to gap junction permeability and level of connexin-43 expression in astrocytes in primary cultures from four brain regions. Neuroscience 92:255-265.

Bosman LWJ, Houweling AR, Owens CB, Tanke N, Shevchouk OT, Rahmati N, Teunissen WHT, Ju C, Gong W, Koekkoek SKE, De Zeeuw CI (2011) Anatomical pathways involved in generating and sensing rhythmic whisker movements. Front Integr Neurosci 5:53.

Bourassa J, Pinault D and Deschênes M (1995) Corticothalamic projections from the cortical barrel field to the somatosensory thalamus in rats: a single-fibre study using biocytin as an anterograde tracer. Eur J Neurosci 7:19-30.

Bosco D, Haefliger JA and Meda P (2011) Connexins: key mediators of endocrine function. Physiol Rev 91:1393-1445.

Brown AM and Ransom BR (2007) Astrocyte glycogen and brain energy metabolism. Glia 55:1263-1271.

Brown AM, Sickmann HM, Fosgerau K, Lund TM, Schousboe A, Waagepetersen HS, Ransom BR (2005) Astrocyte glycogen metabolism is required for neural activity during aglycemia or intense stimulation in mouse white matter. J Neurosci Res 79:74-80.

Brown AM, Wender R and Ransom BR (2001) Metabolic substrates other than glucose support axon function in central white matter. J Neurosci Res 66:839-843.

Brown AM, Tekkok SB, and Ransom BR (2003) Glycogen regulation and functional role in mouse white matter. J Physiol 549:501-512.

Bushong EA, Martone ME, Jones YZ, Ellisman MH (2002) Protoplasmic astrocytes in CA1 stratum radiatum occupy separate anatomical domains. J Neurosci 22:183-192.

Butt AM and Ransom BR (1989) Visualization of oligodendrocytes and astrocytes in the intact rat optic nerve by intracellular injection of lucifer yellow and horseradish peroxidase. Glia 2:470-475.

Bryant C, Zhang N, Sokoloff G, Fanselow M, Ennes H, Palmer A, McRoberts J (2008) Behavioral Differences among C57BL/6 Substrains: Implications for Transgenic and Knockout Studies. J Neurogenet 22:315-331.

Camron D. Bryant, Nanci N. Zhang, Greta Sokoloff, Michael S. Fanselow, Helena S. Ennes, Abraham A. Palmer, and James A. McRoberts (2008) Behavioral Differences among C57BL/6 Substrains: Implications for Transgenic and Knockout Studies. J Neurogenet 22:315-331.

Chen M, Guo D, Xia Y, Yao D (2017) Control of Absence Seizures by the Thalamic Feed-Forward Inhibition. Front Comput Neurosci 11:31.

Chuquet J, Quilichini P, Nimchinsky EA, Buzsáki G (2010) Predominant enhancement of glucose uptake in astrocytes versus neurons during activation of the somatosensory cortex. J Neurosci 30:15298-15303.

Claus L, Philippot C, Griemsmann S, Timmermann A, Jabs R, Henneberger C, Kettenmann H, Steinhäuser C (2018) Barreloid Borders and Neuronal Activity Shape Panglial Gap Junction-Coupled Networks in the Mouse Thalamus. Cereb Cortex 28:213-222.

Cornell-Bell AH, Finkbeiner SM, Cooper MS, Smith SJ (1990) Glutamate induces calcium waves in cultured astrocytes: long-range glial signaling. Science 247:470-473.

Coulter DA and Eid T (2012) Astrocytic regulation of glutamate homeostasis in epilepsy. Glia 60:1215-1226.

Coulter D and Steinhauser C (2015) Role of Astrocytes in Epilpesy. Cold Spring Harb Perspect Med 5:a022434.

Crick F and Koch C (2003) A framework for consciousness. Nat Neurosci 6:119-126.

Dahl E, Manthey D, Chen Y, Schwarz HJ, Chang YS, Lalley PA, Nicholson BJ, Willecke K (1996) Molecular cloning and functional expression of mouse connexin-30,a gap junction gene highly expressed in adult brain and skin. J Biol Chem 271:17903-17910.

D'Ambrosio R, Gordon DS and Winn HR (2002) Differential Role of KIR Channel and Na+/K+-Pump in the Regulation of Extracellular K+ in Rat Hippocampus. J Neurophysiol 87: 87–102.

Del Río Hortega P (1921) Glía con pocas prolongaciones (oligodendroglía). Bol Soc Esp Biol XXI:1–43.

De Pina-Benabou MH, Srinivas M, Spray DC, Scemes E (2001) Calmodulin kinase pathway mediates the K+-induced increase in Gap junctional communication between mouse spinal cord astrocytes. J Neurosci 21:6635–6643.

Dermietzel R, Traub O, Hwang TK, Beyer E, Bennett MV, Spray DC, Willecke K (1989) Differential expression of three gap junction proteins in developing and mature brain tissues. Proc Natl Acad Sci U S A 86:10148-10152.

Dermietzel R, Farooq M, Kessler JA, Althaus H, Hertzberg EL, Spray DC (1997) Oligodendrocytes express gap junction proteins connexin32 and connexin45. Glia 20:101-114

Djukic B, Casper KB, Philpot BD, Chin LS, McCarthy KD (2007) Conditional knock-out of Kir4.1 leads to glial membrane depolarization, inhibition of potassium and glutamate uptake, and enhanced short-term synaptic potentiation. J Neurosci 27:11354-11365.

Downes N and Mullins P (2014) The development of myelin in the brain of the juvenile rat. Toxicol Pathol 42:913-922.

Dringen R, Gebhardt R and Hamprecht B (1993) Glycogen in astrocytes: possible function as lactate supply for neighboring cells. Brain Res 623:208-214.

Eaton SA and Salt TE (1996) Role of N-methyl-D-aspartate and metabotropic glutamate receptors in corticothalamic excitatory postsynaptic potentials in vivo. Neuroscience 73:1-5.

Elsayed M and Magistretti PJ (2015) A New Outlook on Mental Illnesses: Glial Involvement Beyond the Glue. Front Cell Neurosci 9:468.

Enkvist MO and McCarthy KD (1994) Astroglial gap junction communication is increased by treatment with either glutamate or high K+ concentration. J Neurochem 62:489-495.

Fischer G and Kettenmann H (1985) Cultured astrocytes form a syncytium after maturation. Exp Cell Res 159:273-279.

Frassoni C, Amadeo A, Ortino B, Jaranowska A, Spreafico R (2000) Organization of radial and non-radial glia in the developing rat thalamus. J Comp Neurol 428:527-542.

Funfschilling U, Supplie LM, Mahad D, Boretius S, Saab AS, Edgar J, Brinkmann BG, Kassmann CM, Tzvetanova ID, Mobius W, Diaz F, Meijer D, Suter U, Hamprecht B, Sereda MW, Moraes CT, Frahm J, Goebbels S, and Nave KA (2012) Glycolytic oligodendrocytes maintain myelin and long-term axonal integrity. Nature 485:517-521.

Fuss B, Mallon B, Phan T, Ohlemeyer C, Kirchho F, Nishiyama A, Macklin WB (2000) Purification and analysis of in vivo-differentiated oligodendrocytes expressing the green fluorescent protein. Dev Biol 218:259-274.

Giaume C, Koulakoff A, Roux L, Holcman D, Rouach N (2010) Astroglial networks: a step further in neuroglial and gliovascular interactions. Nat Rev Neurosci 11:87-99.

Giaume C and Naus CC (2013) Connexins, gap junctions, and glia. WIREs Membr Transp Signal 2:133-142.

Giaume C, Theis M (2010) Pharmacological and genetic approaches to study connexin mediated channels in glial cells of the central nervous system. Brain Res Rev 63:160-176.

Goldberg GS, Valiunas V and Brink PR (2004) Selective permeability of gap junction channels. Biochim Biophys Acta 1662:96-101.

Golgi C (1886) *Sulla fine anatomia degli organi centrali del sisterna nervosa*. Milan: Hoepli.

Goodenough DA, Goliger JA and Paul DL (1996) Connexins, connexons, and intercellular communication. Annu Rev Biochem 65:475-502.

Gordji-Nejad A, Matusch A, Li S, Kroll T, Beer S, Elmenhorst D, and Bauer A (2018) Phosphocreatine Levels in the Left Thalamus Decline during Wakefulness and Increase after a Nap. J Neurosci 38:10552-10565.

Grant E, Hoerder-Suabedissen A, Molnár Z (2012) Development of the corticothalamic projections. Front Neurosci 6:53.

Griemsmann S (2015) Characterization of panglial gap junction networks in the thalamus and hippocampus reveals glial heterogeneity. Thesis http://hss.ulb.uni-bonn.de/2015/4008/4008.htm

Griemsmann S, Hoft SP, Bedner P, Zhang J, von Staden E, Beinhauer A, Degen J, Dublin P, Cope DW, Richter N, Crunelli V, Jabs R, Willecke K, Theis M, Seifert G, Kettenmann H, and Steinhäuser C (2015) Characterization of Panglial Gap Junction Networks in the Thalamus, Neocortex, and Hippocampus Reveals a Unique Population of Glial Cells. Cereb Cortex 25:3420-3433.

Griffiths I, Klugmann M, Anderson T, Yool D, Thomson C, Schwab MH, Schneider A, Zimmermann F, McCulloch M, Nadon N, Nave KA (1998) Axonal swellings and degeneration in mice lacking the major proteolipid of myelin. Science 280:1610-1613.

Grosche A, Grosche J, Tackenberg M, Scheller D, Gerstner G, Gumprecht A, Pannicke T, Hirrlinger PG, Wilhelmsson U, Hüttmann K, Härtig W, Steinhäuser C, Pekny M, Reichenbach A (2013) Versatile and Simple Approach to Determine Astrocyte Territories in Mouse Neocortex and Hippocampus. PLoS One 8:e69143.

Haidarliu S and Ahissar E (2001) Size gradients of barreloids in the rat thalamus. J Comp Neurol 429:372-387.

Halassa MM, Fellin T and Haydon PG (2007) The tripartite synapse: roles for gliotransmission in health and disease. Trends Mol Med 13:54-63.

Haydon PG and Carmignoto G (2006) Astrocyte control of synaptic transmission and neurovascular coupling. Physiol Rev 86:1009-1031.

Henneberger C, Papouin T, Oliet SHR, Rusakov DA (2010) Long-term potentiation depends on release of D-serine from astrocytes. Nature 463:232-236.

Hirrlinger J and Nave KA (2014) Adapting brain metabolism to myelination and long-range signal transduction Glia 62:1749-1761.

Hoft S, Griemsmann S, Seifert G, Steinhäuser C (2014) Heterogeneity in expression of functional ionotropic glutamate and GABA receptors in astrocytes across brain regions: insights from the thalamus. Philos Trans R Soc Lond B Biol Sci. 369: 20130602.

Hoogland TM, Kuhn B, Göbel W, Huang W, Nakai J, Helmchen F, Flint J, Wang SS (2009) Radially expanding transglial calcium waves in the intact cerebellum. Proc Natl Acad Sci U S A 106:3496-3501.

Houades V, Koulakoff A, Ezan P, Seif I, Giaume C (2008) Gap junction-mediated astrocytic networks in the mouse barrel cortex. *J Neurosci* 28:5207–5217.

Houades V, Rouach N, Ezan P, Kirchhoff F, Koulakoff A, Giaume C (2006) Shapes of astrocyte networks in the juvenile brain. Neuron Glia Biol 2:3-14.

Iadecola C and Nedergaard M (2007) Glial regulation of the cerebral microvasculature. Nat Neurosci 10:1369-1376.

Ito M (1988) Response properties and topography of vibrissa-sensitive VPM neurons in the rat. J Neurophysiol 60:1181–1197.

Kacem K, Lacombe P, Seylaz J, Bonvento G (1998) Structural organization of the perivascular astrocyte endfeet and their relationship with the endothelial glucose transporter: A confocal microscopy study. Glia 23:1-10.

Kafitz KW, Meier SD, Stephan J, Rose CR (2008) Developmental profile and properties of sulforhodamine 101-labeled glial cells in acute brain slices of rat hippocampus. J Neurosci Methods 169:84-92.

Kang J, Kang N, Yu Y, Zhang J, Petersen N, Tian GF, Nedergaard M (2010) Sulforhodamine 101 induces long-term potentiation of intrinsic excitability and synaptic effcacy in hippocampal CA1 pyramidal neurons. Neuroscience 169:1601-1609.

Kettenmann H and Ransom BR (2005) Neuroglia. Oxford University Press, Oxford.

Klugmann M, Schwab MH, Pühlhofer A, Schneider A, Zimmermann F, Griffiths IR, Nave KA (1997) Assembly of CNS myelin in the absence of proteolipid protein. Neuron 18:59-70.

Kuchibhotla KV, Lattarulo CR, Hyman BT, Bacskai BJ (2009) Synchronous hyperactivity and intercellular calcium waves in astrocytes in Alzheimer mice. Science 323:1211-1215.

Kunzelmann P, Blümcke I, Traub O, Dermietzel R, Willecke K (1997) Coexpression of connexin45 and -32 in oligodendrocytes of rat brain. J Neurocytol 26:17-22.

Kunzelmann P, Schröder W, Traub O, Steinhäuser C, Dermietzel R, Willecke K (1999) Late onset and increasing expression of the gap junction protein connexin30 in adult murine brain and long-term cultured astrocytes. Glia 25:111-119.

Land PW and Akhtar ND (1987) Chronic sensory deprivation affects cytochrome oxidase staining and glutamic acid decarboxylase immunoreactivity in adult rat ventrobasal thalamus. Brain Res 425:178-181.

Landisman CE, Long MA, Beierlein M, Deans MR, Paul DL, Connors BW (2002) Electrical synapses in the thalamic reticular nucleus. J Neurosci 22:1002-1009.

Langer J, Stephan J, Theis M, Rose CR (2012) Gap junctions mediate intercellular spread of sodium between hippocampal astrocytes in situ. Glia 60:239-252.

Lappe-Siefke C, Goebbels S, Gravel M, Nicksch E, Lee J, Braun PE, Griffiths IR, Nave KA (2003) Disruption of Cnp1 uncouples oligodendroglial functions in axonal support and myelination. Nat Genet 33:366-374.

Lavalée P and Deschênes M (2004) Dendroarchitecture and lateral inhibition in thalamic barreloids. J Neurosci 24:6098-6105.

Lee SC, Cruikshank SJ and Connors BW (2010) Electrical and chemical synapses between relay neurons in developing thalamus. J Physiol 588:2403-2415.

Lee SC, Patrick SL, Richardson KA, Connors BW (2014) Two functionally distinct networks of gap junction-coupled inhibitory neurons in the thalamic reticular nucleus. J Neurosci 34:13170-13182.

Lee Y, Morrison BM, Li Y, Lengacher S, Farah MH, Ho_man PN, Liu Y, Tsingalia A, Jin L, Zhang PW, Pellerin L, Magistretti PJ, Rothstein JD (2012) Oligodendroglia metabolically support axons and contribute to neurodegeneration. Nature 487:443-448.

Lenhossék MV (1891) Zur Kenntnis der Neuroglia des menschlichen Ruckenmarkes. Verh Anat Ges. 5:193–221.

Lerchundi R, Fernández-Moncada I, Contreras-Baeza Y, Sotelo-Hitschfeld T, Machler P, Wyss MT, Stobart J, Baeza-Lehnert F, Alegría K, Weber B and Barros LF (2015) $NH4^+$ triggers the release of astrocytic lactate via mitochondrial pyruvate shunting. Proc Natl Acad Sci U S A 112:11090–11095.

Li H and Crair MC (2011) How do barrels form in somatosensory cortex? Ann N Y Acad Sci 1225:119-129.

Li X, Penes M, Odermatt B, Willecke K, Nagy JI (2008) Ablation of Cx47 in transgenic mice leads to the loss of MUPP1, ZONAB and multiple connexins at oligodendrocyte-astrocyte gap junctions. Eur J Neurosci 28:1507-1517.

Loers G, Aboul-Enein F, Bartsch U, Lassmann H, Schachner M (2004) Comparison of myelin, axon, lipid, and immunopathology in the central nervous system of differentially myelin-compromised mutant mice: a morphological and biochemical study. Mol Cell Neurosci 27:175-189.

Long MA, Landisman CE and Connors BW (2004) Small clusters of electrically coupled neurons generate synchronous rhythms in the thalamic reticular nucleus. J Neurosci 24:341-349.

Lutz SE, Zhao Y, Gulinello M, Lee SC, Raine CS, Brosnan CF (2009) Deletion of astrocyte connexins 43 and 30 leads to a dysmyelinating phenotype and hippocampal CA1 vacuolation. J Neurosci 29:7743-7752.

MacVicar BA and Newman EA (2015) Astrocyte regulation of blood flow in the brain. Cold Spring Harb Perspect Biol 7:a020388.

Magistretti PJ (2006) Neuron-glia metabolic coupling and plasticity. J Exp Biol 209:2304-2311.

Magistretti PJ and Allaman I (2015) A cellular perspective on brain energy metabolism and functional imaging. Neuron 86:883-901.

Magistretti PJ and Allaman I (2018) Lactate in the brain: from metabolic end-product to signalling molecule. Nat Rev Neurosci 19:235-249.

Magistretti PJ and Chatton JY (2005) Relationship between L-glutamate-regulated intracellular Na+ dynamics and ATP hydrolysis in astrocytes. J Neural Transm 112:77–85.

Magistretti PJ and Pellerin L (1999) Cellular mechanisms of brain energy metabolism and their relevance to functional brain imaging. Philos Trans R Soc Lond B Biol Sci 354:1155-1163.

Magistretti PJ, Sorg O, Yu N, Martin J-L, Pellerin L (1993) Neurotransmitters regulate energy metabolism in astrocytes: Implications for the metabolic trafficking between neural cells. Developmental Neuroscience 15:306-312.

Magistretti PJ, Sorg O, Naichen Y, Pellerin L, de Rham S, Martin JL (1994) Regulation of astrocyte energy metabolism by neurotransmitters. Ren Physiol Biochem 17:168-71.

Maglione M, Tress O, Haas B, Karram K, Trotter J, Willecke K, Kettenmann H (2010) Oligodendrocytes in mouse corpus callosum are coupled via gap junction channels formed by connexin47 and connexin32. Glia 58:1104-1117.

Magnotti LM, Goodenough DA and Paul DL (2011) Functional heterotypic interactions between astrocyte and oligodendrocyte connexins. Glia 59:26-34.

Marrero H and Orkand RK (1996) Nerve impulses increase glial intercellular permeability. Glia 16:285–289.

Mathiisen TM, Lehre KP, Danbolt NC, Ottersen OP (2010) The perivascular astroglial sheath provides a complete covering of the brain microvessels: an electron microscopic 3D reconstruction. Glia 58:1094-1103.

Matsui K, Jahr CE and Rubio ME (2005) High-concentration rapid transients of glutamate mediate neural-glial communication via ectopic release. J Neurosci 25:7538-7547.

Matthias K, Kirchhoff F, Seifert G, Hüttmann K, Matyash M, Kettenmann H, Steinhäuser C (2003) Segregated expression of AMPA-type glutamate receptors and glutamate transporters defines distinct astrocyte populations in the mouse hippocampus. J Neurosci 23:1750-1758.

Matyash V and Kettenmann H (2010) Heterogeneity in astrocyte morphology and physiology. Brain Res Rev 63:2–10.

Martinez-Hernandez A, Bell KP and Norenberg MD (1977) Glutamine synthetase: glial localization in brain. Science 195:1356-1358.

May D, Tress O, Seifert G, Willecke K (2013) Connexin47 Protein Phosphorylation and Stability in Oligodendrocytes Depend on Expression of Connexin43 Protein in Astrocytes. J Neuroci 33:7985-7996.

Menichella DM, Goodenough DA, Sirkowski E, Scherer SS, Paul DL (2003) Connexins are critical for normal myelination in the CNS. J Neurosci 23:5963-5973.

Menichella DM, Majdan M, Awatramani R, Goodenough DA, Sirkowski E, Scherer SS, Paul DL (2006) Genetic and physiological evidence that oligodendrocyte gap junctions contribute to spatial buffering of potassium released during neuronal activity. J Neurosci 26:10984-10991.

Mergenthaler P, Lindauer U, Dienel GA, Meisel A (2013) Sugar for the brain: the role of glucose in physiological and pathological brain function. Trends Neurosci 36:587-597.

Meyer N, Richter N, Fan Z, Siemonsmeier G, Pivneva T, Jordan P, Steinhäuser C, Semtner M, Nolte C, Kettenmann H (2018) Oligodendrocytes in the Mouse Corpus Callosum Maintain Axonal Function by Delivery of Glucose. Cell Rep 22:2383-2394.

Mink JW, Blumenschine RJ and Adams DB (1981) Ratio of central nervous system to body metabolism in vertebrates: its constancy and functional basis. Am J Physiol 241:R203-12.

Moriyoshi K, Richards LJ, Akazawa C, O'Leary DD, Nakanishi S (1996) Labeling neural cells using adenoviral gene transfer of membrane-targeted GFP. Neuron 16:255-60.

Morgello S, Uson RR, Schwartz EJ, Haber RS (1995) The human blood-brain barrier glucose transporter (GLUT1) is a glucose transporter of gray matter astrocytes. Glia 14:43-54.

Morrison BM, Lee Y and Rothstein JD (2013) Oligodendroglia: metabolic supporters of axons. Trends Cell Biol 23:644–651.

Mosconi T, Woolsey TA and Jacquin MF (2010) Passive vs. active touch-induced activity in the developing whisker pathway. Eur J Neurosci 32:1354–1363.

Nagy JI, Li X, Rempel J, Stelmack G, Patel D, Staines WA, Yasumura T, Rash JE (2001) Connexin26 in adult rodent central nervous system: demonstration at astrocytic gap junctions and colocalization with connexin30 and connexin43. J Comp Neurol 441:302-323.

Nagy JI, Lynn BD, Tress O, Willecke K, Rash JE (2011) Connexin26 expression in brain parenchymal cells demonstrated by targeted connexin ablation in transgenic mice. Eur J Neurosci 34:263-271.

Nagy JI, Patel D, Ochalski PA, Stelmack GL (1999) Connexin30 in rodent, cat and human brain: selective expression in gray matter astrocytes, co-localization with connexin43 at gap junctions and late developmental appearance. Neuroscience 88:447-468.

Nagy JI, Dudek FE and Rash JE (2004) Update on connexins and gap junctions in neurons and glia in the mammalian nervous system. Brain Res Brain Res Rev 47:191-215.

Nagy JI, Ionescu AV, Lynn BD, Rash JE (2003) Connexin29 and connexin32 at oligodendrocyte and astrocyte gap junctions and in myelin of the mouse central nervous system. J Comp Neurol 464:356-370.

Nagy JI and Rash JE (2003) Astrocyte and oligodendrocyte connexins of the glial syncytium in relation to astrocyte anatomical domains and spatial buffering. Cell Commun Adhes 10:401-406.

Navarrete M, Perea G, Maglio L, Pastor J, García de Sola R, Araque A (2013) Astrocyte calcium signal and gliotransmission in human brain tissue. Cereb Cortex 23:1240-1246.

Navarrete M and Araque A (2014) The Cajal school and the physiological role of astrocytes: a way of thinking. Front Neuroanat 8:33.

Navarrete M, Perea G, Fernandez de Sevilla D, Gómez-Gonzalo M, Núñez A, Martín ED, Araque A (2012) Astrocytes mediate in vivo cholinergic-induced synaptic plasticity. PLoS Biol 10: e1001259.

Nedergaard M, Ransom B and Goldman SA (2003) New roles for astrocytes: redefining the functional architecture of the brain. Trends Neurosci 26:523-530.

Neher E, Sakmann B (1976) Single-channel currents recorded from membrane of denervated frog muscle fibres. Nature 260:799-802.

Nelles E, Bützler C, Jung D, Temme A, Gabriel HD, Dahl U, Traub O, Stümpel F, Jungermann K, Zielasek J, Toyka KV, Dermietzel R, Willecke K (1996) Defective propagation of signals generated by sympathetic nerve stimulation in the liver of connexin32-deficient mice. Proc Natl Acad Sci USA 93:9565-9570.

Niepel G, Tench ChR, Morgan PS, Evangelou N, Auer DP, Constantinescu CS (2006) Deep gray matter and fatigue in MS: a T1 relaxation time study. J Neurol 253:896:902.

Niermann H, Amiry-Moghaddam M, Holthoff K, Witte OW, Ottersen OP (2001) A novel role of vasopressin in the brain: modulation of activity-dependent water flux in the neocortex. J Neurosci 21:3045-3051.

Nimmerjahn A, Kirchhoff F, Kerr JND, Helmchen F (2004) Sulforhodamine 101 as a specific marker of astroglia in the neocortex in vivo. Nat Methods 1:31-37.

Nimmerjahn A, Mukamel EA and Schnitzer MJ (2009) Motor behavior activates Bergmann glial networks. Neuron 62:400-412.

Nishiyama A, Dahlin KJ, Prince JT, Johnstone SR, Stallcup WB (1991) The primary structure of NG2, a novel membrane-spanning proteoglycan. J Cell Biol 114:359-371.

Nolte C, Matyash M, Pivneva T, Schipke CG, Ohlemeyer C, Hanisch UK, Kirchhoff F, Kettenmann H (2001) GFAP promoter-controlled EGFP-expressing transgenic mice: a tool to visualize astrocytes and astrogliosis in living brain tissue. Glia 33:72-86.

Odermatt B, Wellershaus K, Wallraff A, Seifert G, Degen J, Euwens C, Fuss B, Büssow H, Schilling K, Steinhäuser C, Willecke K (2003) Connexin 47 (Cx47) deficient mice with enhanced green fluorescent protein reporter gene reveal predominant oligodendrocytic expression of Cx47 and display vacuolized myelin in the CNS. J Neurosci 23:4549-4559.

Oe Y, Baba O, Ashida H, Nakamura KC, and Hirase H (2016) Glycogen distribution in the microwave-fixed mouse brain reveals heterogeneous astrocytic patterns. Glia 64:1532-1545.

Orkand RK (1986) Introductory Remarks: Glial-Interstitial Fluid Exchange. Ann N Y Acad Sci 481:269–272.

Orthmann-Murphy JL, Freidin M, Fischer E, Scherer SS, Abrams CK (2007) Two distinct heterotypic channels mediate gap junction coupling between astrocyte and oligodendrocyte connexins. J Neurosci 27:13949-13957.

Pannasch U, Freche D, Dallérac G, Ghézali G, Escartin C, Ezan P, Cohen-Salmon M, Benchenane K, Abudara V, Dufour A, Lübke JHR, Déglon N, Knott G, Holcman D, Rouach N (2014) Connexin 30 sets synaptic strength by controlling astroglial synapse invasion. Nat Neurosci 17:549-558.

Pannasch U and Rouach N (2013) Emerging role for astroglial networks in information processing: from synapse to behavior. Trends Neurosci 36:405-417.

Pannasch U, Vargová L, Reingruber J, Ezan P, Holcman D, Giaume C, Syková E, Rouach N (2011) Astroglial networks scale synaptic activity and plasticity. Proc Natl Acad Sci U S A 108:8467-8472.

Parpura V, Basarsky TA, Liu F, Jeftinija K, Jeftinija S, Haydon PG (1994) Glutamate-mediated astrocyte-neuron signalling. Nature 369:744-747.

Parri HR, Gould TM and Crunelli V (2010) Sensory and cortical activation of distinct glial cell subtypes in the somatosensory thalamus of young rats. Eur J Neurosci 32:29–40.

Pekny M, Wilhelmsson U and Pekna M (2014) The dual role of astrocyte activation and reactive gliosis. Neurosci Lett 565:30-38.

Pellerin L (2003) Lactate as a pivotal element in neuron-glia metabolic cooperation. Neurochem Int 43:331-338.

Pellerin L, Bouzier-Sore AK, Aubert A, Serres S, Merle M, Costalat R, Magistretti PJ (2007) Activity-dependent regulation of energy metabolism by astrocytes: An update. Glia 55:1251-1562.

Pellerin L and Magistretti PJ (1994) Glutamate uptake into astrocytes stimulates aerobic glycolysis: a mechanism coupling neuronal activity to glucose utilization. Proc Natl Acad Sci U S A 91:10625-10629.

Pellerin L and Magistretti PJ (2012) Sweet sixteen for ANLS. J Cereb Blood Flow Metab 32:1152-1166.

Perea G, Navarrete M and Araque A (2009) Tripartite synapses: astrocytes process and control synaptic information. Trends Neurosci 32:421-431.

Philips T and Rothstein JD (2017) Oligodendroglia: metabolic supporters of neurons. J Ckin Invest 127:3271-3280.

Pinault D (2011) Dysfunctional thalamus-related networks in schizophrenia. Schizophr Bull 37:238-243.

Pirttimaki TM and Parri HR (2012) Glutamatergic input-output properties of thalamic astrocytes. Neuroscience 205:18–28.

Pellerin L and Magistretti PJ (1994) Glutamate uptake into astrocytes stimulates aerobic glycolysis: a mechanism coupling neuronal activity to glucose utilization. Proc Natl Acad Sci U S A 91:10625-10629.

Pellerin L and Magistretti PJ (2012) Sweet sixteen for ANLS. J Cereb Blood Flow Metab 32:1152-1166.

Pierre K and Pellerin L (2005) Monocarboxylate transporters in the central nervous system: distribution, regulation and function. J Neurochem 94:1-14.

Rafiki A, Boulland JL, Halestrap AP, Ottersen OP, and Bergersen L (2003) Highly differential expression of the monocarboxylate transporters MCT2 and MCT4 in the developing rat brain. Neuroscience 122:677-688.

Ramón y Cajal S (1897) Algo sobre la significación fisiológica de la neuroglia. Revista Trimestral Micrografía 1:3–47.

Rampon C, Jiang CH, Dong H, Tang YP, Lockhart DJ, Schultz PG, Tsien JZ, Hu Y (2000) ffects of environmental enrichment on gene expression in the brain. Proc Natl Acad Sci U S A 97:12880-12884.

Ransom CB, Ransom BR and Sontheimer H (2000) Activity-dependent extracellular K+ accumulation in rat optic nerve: the role of glial and axonal Na+ pumps. J Physiol 522: 427–442.

Rinholm JE, Hamilton NB, Kessaris N, Richardson WD, Bergersen LH, and Attwell D (2011) Regulation of oligodendrocyte development and myelination by glucose and lactate. J Neurosci 31:538-548.

Rouach N, Glowinski J and Giaume C (2000) Activity-dependent neuronal control of gap-junctional communication in astrocytes. J Cell Biol 149:1513–1526.

Rouach N, Koulako A, Abudara V, Willecke K, Giaume C (2008) Astroglial metabolic networks sustain hippocampal synaptic transmission. Science 322:1551-1555.

Roux L, Benchenane K, Rothstein JD, Bonvento G, Giaume C (2011) Plasticity of astroglial networks in olfactory glomeruli. Proc Natl Acad Sci U S A 108:18442–18446.

Saab AS, Tzvetavona ID, Trevisiol A, Baltan S, Dibaj P, Kusch K, Möbius W, Goetze B, Jahn HM, Huang W, Steffens H, Schomburg ED, Pérez-Samartín A, Pérez-Cerdá F, Bakhtiari D, Matute C, Löwel S, Griesinger C, Hirrlinger J, Kirchhoff F, Nave KA (2016) Oligodendroglial NMDA Receptors Regulate Glucose Import and Axonal Energy Metabolism. Neuron 91:119-132.

Scemes E and Giaume C (2006) Astrocyte calcium waves: what they are and what they do. Glia 54:716-725.

Schools GP, Zhou M and Kimelberg HK (2006) Development of gap junctions in hippocampal astrocytes: evidence that whole cell electrophysiological phenotype is an intrinsic property of the individual cell. J Neurophysiol 96:1383–1392.

Seifert G, Huttmann K, Binder DK, Hartmann C, Wyczynski A, Neusch C, Steinhauser C (2009) Analysis of Astroglial K+ Channel expression in the developing hippocampus reveals a predominant role of the Kir4.1 Subunit. J Neurosci 29:7474-7488.

Sherman DL and Brophy PJ (2005) Mechanisms of axon ensheathment and myelin growth. Nat Rev Neurosci 6:683-690.

Sherman SM and Guillery RW (2002) The role of the thalamus in the flow of information to the cortex. Philos Trans R Soc Lond B Biol Sci 357:1695-1708.

Simard M, Arcuino G, Takano T, Liu QS, Nedergaard M (2003) Signaling at the gliovascular interface. J Neurosci 23:9254-9262.

Simons M and Nave KA (2016) Oligodendrocytes: Myelination and Axonal Support. Cold Spring Harb Perspect Biol 8:a020479.

Sofroniew MV and Vinters HV (2010) Astrocytes: biology and pathology. 119:7-35.

Söhl G and Willecke K (2003) An update on connexin genes and their nomenclature in mouse and man. Cell Commun Adhes 10:173-180.

Somjen GG (1975) Electrophysiology of Neuroglia. Annu Rev Physiol 37:163–190.

Srinivas M, Verselis VK and White TW (2018) Human diseases associated with connexin mutations. Biochim Biophys Acta Biomembr 1860:192-201.

Stohschein S, Hüttmann K, Gabriel S, Binder D, Heinemann U, Steinhäuser C (2011) Impact of aquaporin-4 channels on K^+ buffering and gap junction coupling in the hippocampus. Glia 59:973-980.

Sugitani M, Yano J, Sugai T, Ooyama H (1990) Somatotopic organization and columnar structure of vibrissae representation in the rat ventrobasal complex. Exp Brain Res 81:346–352.

Suzuki A, Stern SA, Bozdagi O, Huntley GW, Walker RH, Magistretti PJ, Alberini CM (2011). Astrocyte-neuron lactate transport is required for long-term memory formation. Cell 44:810-823.

Sun W, McConnell E, Pare JF, Xu Q, Chen M, Peng W, Lovatt D, Han X, Smith Y, Nedergaard M (2003) Glutamate-dependent neuroglial calcium signaling differs between young and adult brain. Science 339:197-200.

Tekkök SB, Brown AM, Westenbroek R, Pellerin L, Ransom BR (2005) Transfer of glycogen-derived lactate from astrocytes to axons via specific monocarboxylate transporters supports mouse optic nerve activity. J Neurosci Res 81:644-652.

Theis M, Jauch R, Zhuo L, Speidel D, Wallra_ A, Döring B, Frisch C, Söhl G, Teubner B, Euwens C, Huston J, Steinhäuser C, Messing A, Heinemann U, Willecke K (2003) Accelerated hippocampal spreading depression and enhanced locomotory activity in mice with astrocyte-directed inactivation of connexin43. J Neurosci 23:766-776.

Tress O, Maglione M, May D, Pivneva T, Richter N, Seyfarth J, Binder S, Zlomuzica A, Seifert G, Theis M, Dere E, Kettenmann H, Willecke K (2012) Panglial gap junctional communication is essential for maintenance of myelin in the CNS. J Neurosci 32:7499-7518.

Uhlenberg B, Schuelke M, Rüschendorf F, Ruf N, Kaindl AM, Henneke M, Thiele H, Stoltenburg-Didinger G, Aksu F, Topaloğlu H, Nürnberg P, Hübner C, Weschke B, Gärtner J (2004) Mutations in the gene encoding gap junction protein alpha 12 (connexin 46.6) cause Pelizaeus-Merzbacher-like disease. Am J Hum Genet 75:251-260.

Van Den Berg CJ and Garfinkel D (1971) A simulation study of brain compartments. Metabolism of glutamate and related substances in mouse brain. Biochem J 123:211-218.

Van Der Loos H (1976) Barreloids in mouse somatosensory thalamus. Neurosci Lett 2:1-6.

Varga C, Sík A, Lavallée P, Deschênes M (2002) Dendroarchitecture of relay cells in thalamic barreloids: a substrate for cross-whisker modulation. J Neurosci 22:6186-6194.

Verkhratsky A and Nedergaard M (2018) Physiology of Astroglia. Physiol Rev 98:239-389.

Virchow R (1856) Die Cellularpathologie in ihrer Begründung auf physiologische and pathologische Gewebelehre. Zwanzig Vorlesungen gehalten während der Monate Februar, März und April 1858 im pathologischen Institut zu Berlin. Berlin: August Hirschwald, p. 440.

Wallraff A, Odermatt B, Willecke K, Steinhäuser C (2004) Distinct types of astroglial cells in the hippocampus differ in gap junction coupling. Glia 48:36–43.

Wallraff A, Köhling R, Heinemann U, Theis M, Willecke K, Steinhäuser C (2006) The impact of astrocytic gap junctional coupling on potassium buffering in the hippocampus. J Neurosci 26:5438-5447.

Wang DD and Bordey A (2008) The astrocyte odyssey. Prog Neurobiol 86:342-367.

Wasseff SK and Scherer SS (2011) Cx32 and Cx47 mediate oligodendrocyte:astrocyte and oligodendrocyte:oligodendrocyte gap junction coupling. Neurobiol Dis 42:506-513.

Waterston RH, Lindblad-Toh K, Birney E, Rogers J, Abril JF, Agarwal P, et al. (2002) Initial sequencing and comparative analysis of the mouse genome. Nature 420:520–562.

Wender R, Brown AM, Fern R, Swanson RA, Farrell K, Ransom BR (2000) Astrocytic glycogen influences axon function and survival during glucose deprivation in central white matter. J Neurosci 20:6804-6810.

White TW and Bruzzone R (1996) Multiple connexin proteins in single intercellular channels: Connexin compatibility and functional consequences. J Bioenerg Biomembr 28:339-350.

Wilhelmsson U, Li L, Pekna M, Berthold CH, Blom S, Eliasson C, Renner O, Bushong E, Ellisman M, Morgan TE, Pekny M (2004) Absence of glial fibrillary acidic protein and vimentin prevents hypertrophy of astrocytic processes and improves post-traumatic regeneration. J Neurosci 24:5016-5021.

Wilhelmsson U, Bushong EA, Price DL, Smarr BL, Phung V, Terada M, Ellisman MH, Pekny M(2006) Redefining the concept of reactive astrocytes as cells that remain within their unique domains upon reaction to injury. Proc of the Natl Acad of Sci U S A 103:17513-17518.

Willecke K, Eiberger J, Degen J, Eckardt D, Romualdi A, Güldenagel M, Deutsch U, Söhl G (2002) Structural and functional diversity of connexin genes in the mouse and human genome. Biol Chem 383:725-737.

Yamamoto T, Iwasaki Y, Sato Y, Yamamoto H, and Konno H (1989) Astrocytic pathology of methionine sulfoximine-induced encephalopathy. Acta Neuropathol 77:357-368.

Yamamoto T, Ochalski A, Hertzberg EL, Nagy JI (1990) On the organization of astrocytic gap junctions in rat brain as suggested by LM and EM immunohistochemistry of connexin43 expression. J Comp Neurol 302:853-883.

Young KM, Psachoulia K, Tripathi RB, Dunn SJ, Cossell L, Attwell D, Tohyama K and Richardson WD (2013) Oligodendrocyte dynamics in the healthy adult CNS: evidence for myelin remodeling. Neuron 77:873-885.

Xin W and Bonci Antonello (2018) Functional Astrocyte Heterogeneity and Implications for Their Role in Shaping Neurotransmission. Front Cell Neurosci 12:141.

Zantua JB, Wasserstrom SP, Arends JJ, Jacquin MF, Woolsey (1996) Postnatal development of mouse "whisker" thalamus: ventroposterior medial nucleus (VPM), barreloids, and their thalamocortical relay neurons. Somatosens Mot Res 13:307-322.

Zhang Y and Barres BA (2010) Astrocyte heterogeneity: an underappreciated topic in neurobiology. 20:588-594.

Zolnik TA and Connors BW (2016) Electrical synapses and the development of inhibitory circuits in the thalamus. J Physiol 594:2579-2592.